Fakultät für Medizin der Technischen Universität München

Substrates and functions of the Alzheimer's disease proteases ADAM10, BACE1, and MT5-MMP

Julia Herber

Vollständiger Abdruck der von der Fakultät für Medizin der Technischen Universität München zur Erlangung des akademischen Grades eines Doktors der Naturwissenschaften (Dr. rer. nat.) genehmigten Dissertation.

Vorsitzender: Prof. Dr. Dr. Andreas Pichlmair

Prüfer der Dissertation:

1. Prof. Dr. Stefan Lichtenthaler
2. Prof. Dr. Dieter Langosch

Die Dissertation wurde am 31.07.2018 bei der Technischen Universität München eingereicht und durch die Fakultät für Medizin am 20.02.2019 angenommen.

Technische Universität München

Substrates and functions of the Alzheimer's disease proteases ADAM10, BACE1, and MT5-MMP

von

Julia Herber

Dissertation

vorgelegt bei der Medizinischen Fakultät der Technischen Universität München zur Erlangung des akademischen Grades

Doktor der Naturwissenschaften (Dr. rer. nat.)

München, den 19.07.2018

Diese Dissertation wurde am Lehrstuhl für Neuroproteomik der medizinischen Fakultät an der Technischen Universität München und dem Deutschen Zentrum für Neurodegenerative Erkrankungen in München unter der Betreuung von Herrn Prof. Dr. Stefan Lichtenthaler verfasst.

Contents

Abstract

Alzheimer's disease (AD) is the most common form of age-related dementia and manifests as atrophy of the brain, loss of memory, and cognitive decline. Histologically the disease has two major hallmarks: neurofibrillary tau tangles and amyloid β (Aβ) deposits, which induce neurotoxicity, inflammation, and eventually lead to neuronal death. Although the molecular pathological mechanisms are relatively well studied, available drugs only treat the disease symptoms, but preventive treatment or a cure do not yet exist. Drug development is currently guided by the amyloid cascade hypothesis, in which proteolytic processing of the amyloid precursor protein (APP) is a driving process in the pathological progression of AD: Sequential APP processing by β- and γ-secretases releases the toxic Aβ peptide, which is prone to aggregation and forms Aβ-plaques.

ADAM10, BACE1, and MT5-MMP are three APP-cleaving proteases and therefore represent potential drug targets to modulate Aβ-generation. Although ADAM10 and BACE1 are already investigated in the clinic, their substrates are still not fully known, which poses the risk of side effects upon therapeutic modulation of these proteases. Therefore, this dissertation uses proteomic, biochemical, and molecular biological techniques to identify and/or validate additional substrates of these three proteases.

Stimulation of the α-secretase ADAM10 is a promising therapeutic approach in AD drug development. Yet, research in the last years began to reveal a high physiological relevance of ADAM10 in the brain. The here presented study validates two newly identified substrate candidates NrCAM and NEO1 as physiological ADAM10 substrates. The two proteins demonstrate a function for ADAM10 in neurite outgrowth and regulation of axon targeting by NrCAM-cleavage and point towards an important role for ADAM10 in the brain.

Currently, the β-secretase BACE1 is a major target in AD treatment. However, clinical BACE1 inhibition caused side effects in patients and highlights limited knowledge of the substrates and physiological roles of the protease. So far, BACE1 functions have been mainly studied by investigating cleaved soluble substrate fragments. The here presented dissertation therefore investigated the effects of pharmacological BACE1 inhibition on the neuronal cell surface proteome by mass spectrometry. To make this possible, the new method *surface-spanning protein enrichment with click sugars* (SUSPECS) was developed. The new method allows to specifically label, enrich, and purify cell surface proteins. The results obtained here indicate secondary cell surface changes and moreover show that BACE1 regulates the abundance of only few substrates in the cell surface. These substrates strongly accumulated upon inhibition of the protease and, in addition to the observed secondary changes, could be responsible for adverse effects. Therefore, this new information can be used in further studies to investigate and explain such side effects. The results presented here on BACE1 and recent outcome of clinical trials emphasize the importance to investigate additional drug targets in order to safely modulate the disease.

MT5-MMP represents such an alternative therapeutic target, since its deficiency was beneficial for pathology outcome in an AD mouse model and resulted in cognitive improvement. Using optimized proteome analysis of murine cerebrospinal fluid, the here presented work shows that the protease has significant effects in an AD background, but has only limited functions under physiological conditions. Thus, modulation or inhibition of MT5-MMP activity would result in substantially fewer side effects and therefore represents a promising new strategy for AD therapeutics.

Zusammenfassung

Die Alzheimer-Krankheit (Alzheimer's disease, AD) ist die häufigste Form der altersbedingten Demenz und manifestiert sich als Atrophie des Gehirns, Gedächtnisverlust und kognitiver Verfall. Die histologischen Hauptmerkmale der Krankheit sind neurofibrilläre Tau-Bündel und Amyloid-β (Aβ) Ablagerungen im Gehirn. Diese führen zu Neurotoxizität, Entzündungen und schließlich neuronalem Tod. Obwohl die molekularpathologischen Mechanismen relativ gut untersucht sind, schlichten Medikamente nur die Krankheitssymptome, aber eine Prävention oder Heilung ist noch nicht möglich. Derzeit wird die Medikamentenentwicklung von der Amyloid-Kaskadenhypothese bestimmt, bei der die proteolytische Prozessierung des Amyloid-Vorläuferproteins (APP) ein treibender Prozess des pathologischen AD Verlaufs ist: Sequentielle APP-Spaltung durch β- und γ-Sekretasen setzt das toxische Aβ-Peptid frei, das aggregiert und die toxischen Aβ-Plaques bildet.

ADAM10, BACE1 und MT5-MMP sind drei APP-spaltende Proteasen und repräsentieren potentielle Medikamentenziele, um die Aβ-Bildung zu beeinflussen. Obwohl ADAM10 und BACE1 Medikamente bereits in klinischen Studien untersucht wurden, ist noch nicht vollständig bekannt, welche Substrate von ihnen geschnitten werden, was ein Risiko für Nebenwirkungen darstellt. Diese Dissertation verwendet proteomische, biochemische und molekularbiologische Methoden, um zusätzliche Substrate der drei Proteasen zu identifizieren und /oder zu validieren.

Stimulation der α-Sekretase ADAM10 ist ein vielversprechender therapeutischer Ansatz in der Entwicklung von AD-Medikamenten. Allerdings zeigt die Forschung der letzten Jahre auch eine hohe physiologische Relevanz für ADAM10 im Gehirn und erschwert die Modulation der Protease für therapeutische Zwecke. Die hier vorliegende Dissertation validiert zwei zusätzliche, neue Substratkandidaten von ADAM10: NrCAM und NEO1. Die beiden Proteine zeigen eine Funktion für ADAM10 im Neuritenwachstum und bei der Regulation des Axon-Targetings und bestätigen die wichtige Rolle von ADAM10 im Gehirn.

Aktuell ist die β-Sekretase BACE1 ein Hauptziel der AD-Therapie. Allerdings führt die klinische BACE1-Inhibition zu Nebenwirkungen bei Patienten und hebt das begrenzte Wissen über die Substrate und die physiologische Funktion der Protease hervor. Bisher sind BACE1 Funktionen größtenteils anhand gespaltener löslicher Substratfragmente untersucht worden. Diese Doktorarbeit untersucht die Auswirkungen der pharmakologischen BACE1-Inhibition auf das neuronale Zelloberflächenproteom mittels Massenspektrometrie. Um dies zu ermöglichen, wurde die neue Methode *surface-spanning protein enrichment with click sugars* (SUSPECS) entwickelt. Mit ihr können Zelloberflächenproteine spezifisch markiert, angereichert und aufgereinigt werden. Hier erhaltene Ergebnisse weisen sekundäre Veränderungen in der Zelloberfläche auf, die verantwortlich für Nebenwirkungen sein könnten und in weiteren Studien genutzt werden können, um diese zu untersuchen. Weiterhin zeigen die Ergebnisse, dass BACE1 nur die Menge weniger Substrate an der Zelloberfläche reguliert und die Inhibition der Protease einen enormen Anstieg dieser Substrate zur Folge hatte. Die vorgestellten BACE1 Resultate und Entwicklungen der klinischen Studien machen klar, wie wichtig es ist, zusätzliche Arzneimittelziele zu untersuchen, um den Krankheitsverlauf sicher beeinflussen zu können.

MT5-MMP stellt ein solches alternatives therapeutisches Ziel dar, da ein genetischer Knockout der Protease sich vorteilhaft auf den pathologischen Zustand eines AD-Mausmodells auswirkte und zu kognitiver Verbesserung führte. Die vorliegende Arbeit zeigt mit optimierter Proteomanalyse von muriner Cerebrospinalflüssigkeit, dass die Protease deutliche Auswirkungen in einem AD-Hintergrund, aber nur begrenzte Funktionen unter physiologischen Bedingungen hat. Die Hemmung der MT5-MMP-Aktivität würde folglich in wesentlich weniger Nebenwirkungen resultieren und stellt daher eine vielversprechende neue Strategie für AD-Therapeutika dar.

1 Introduction

1.1 Alzheimer's disease

In 1907, Alois Alzheimer proclaimed a "peculiar disease of the cerebral cortex" and reported in detail the symptoms of his patient Auguste Deter. The 51-year-old woman showed "rapidly worsening memory weakness", "complete perplexity", and was "disoriented to time and place". Four and a half years later the patient died. After post mortem examination of the brain, he described atrophic tissue, gliosis, neurofibrillary tangles, and amyloid plaques (Alzheimer, 1907; Strassnig and Ganguli, 2005) – which still are the main characteristics of the disease.

1.1.1 Epidemiology

Nowadays, Alzheimer's disease (AD) is the most common type of neurodegenerative disorder accounting for 60 - 80% of dementia cases. More than 47 million people are affected worldwide (Alz.co.uk) and suffer loss of memory, cognitive functions, and physical abilities – eventually leading to death. Aging is the most relevant risk factor for AD and the fact of increased life expectancy in western countries predicts a dramatic rise of patient numbers in the future. In addition to patients, the severe disease progression has a deep impact on relatives and caregivers regarding social, psychological, physical, and economic elements of life (Querfurth and LaFerla, 2010). These wide-ranging consequences highlight AD as one of the most challenging diseases in the future. Currently available treatments can only temporarily slow the worsening of symptoms, but at this point there are no drugs that are able to prevent or delay the onset of AD, or much less to cure AD. Although no disease-modifying treatment is available, the molecular mechanisms are relatively well studied (Folch et al., 2016; Lang, 2010) and a variety of new drugs are under investigation (clinicaltrials.gov).

1.1.2 Pathology

The most significant characteristic of an Alzheimer's diseased brain is the pronounced regression of brain tissue/size. This atrophy equally affects both hemispheres in a symmetrical manner, predominantly in areas important for cognitive function and memory, i.e. cortical and hippocampal regions, and is the result of inflammation-induced neuronal cell loss (Mouton et al., 1998; Tabatabaei-Jafari et al., 2015). These areas show high occurrence of intracellular accumulation of neurofibrillary tangles (NFT) containing hyperphosphorylated tau and the formation of extracellular amyloid-β (Aβ) plaques, which are the two neuropathological hallmarks of the disease (Goedert et al., 1991; Selkoe, 2011) (Figure 1). The research of the last years further indicates the importance of additional changes in the AD brain being of inflammatory, immunological, and neurovascular nature (Ardura-Fabregat et al., 2017; Kisler et al., 2017). However, the common idea of AD pathogenesis suggests that accumulation of Aβ is a required, although perhaps not sufficient, process in triggering molecular events leading to neuroinflammation, neurodegeneration, cell death and finally to the clinical manifestation of AD. This explanation of the AD pathology is referred to as amyloid cascade hypothesis, which is guiding the development of potential treatments (Hardy, 2009; Selkoe and Hardy, 2016).

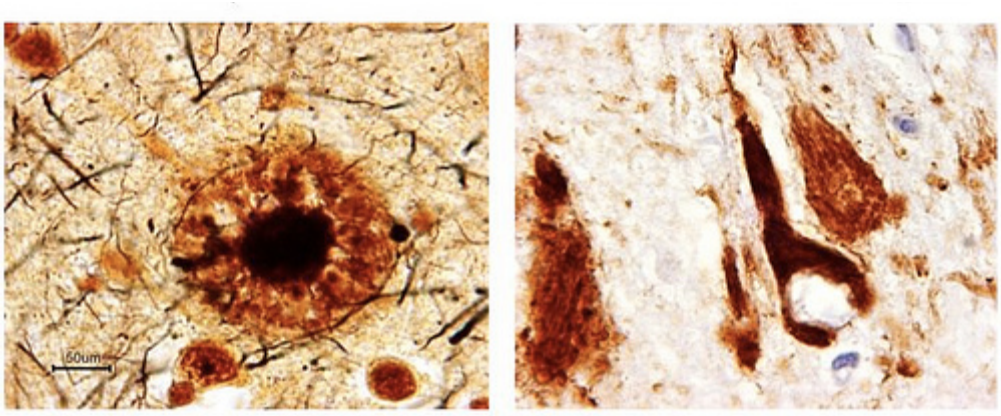

Figure 1: Neuropathological hallmarks of Alzheimer's disease. Left: Extracellular senile plaque composed of aggregated Aβ peptide with a dense core region and diffused halo. **Right:** Intracellular neurofibrillary tau-tangle developed from hyperphosphorylated and aggregated tau protein. (Pictures: www.alz101.blogspot.de)

1.1.3 Molecular pathogenesis and the amyloid cascade hypothesis

The 4 kDa Aβ peptide is the major constituent of amyloid plaques. In 1984/85 Glenner & Wong and Masters & Beyreuther isolated this peptide from postmortem AD brains and identified the amino acid sequence. They suggested the progressive buildup of amyloid plaques to be causative for the disease (Glenner and Wong, 1984; Masters et al., 1985). Shortly afterwards, the amyloid precursor protein (APP) was identified to be the source of Aβ, which is liberated through proteolytical processing (Kang et al., 1987), and led to the formation of the amyloid cascade hypothesis (Beyreuther and Masters, 1991; Hardy and Higgins, 1992; Selkoe, 1991): It postulates Aβ aggregation as driving force and crucial step in the beginning of disease pathology, initiating neurotoxicity and eventually resulting in neuronal death and dementia (Hardy and Selkoe, 2002).

Aβ is the product of consecutive proteolysis of APP, where first the beta-site APP cleaving enzyme 1 (BACE1) removes the protein ectodomain, and subsequent cleavage by the γ-secretase releases the Aβ peptide into the extracellular space (De Strooper et al., 2010). Regulated intramembrane proteolysis (RIP) of APP is a physiological process and common for many transmembrane proteins (Lichtenthaler et al., 2011). As proteolytic fragment of APP, Aβ (varying from 38–43 residues due to differential processing by gamma-secretase) is generated normally throughout life by almost all mammalian cells (Haass et al., 1992; Seubert et al., 1992; Shoji et al., 1992). However, increased or unbalanced production or decreased degradation of specific Aβ species over time leads to the formation of oligomeric Aβ and ultimately to aggregation forming extracellular plaques. Initially, the accumulation of toxic Aβ oligomers triggers synaptic alterations followed by spine reduction and loss. With disease progression, neuronal dystrophies and inflammatory processes lead to neuronal cell death and the loss of structural and functional connectivity inside the brain (Haass and Selkoe, 2007).

1.1.4 Tau pathology in AD

Although neurofibrillary tangles (NFTs) are the other main histopathological hallmark of AD, they were not considered in the initial form of the amyloid cascade hypothesis. However, after studies showed that Aβ oligomers could promote tau hyperphosphorylation (Jin et al., 2011; Ryan et al., 2009) the hypothesis was revised and adjusted (Hardy and Selkoe, 2002). Since then, research demonstrated that Aβ accumulation proceeds and leads to progressive tau deposition, but the reciprocal effect could not be observed (Selkoe and Hardy, 2016).

The major component of neurofibrillary tangles is the microtubule-associated protein tau, a 68 kDa protein. It is involved in formation and reorganization of microtubules in healthy neurons (Gallyas, 1971). Tau-phosphorylation is a physiological process and occurs at sites, where tau is interacting with microtubules. In pathological conditions it can be hyperphosphorylated and misfolded (Grundke-Iqbal et al., 1986a; Grundke-Iqbal et al., 1986b; Iqbal et al., 1986). Increased stage of phosphorylation causes the protein to form fibrils and tangles (Alonso et al., 2001) and tau accumulation was shown to affect neuronal metabolism and function: it impairs synaptic function and mitochondrial dynamics, induces endoplasmatic reticulum (ER) stress and activates microglia resulting in inflammation (Yang and Wang, 2018). Interesting observations show an anti-apoptotic purpose of tau hyperphosphorylation (Li et al., 2007; Wang and Liu, 2008) and suggest tau to play a dual role in AD neurodegeneration: while transient tau phosphorylation prevents acute apoptosis, persistent tau hyperphosphorylation and accumulation induces chronic neurodegenerative mechanisms as described above (Yang and Wang, 2018).

1.1.5 Drug development and therapeutic approaches

Several therapeutic approaches have been developed and tested in the past to find effective strategies for the treatment of Alzheimer's disease. Currently approved and available drugs for treatment only target and help to ease the symptoms of the disease: cholinesterase inhibitors such as Donepezil and the NMDA receptor antagonist Memantine help preventing cognitive decline (Howard et al., 2012). Many drugs have failed in clinical trials or were terminated, because they did not meet the set disease modifying goals or because of adverse effects upon drug treatment.

Until today, anti-Aβ approaches are dominating the area of AD drug development and therapeutics. Strategies include approaches to 1) reduce Aβ production, using beta-site amyloid cleaving enzyme 1 (BACE1) inhibitors, and γ-secretase inhibitors and modulators, and 2) prevent Aβ aggregation and improve Aβ clearance with monoclonal antibodies in passive immunization and vaccines in active immunization.

The major problems with γ-secretase inhibitors were their unforeseen, severe side effects, due to chronic inhibition of Notch signaling. Thus, the inhibitor Semagacestat failed in clinical Phase III, but also modulators such as Tarenfluribil did not have the expected positive outcomes (De Strooper, 2014; Doody et al., 2013; Green et al., 2009).

Since Aβ oligomers are considered to be the neurotoxic species in AD pathology, drugs like Tramiprosate were developed to prevent Aβ aggregation, but unfortunately failed to demonstrate major clinical improvements in Phase III clinical trials (Aisen et al., 2011). On the contrary, promoting Aβ clearance with immunization against the Aβ peptide itself seemed very promising at that time. Active immunization stimulates self-production of antibodies against Aβ, whereas passive immunization is based on *in vitro* generated Aβ antibodies. Immunization stimulates the patient's immune system and enhances Aβ clearance via microglia-mediated phagocytosis of the Aβ antibody/plaque-complex. Unfortunately, active immunization for immunotherapy resulted in brain inflammation. A number of anti-Aβ humanized monoclonal antibodies have been tested, but terminated on the basis of two Phase III clinical studies: The monoclonal antibodies Bapineuzamab and Solanazumab did not improve cognition and memory of AD patients. However, the less aggressive passive immunization is still a promising therapeutic approach and the antibody Gantenerumab is currently being tested in two Phase III clinical trials with prodromal AD (Doody et al., 2014; Salloway et al., 2014; Vandenberghe et al., 2016).

In the last years, increasing pharmacological alternative strategies are focusing on the inhibition of tau-phosphorylation in order to prevent tau aggregation or promote disassembly. This strategy is mainly targeting the kinase GSK-3β, which is responsible for tau phosphorylation. So far, drugs targeting GSK-3β have shown no or adverse effects (Lonergan

and Luxenberg, 2009), but research in this field is ongoing and improving (Liang and Li, 2018).
Currently, inhibition of BACE1 is still a promising strategy to lower Aβ generation, since developed inhibitors have the required specificity and are small molecules that can cross the blood-brain-barrier. At the same time, they are still able to block the large active site of BACE1 (Vassar, 2014). Different pharma companies have developed BACE inhibitors which are being tested in clinical trials, for primary and secondary prevention strategies. Primary strategies are aiming to prevent the onset of the disease, whereas secondary strategies are applied, when the disease already manifested. Although recently the BACE inhibitor Verubecestat was terminated in two Phase III trials with mild-to-moderate AD (Egan et al., 2018), there are still several other BACE1 inhibitors being tested, which are applied e.g. at an much earlier disease stage (clinicaltrials.gov). Another BACE inhibitor, Atabecestat, was just now prematurely stopped in two studies in Phase II/III and Phase III, because of observed liver toxicity. The Phase II/III trial tested early intervention in a late-onset preclinical stage Alzheimer's disease. It is still unclear, if the toxicity was caused by BACE inhibition or an off-target effect (Janssen, 2018). BACE inhibitors will therefore need to demonstrate their clinical efficacy in Phase III trials, in the next years. Raised concerns due to the complex BACE knockout mouse phenotypes and the various physiological functions of the protease, have now unfortunately been justified with the failed Verubecestat trial, which showed side effects such as skin rashes, sleep disturbance, suicidal ideation, weight loss, and hair color change (Egan et al., 2018). Particularly now, BACE inhibitor clinical trials and research on BACE has to continue to describe underlying early molecular events in AD onset and progression in order to complete the picture and allow safe drug development.

1.2 Ectodomain shedding and regulated intramembrane proteolysis

Proteolysis of transmembrane proteins and the release of their ectodomains into the extracellular space is often called *shedding*. Shedding of ectodomains is vital for various physiological cellular processes including differentiation, axon guidance, neurite outgrowth, cell adhesion, signaling, cell-cell communication, and many more. This mechanism is evolutionarily conserved from bacteria to humans. Shedding of a protein's ectodomain can be followed by an additional proteolysis step, mediated by intramembrane proteases: The combination of these processes is referred to as *regulated intramembrane proteolysis* (RIP) (Brown et al., 2000; Lichtenthaler et al., 2011) (Figure 2). RIP generally controls the amount of transmembrane proteins at the cell surface and is frequently comprised by two sequential proteolytic events: The first is mediated by membrane-bound proteases, which cleave their transmembrane substrates and liberate their soluble ectodomains into the extracellular milieu. Shedding of large ectodomains is the requirement for the second proteolytic event, carried out by intramembrane proteases to release membrane-bound fragments. Thus, in controversy to the name, shedding is the regulating step during the proteolytic sequence of RIP (Reiss and Saftig, 2009). The release of proteolytic fragments by RIP into the extracellular space and the cytosol can 1) be necessary to trigger the function of a transmembrane protein, acting through its cleaved forms e.g. in the case of cytokines or 2) terminate the function of proteins by releasing them from the membrane e.g. release of cell surface receptors to inhibit ligand binding (Lal and Caplan, 2011; Lichtenthaler et al., 2011).
Proteases responsible for the ectodomain shedding are called *sheddases* which mostly belong to the families of the a-disintegrin-and-metalloprotease (ADAM), the beta-site amyloid precursor protein cleaving enzymes (BACE), and membrane-type matrix metalloproteases (MT-MMP) (Blobel, 2005; Hayashida et al., 2010; Itoh, 2015; Vassar et al., 2014). The majority of transmembrane proteins that are targets of sheddases and RIP are single-pass

transmembrane proteins with type I orientation (N-terminus exposed to the extracellular/luminal compartment) or type II orientation (N-terminus exposed towards the cytosol) (Lal and Caplan, 2011; Muller et al., 2016). Moreover, glycophosphatidylinositol (GPI)-anchored proteins and proteins with several transmembrane domains have been described as RIP substrates (Altmeppen et al., 2011; Dislich et al., 2015; Fleck et al., 2012; Hemming et al., 2009).
Intramembrane proteases mediate the second proteolytic step of RIP, during which a short protein fragment is released into the extracellular space and the intracellular domain is liberated into the cytosol. Four protease families are able to cleave proteins within their transmembrane in the hydrophobic environment of the lipid bilayer (Ha, 2009). Usually, γ-secretase and rhomboid proteases cleave type I transmembrane proteins, whereas type II transmembrane proteins are processed by signal-peptide peptidase (like) and site-2 protease (Voss et al., 2013).

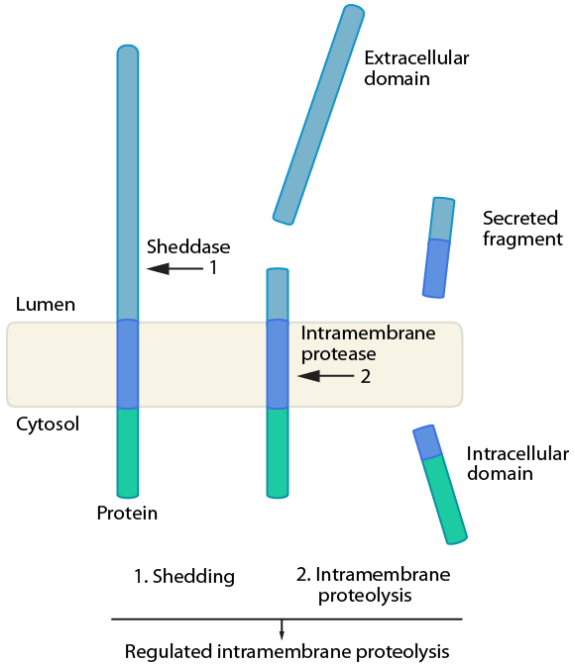

Figure 2: Regulated intramembrane proteolysis.
Regulated intramembrane proteolysis (RIP) is a two-step proteolytic process: The first step is known as shedding, during which the ectodomain of a transmembrane protein is cleaved off by a membrane-bound protease also termed shaddase. In the following step, an intramembrane protease cleaves the remaining membrane-bound fragment within its transmembrane domain and releases a secreted fragment into the extracellular space and the intracellular domain into the cytoplasm.

1.2.1 RIP mechanisms regulate cell communication, signaling, and pathways

RIP is a mechanism to control the availability of soluble ligands during cell-cell communication, but also regulate the amount of cell surface ligands and receptors.
A well-studied example of such a mechanism is the type II transmembrane protein tumor necrosis factor-α (TNFα) – a RIP substrate, whose extracellular domain acts as a signaling molecule. TNFα is a highly active cytokine and controls cell growth, cell differentiation, and cell death. In order to trigger an immune response, ADAM17 cleaves off the TNFα ectodomain and releases the pro-inflammatory cytokine from the cell surface (Black et al., 1997; Saftig and Reiss, 2011). In addition, intramembrane proteolysis of the remaining membrane-bound TNFα fragment by SPPL2a or SPPL2b releases the TNFα intracellular domain (ICD) into the cytosol, which drives the expression of the pro-inflammatory cytokine interleukin-12 (IL-12)

(Friedmann et al., 2006). Comparable to TNFα, some growth factors, such as EGF-like growth factors and neuregulins, are inactive in their membrane-bound form and need to be activated by proteolytic shedding (Blobel, 2005).
RIP does not only control soluble ligands, but also modulates the activity of signaling receptors: On one hand, ectodomain shedding activates the cytokine TNFα and on the other hand, shedding of the TNF receptor proteolytically releases it from the membrane and terminates its signaling (D'Alessio et al., 2012; Deng et al., 2015). Another receptor that is tightly regulated through RIP is Notch, a cell surface receptor controlling cell-fate decisions. If Notch binds its ligand on the adjacent cell, the receptor undergoes a conformational change, which allows proteolytic shedding by ADAM10 (Hartmann et al., 2002). The remaining membrane fragment of Notch is then cleaved by γ-secretase, which releases the intracellular domain that translocates to the nucleus and acts as transcription factor (Arumugam et al., 2011). Additionally, RIP can regulate adhesive functions by ectodomain cleavage of cell adhesion molecules (Solanas et al., 2011).
Taken together, RIP is a mechanism to either activate or terminate protein function while proper activity of involved proteases is essential for regulating various cellular processes. A deregulation of the RIP mechanism is therefore associated with numerous diseases, such as cancer and Alzheimer's disease (AD) (Lichtenthaler et al., 2011; Saftig and Reiss, 2011).

1.2.2 The amyloid precursor protein (APP) and its processing

The amyloid precursor protein was first cloned in 1987 (Goldgaber et al., 1987; Kang et al., 1987; Tanzi et al., 1987). It is present ubiquitously in the body, but due to alternative splicing its expression varies in isoforms from 695, 751, and 770 amino acids between the brain and periphery (Sandbrink et al., 1994). Neuronal cells predominantly contain APP-695, whereas the other two variants are the dominant species in peripheral cells (Li et al., 1999). The APP-gene family contains other two members – the APP-like proteins 1 and 2 (APLP1 and APLP2). Although all three proteins share functional and structural similarity only APP gives rise to Aβ peptides (Shariati and De Strooper, 2013).
APP is a type 1 transmembrane protein with a large N-terminal part located in the lumen/ extracellular space and a short cytoplasmic part. During its transport to the cell membrane through the secretory pathway, it undergoes sequential cleavages by α-, β-, and γ-secretases (Figure 3A) (Lichtenthaler et al., 2011). Cleavage by α- or β-secretase liberates nearly the whole ectodomain and results in the soluble fragments sAPP-α and sAPP-β and the membrane-bound carboxyl-terminal fragments α-CTF and β-CTF, which can be further processed by γ-protease. The γ-cleavage sites are within the APP transmembrane region and release the peptides P3 (from α-CTF), Aβ (from β-CTF) and in both cases a short intracellular domain (AICD) on the cytoplasmic side. Processing by β-secretase gives rise to aggregation-prone Aβ peptide species, which accumulate to oligomers and eventually form plaques. This event was therefore described as amyloidogenic pathway. Cleavage by α-secretase occurs within the Aβ region and hence prevents the formation of the aggregating peptide (Lichtenthaler et al., 2011).
BACE1 is the major β-secretase in the brain and responsible for the amyloidogenic processing of APP (Hussain et al., 1999; Lin et al., 2000; Sinha et al., 1999; Vassar, 1999; Yan et al., 1999). As described in this section in detail, APP cleavage by BACE1 releases the soluble ectodomain sAPPβ into the extracellular space and generates the N-terminus of the Aβ peptide. Thus, β-secretase cleavage mediates the initial and rate-limiting step in Aβ-production. The non-amyloidogenic pathway is predominantly mediated by the α-secretase ADAM10 (Kuhn et al., 2010), which cleaves inside the Aβ peptide and leaves a slightly shorter (α-)CTF inside the membrane. The membrane bound α-CTF (or C83) and β-CTF (or C99) are further processed by the γ-secretase, which in case of β-CTF, liberates the Aβ peptide from the membrane into the extracellular space and at the same time releases the

AICD into the cytoplasm. γ-secretase is a complex with four subunits: presenilin 1 or 2, nicastrin, APH-1, and PEN-2 (Edbauer et al., 2002; Edbauer et al., 2003). Intramembrane cleavage by γ-secretase generates multiple Aβ species of different length (Fukumori et al., 2010; Portelius et al., 2011; Steiner et al., 2008) with Aβ40 being the predominant one. The highly aggregating Aβ42 consists of only 10% of the total amount (Selkoe, 2004).

Additional studies report the physiological proteolysis of APP by additional proteases; the protease meprin β was demonstrated to cleave APP at the BACE1-site (or in close proximity) and thereby contributes to Aβ generation. Additionally, meprin β is able to cleave APP in its ectodomain distal from the Aβ region (Bien et al., 2012; Jefferson et al., 2011). Asparagine endopeptidase (AEP) was described as APP δ-secretase and cleaves the protein N-terminally of the Aβ peptide sequence (Zhang et al., 2015b). Selected members of the membrane-type matrix metalloproteases (MT-MMPs) are also involved in alternative APP processing and are so-called η-secretases (Figure 3B) (Ahmad et al., 2006; Willem et al., 2015). η-secretase cleaves APP in the ectodomain, but further away from the transmembrane region. It thereby generates a shorter soluble fragment – sAPP-η – that is released into the extracellular space. The remaining membrane-bound η-CTF can then be further processed by α- or β-secretase as described above. However, since the APP ectodomain has already been partly cleaved off, subsequent processing by α- or β-, and γ-secretase results in the release of short fragments, termed Aη-α and Aη-β instead of the earlier mentioned sAPP-α and sAPP-β (Figure 3B). η-secretase cleavage is partly mediated by the protease MT5-MMP (Ahmad et al., 2006; Baranger et al., 2016b; Willem et al., 2015).

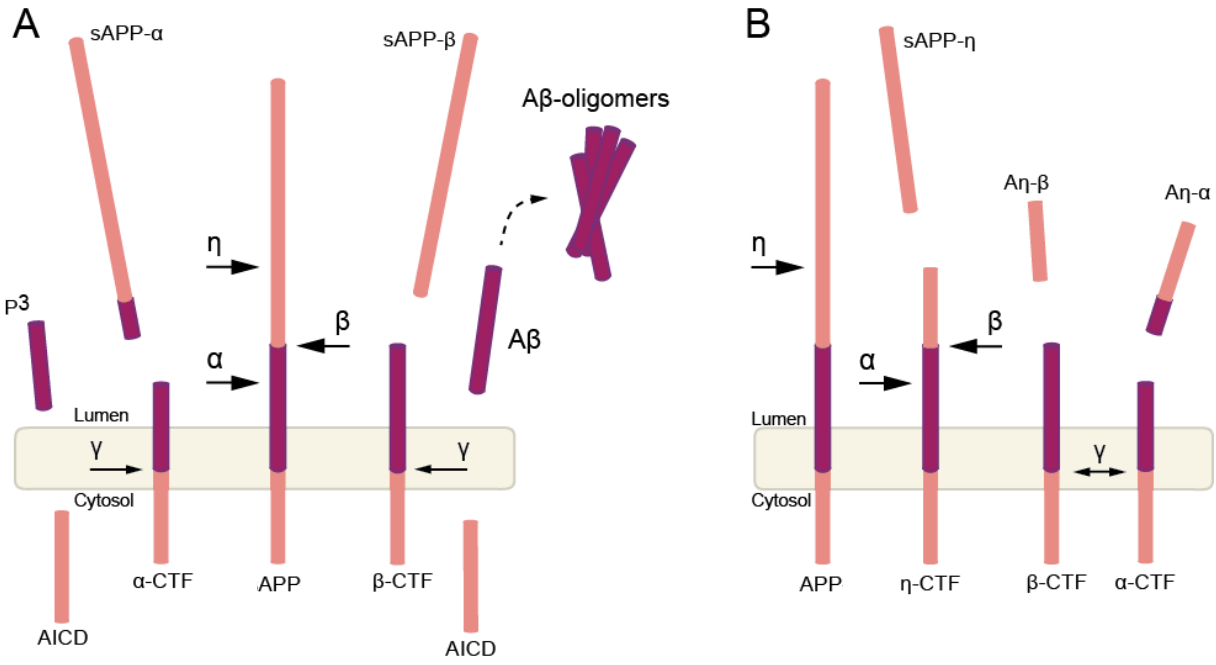

Figure 3: Proteolytic processing of the amyloid precursor protein. A) Two competing RIP pathways proteolytically cleave the transmembrane amyloid precursor protein (APP). Concomitant cleavage by β-secretase and γ-secretase generates the aggregating Aβ peptide species and is referred to as the amyloidogenic pathway. β-cleavage results in shedding of the ectodomain (sAPP-β) and a membrane-bound C-terminal fragment (β-CTF/C99), which is the processed by γ-secretase to Aβ and a APP intracellular domain (AICD). Alternatively, APP is first processed in a non-amyloidogenic pathway and cleaved by α-secretase resulting in the soluble APP ectodomain sAPP-α and a C-terminal fragment (α-CTF/C83). γ-cleavage of α-CTF then secretes the p3 peptide into the extracellular space and the AICD into the cytosol. **B)** η-secretase cleaves APP more distant from the membrane and releases a shorter ectodomain fragment (sAPP-η). The longer CTF fragment inside the membrane (η-CTF) can be further processed by α- or β-secretase, releasing additional small soluble fragments Aη-α and Aη-β, leaving the CTFs ready for γ-secretase cleavage as shown in panel **A**.

1.2.3 Alpha-secretase: ADAM10

The zinc-dependent a-disintegrin-and-metalloprotease 10 (ADAM10) is a type 1 membrane protein and belongs to a large family of membrane-bound proteases. Its ubiquitous expression, evolutionarily conserved state, and the embryonic lethality of ADAM10 knockout mice underline the protease's essential role in development and differentiation, cell-to-cell communication, and signaling (Bercher and Blobel, 2003; Schlondorff and Blobel, 1999; Weber and Saftig, 2012). ADAM10 has extensively studied and well-described functions in the periphery, e.g. the immune system, but its involvement in the central nervous system is still poorly understood (Reiss and Saftig, 2009; Saftig and Lichtenthaler, 2015).

ADAM10 was identified as physiologically relevant α-secretase in the brain, where it constitutively cleaves APP and generates the soluble sAPP-α fragment (Colombo et al., 2013; Jorissen et al., 2010; Kuhn et al., 2010; Lammich et al., 1999; Prox et al., 2013). Mildly elevated ADAM10 protein levels have been shown to increase APP α-cleavage and benefit AD pathology in mice without significant effects on Notch signaling, another substrate (Postina et al., 2004; Prinzen et al., 2009), which was the starting point to investigate ADAM10 as therapeutic target in AD. In favor, several studies demonstrated that lowered or inactive ADAM10 shifts APP processing towards β-cleavage and thus increased Aβ levels and AD pathology in vivo (Postina et al., 2004; Schmitt et al., 2006). Similar effects were shown in human individuals with a family history of late-onset AD, which were heterozygous carriers of two mutations rendering ADAM10 inactive (Kim et al., 2009; Suh et al., 2013). ADAM10's therapeutic potential has been confirmed by a clinical trial, where a small cohort of 21 patients with mild to moderate AD was treated with Acitretin – an approved drug against psoriasis – and presented elevated sAPPα levels in cerebrospinal fluid (CSF) after 4 weeks (Endres et al., 2014). Mechanistically, Acitretin increases ADAM10 expression and stimulates APP α-cleavage *in vitro* and *in vivo* (Tippmann et al., 2009). However, treatment over the short period of 4 weeks did not alter CSF Aβ levels in patients (Endres et al., 2014).

Despite the promising potential of ADAM10 as AD drug-target, its physiological functions in the brain are not yet well understood. Due to above-mentioned lethality of knockout mice, knowledge about the ADAM10 substrate repertoire is limited, which are aggravating circumstances for drug-development. Nevertheless, in the last 10-15 years studies *in vitro* and with conditional ADAM10-deficient mice succeeded in the validation of a number of additional protease substrates in the nervous system. Together with the description of new substrates such as APLP2, CDH2 (N-cadherin), NCAM, EFNA2 and 5, L1CAM, MEP1B, and NLGN1, new ADAM10 functions were discovered - as reviewed previously (Saftig and Lichtenthaler, 2015). Recently, a systematic approach using proteomic analysis in our laboratory identified 91 mostly novel substrate candidates in ADAM10-deficient neurons, underlining a major role for ADAM10 in the brain (Kuhn et al., 2016). Consequently, it becomes more and more important to first fully understand the properties and involvement of ADAM10 substrates and functions in the brain, to allow successful and safe drug development and therapeutics.

1.2.4 Beta-secretase: BACE1

In 1999, the transmembrane aspartyl protease BACE1 (β-site APP cleaving enzyme 1) was discovered to be responsible for the release of sAPPβ (Vassar et al., 1999). The enzyme BACE1 has a closely related homolog BACE2. The two proteases show distinct cleavage specificity, but are also known to share substrates, such as APP, JAG1, and the SEZ6 family proteins (Farzan et al., 2000; He et al., 2014; Pigoni et al., 2016). However, they display different cell and tissue expression pattern with BACE1 being the predominant form in brain, which is specifically expressed in neurons and oligodendrocytes (Sharma et al., 2015).

BACE2 was shown to be expressed at a low level in all major brain cell types, but expression levels vary significantly within cell types and brain regions (Dominguez et al., 2005; Voytyuk et al., 2018b). Though APP is also cleaved by BACE2, cleavage occurs within the Aβ domain and does not produce the Aβ peptide (Bennett et al., 2000; Voytyuk et al., 2018b; Yan, 2017). BACE1 has an acidic pH optimum and is mainly localized to endosomes and the trans-Golgi network, where also the majority of Aβ is generated (Hook et al., 2002; Vassar, 1999). Although a measurable amount is located at the cell surface, BACE1 is rapidly internalized and cycles between the plasma membrane and endosomal compartment (Huse et al., 2000).
Since its discovery, a major focus has been the search for specific BACE1 activity inhibitors for Alzheimer's disease (AD) therapy. Several potent BACE1 inhibitors have been successfully developed and are tested in clinical trials (Vassar, 2014; Yan, 2016). In preclinical studies, many inhibitors have been shown to effectively reduce Aβ levels in CSF or brains of different animal models (Fukumoto et al., 2010; Sankaranarayanan et al., 2009). However, some clinical studies with BACE inhibitors in humans have already been terminated, because they did not succeed to lower Aβ levels, did not improve cognition and memory in the tested cohorts, or showed non-mechanism based side effects (Egan et al., 2018; May et al., 2011). Notably, all current BACE1 inhibitors in clinical trials do also inhibit the close homolog BACE2 (Bennett et al., 2000; Farzan et al., 2000). Although, BACE2 is predominantly expressed in peripheral tissue, such as pancreas, kidney, and colon, only little is known about its functions in the brain and potential cross-inhibition could severely interfere with clinical studies targeting BACE1 inhibition (Bennett et al., 2000; Voytyuk et al., 2018a; Voytyuk et al., 2018b). Also, the relevance of BACE inhibitors needs still to be tested in prevention paradigms.
Nevertheless, the extensive research on BACE1 in the last 20 years and the encountered adverse effects upon BACE1 inhibition help to elucidate the complex role of the protease. Studies on BACE1 knockout mice pointed towards diverse biological functions in the brain apart of APP-β-secretion. BACE1 was found to regulate neurogenesis via cleavage of Jag1 and Notch signaling in the early developing hippocampus (He et al., 2014; Hu et al., 2013). Further, it plays a role in myelination during development and re-myelination in adult stages through cleavage of type III NRG1 (Fleck et al., 2013; Hu et al., 2016). The identification of CHL1 as BACE1 substrate revealed a molecular basis of BACE1-dependent axon guidance (Zhou et al., 2012). Other phenotypes observed in BACE1 knockout mice demonstrate an involvement in muscle spindle formation, enhanced sensitivity to insulin, hyperactivity, postnatal lethality and growth retardation, retinal abnormalities, seizures, memory loss and synaptic spine density abnormalities. Despite the described consequences of BACE1 deficiency the mechanisms behind them and involved BACE1 substrates are largely unknown (Vassar et al., 2014; Yan, 2017).
Using unbiased proteomic approaches with BACE1 overexpression or inhibition more than 40 putative substrate candidates were identified using cell based studies (Hemming et al., 2009; Kuhn et al., 2012; Stutzer et al., 2013) or CSF of BACE1 knockout mice (Dislich et al., 2015). Some of the identified candidates could already be validated, such as CHL1, L1CAM, SEZ6, and CNTN2 (Dislich et al., 2015; Pigoni et al., 2016; Zhou et al., 2012).
Further investigation of BACE1 and its substrate candidates will contribute to resolve its full pathophysiological relevance and provide essential knowledge to predict and prevent possible side effects of BACE1 inhibition-based therapeutic approaches. As several BACE1 inhibitors are currently being tested in clinical trials, a better understanding will not only improve treatment, but also aid biomarker discovery and companion diagnostics.

1.2.5 Eta-secretase: MT5-MMP

MT5-MMP belongs to a large family of Zn^{2+} dependent matrix metalloproteases (MMPs). It forms together with 5 other members the subgroup of membrane-type matrix metalloproteases

(MT-MMPs), which are bound to the cell membrane by either expressing a transmembrane domain (as in the case of MT5-MMP) or a glycosylphosphatidylinositol (GPI)-anchor (Itoh, 2015; Pei, 1999). In contrast to the other MT-MMPs, which exhibit a broad tissue expression pattern, MT5-MMP is predominantly expressed in neuronal cells of the peripheral and central nervous system, although it has been detected to a lesser extent in inflammatory cells as well (Bar-Or et al., 2003; Hayashita-Kinoh et al., 2001; Jaworski, 2000; Llano, 1999; Pei, 1999; Warren et al., 2012). As a MMP, also MT5-MMP was shown to be involved in remodeling of the extracellular matrix (ECM) by degradation of proteoglycans and other ECM components, which promotes neurite outgrowth (Hayashita-Kinoh et al., 2001; Wang et al., 1999).
The first study to link MT5-MMP to Alzheimer's disease (AD) found the protease to be localized in dystrophic neurites around Aβ-plaques in post-mortem brains of AD patients (Sekine-Aizawa et al., 2001). Soon after, a functional connection between APP and MT5-MMP was discovered by the observation that MT5-MMP (as well as MT1- and MT3-MMP) can process APP into different truncated APP fragments (Ahmad et al., 2006). Recently, MT5-MMP was demonstrated to cleave APP upstream of the BACE1 cleavage site and mediate the generation of alternative APP soluble and membrane-bound fragments (Willem et al., 2015). This study described MT5-MMP to be the APP η-secretase – however, it did not fully differentiate MT5-MMP from its membrane-bound family members. Further, it demonstrated that a sequential cleavage by the α-secretase ADAM10 results in a short neurotoxic fragment, termed Aη-α, which inhibits long-term potentiation (LTP) *ex vivo* and decreases hippocampal neuronal activity *in vivo* (Willem et al., 2015). In parallel, MT5-MMP deficiency was shown to be beneficial for AD pathology in a mouse model, where it decreased Aβ load and attenuated neurotoxicity through decreased glial reactivity and interleukin-1β (IL-1β) levels, Moreover, LTP and cognitive dysfunctions were prevented, when the protease was not present in AD mice. At the same time the direct interaction of MT5-MMP and APPswe (APP harboring the familial Swedish mutation (Mullan et al., 1992)) was demonstrated to increase the levels of Aβ and the precursor β-CTF/C99 *in vitro* (Baranger et al., 2016b). In another study the same group found evidence *in vitro* and suggested the MT5-MMP to promote trafficking of APP to early endosomes, where amyloidogenic processing occurs (Baranger et al., 2017).
Taken together, these recent findings implicate MT5-MMP as a potential target in drug development for AD. This possibility is supported by the fact that MT5-MMP knockout in mice does not lead to histological defects or developmental deficits in the nervous system (Komori et al., 2004). In contrast, it was reported that under pathological conditions the protease plays a role in neuronal plasticity after sciatic nerve injury (Komori et al., 2004) and is important in the peripheral nervous system for inflammatory response to interleukin-1 beta (IL-1β) and tumor necrosis factor-alpha (TNF-α) (Folgueras et al., 2009). Noteworthy, the pathophysiological mechanisms of action are largely unknown. Apart from a few substrates, such as the before-mentioned proteoglycans, only KISS1 and N-Cadherin have been shown to be functionally processed by MT5-MMP (Itoh, 2015; Porlan et al., 2014; Takino et al., 2003).
It is therefore crucial to elucidate the full involvement of MT5-MMP in normal and pathophysiological processes in the brain, in order to evaluate the full potential of modulating MT5-MMP activity as therapeutic approach. Importantly, targeting MT5-MMP in pathology may have no side effects due to little impact on physiology, which emphasizes the therapeutic value.

1.3 Quantitative proteomics

Quantitative proteomics in research is mainly used for relative quantification of proteomes. A proteome is defined as *protein complement of a cell, tissue, or organism under a specific,*

defined set of conditions (Yu et al., 2010). It is dynamic and differs from cell to cell, changes over time, and may be modulated in response to cell stimuli. Mass spectrometry (MS)-based proteomics, techniques such as Tandem-MS (MS/MS) are commonly used to analyze body fluids and tissues in discovery experiments with the aim to find biomarkers - specific protein markers that are able to distinguish between physiological and pathophysiological states and at the same time provide new strategies for diagnostics (Geyer et al., 2017; Mirzaei and Carrasco, 2016). Moreover, in combination with proteomic analysis of cell line-based experiments, this technology can be utilized to investigate disease mechanisms and drug functions, developing new pharmaceutical treatments. Finally, a major advantage of a system-wide proteomic approach is the possibility to follow changes of the proteome resulting from e.g. knockout or inhibition of a specific gene or protein and, in the long turn, predict and monitor potential side effects of newly discovered drugs in an unbiased manner (Cox and Mann, 2011; Geyer et al., 2017; Mirzaei and Carrasco, 2016). Though, MS-based proteomics has a lot of optimization ahead, it also rapidly developed over the past and is constantly improving. Complemental ongoing progress on quantitative methods is contributing to make MS-based proteomics and whole-proteome quantitation faster and more accessible, raising proteomics to the same powerful level as large-scale genomics (Bensimon et al., 2012; Cox and Mann, 2007; Sabido et al., 2012)

1.3.1 Bottom-up proteomics and LC-MS/MS

The majority of established proteomic workflows are based on bottom-up proteomics. In *bottom-up* proteomics proteins are proteolytically digested into peptides, which are analyzed by LC-MS/MS to identify and characterize parent proteins in a mixture. Here, discovery proteomics was used, which is an unbiased technique aiming for the analysis of a complete proteome (Aebersold and Mann, 2016; Bantscheff et al., 2007; Washburn et al., 2001).

For a typical experiment using bottom-up proteomics a protein sample, obtained from e.g. a homogenized tissue or lysed cell culture is digested with one or more sequence specific enzymes, such as trypsin, and analyzed by LC-MS/MS. Trypsin is commonly used, since it generates peptides with a lysine or an arginine residue at the peptide C-termini which are protonated besides the amino group at the N-termini at acidic pH. Therefore, tryptic peptides can be well ionized in LC-MS/MS analysis. The average length of 9 amino acids of tryptic peptides is also well suited for fragmentation and subsequent peptide identification (Swaney et al., 2010).

In order to increase the number of peptide and protein identifications and quantifications, proteins can be fractionated prior to proteolytic digestion using chromatographic separation or SDS-PAGE. Alternatively, also proteolytic peptides can be fractionated to increase the proteome coverage employing anion or cation exchange chromatography, or reversed phase chromatography at basic pH.

In the next step, proteolytic peptides are subjected to LC-MS/MS analysis. Commonly, peptides are separated by C18 reverse-phase chromatography using nano-flow high-performance liquid chromatography (HPLC) using water and acetonitrile supplemented with 0.1% formic acid as mobile phases. Increasing percentages of the organic solvent elute peptides according to their hydrophobicity.

The LC is online coupled to a mass spectrometer which consists of three parts: An ion source, which ionizes the molecules in the sample, followed by a mass analyzer, where ions are separated, and finally a detector that records the information. Acquired data from the detector is then processed by a computer to generate spectra (Figure 4). For LC-MS/MS in bottom-up proteomics, ElectroSpray Ionization (ESI) is used to generate a continuous stream of positively charged peptide ions which usually contain two or more protons (Fenn et al., 1989). The charge state of an ion or molecule is referred to as *z*. The charge is necessary to allow ion separation in the electrical field of the mass analyzer. Ions are separated according to their m/z ratios in the mass analyzer and are detected afterwards using a detector.

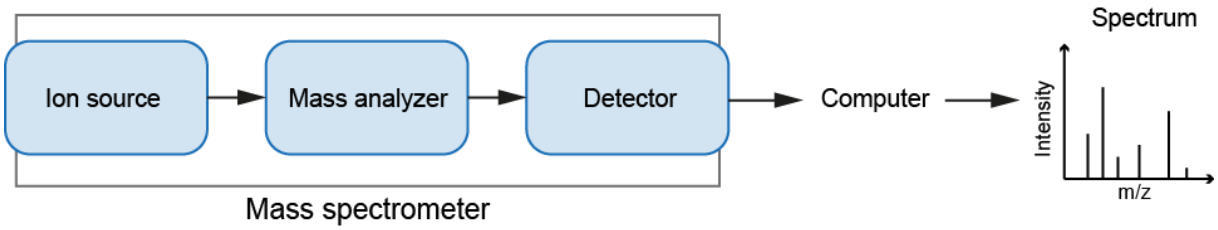

Figure 4: Schematic representation of a mass spectrometer.
A mass spectrometer consists of three parts: 1) An ion source, which ionizes molecules in the sample, followed by 2) a mass analyzer, where ionized molecules are separated according to their mass to charge ratio (m/z) and 3) a detector, which acquires the data. Recorded information is then processed by a computer and visualized as mass spectra.

In this work, three different mass spectrometers were used: an Orbitrap Velos Pro, a Q-Exactive, and a Q-Exactive HF. All of these hybrid mass spectrometers exhibit an orbitrap mass analyzer. The two Q-Exactive instruments own a quadrupole for ion isolation, a Higher-energy Collisional Dissociation (HCD) cell for ion fragmentation, and an orbitrap mass analyzer. The Orbitrap Velos Pro features an ion trap for ion isolation, fragmentation, and detection, as well as a HCD cell and an orbitrap.
The orbitrap works as a mass analyzer as well as a detector. It consists of a spindle-shaped inner electrode, which is negatively charged, confined by an outer barrel-shaped outer electrode. Positively charged peptide ions, which are injected into the orbitrap, are electrostatically trapped and move in a stable trajectory around the central electrode. They rotate in an orbit around the inner electrode and also oscillate along the spindle as z-axis. This harmonic axial oscillation is solely defined by an ion's mass to charge ratio *m/z* and therefore allows high mass accuracy and high-resolution recordings by the orbitrap mass analyser. The oscillations of an ion induce an image current that is detected at the outer electrode operating as mass detector (Figure 5): The frequency of an ion oscillation along the z-axis depends on its m/z ratio and the instrumental constant k: $\omega = \sqrt{\frac{z}{m} \times k}$. When multiple ions are present in the orbitrap, the signals of individual ions will produce cumulative signal. Therefore, Fast Fourier Transformation (FFT) is applied after signal amplification to obtain the frequencies of the individual ion oscillations and to compute its *m/z* ratios and intensities which are finally visualized in a mass spectrum (Hu et al., 2005; Makarov, 2000; Perry et al., 2008).

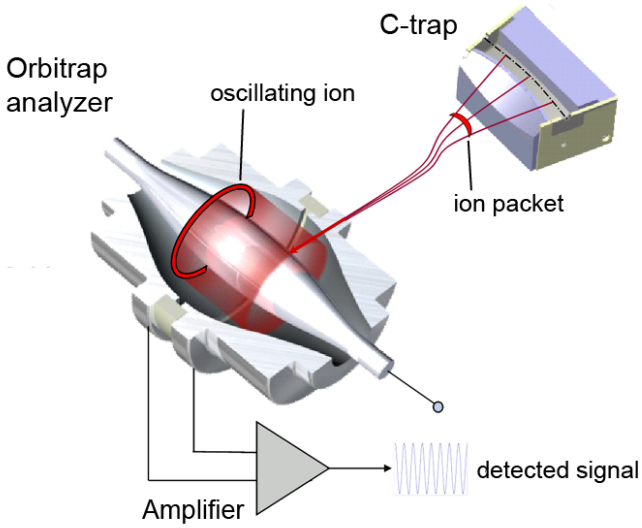

Figure 5: The orbitrap mass analyzer.
Ions are trapped in the C-trap (a bent quadrupole) and condensed into a small ion packet with a certain m/z. The ion packet is injected into the orbitrap through a narrow slit and starts oscillating around the inner spindle-shaped electrode. Axial oscillations induce a current detected by the differential amplifier and converted using Fourier transformation. Picture was taken from Zubarev & Makarov and modified (Zubarev and Makarov, 2013).

In bottom-up discovery experiments, the mass spectrometer records all peptide ions that co-elute at a certain retention time and acquires their mass spectra in a first full scan (MS^1 or MS). This full scan determines the m/z ratios of all co-eluting peptide ions (or precursor ions). However, the peptide masses alone are not sufficient to identify a peptide sequence. Therefore, the instrument switches to acquisition of fragment-ion spectra (MS^2 or MS/MS), in which a selected number of precursor-ions are sequentially isolated and fragmented. Precursor-ions for fragmentation are usually selected based on their signal intensity with the *top-N*-method, where *N* determines the number of MS/MS spectra to be acquired. Fragmentation of the chosen precursor-ions is achieved with the use of an inert gas, such as helium or nitrogen, and collision-induced dissociation (CID) or higher-energy collisional dissociation (HCD), two commonly used fragmentation methods (Olsen et al., 2007). Upon collision, the peptides are disrupted along their peptide backbone. In an ion trap, breakage mainly occurs at the weakest peptide bonds following the lowest energy path whereas in HCD, or also called beam-type CID, fragmentation does not necessarily take place at the weakest peptide bonds. Afterwards, the fragment ions are subjected to the mass analyzer to record the MS/MS signals. A scan cycle usually consists of one full MS and 10-20 MS/MS scans. In Q-Exactive instruments, both full MS and MS/MS scans are acquired in the orbitrap. The Orbitrap Velos Pro offers a parallel acquisition strategy of full MS and MS/MS spectra. While the orbitrap is acquiring the MS scan of the peptide ions, the ion trap records fragment ion spectra of a predefined number of peptide ions at the same time.
The peptide mass provided by the full MS scan and the m/z ratios of the fragment ions from the MS/MS spectra are used together to determine the exact sequence of a peptide using a database search strategy (Figure 6). Briefly, peptide and peptide fragment masses are compared to a protein database of the specific organism, which was in-silico digested with the applied protease to generate a database of all possible proteolytic peptides in the experiment. The database search engine determines the best fitting peptide for each MS/MS spectrum and scores the quality of the individual identifications. Afterwards, a false discovery rate filter

based on the score is applied to control the number of false positive identifications. (Aebersold and Mann, 2016; Nesvizhskii et al., 2007).

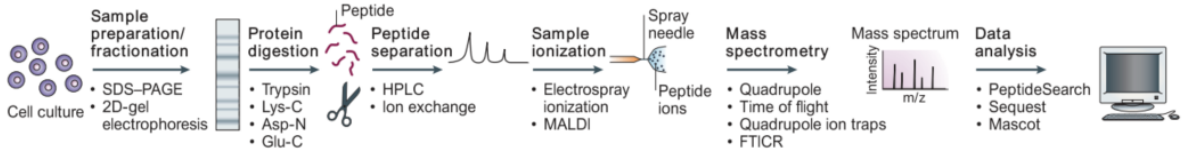

Figure 6: Experimental outline for bottom-up proteomics.
A protein mixture, for example a cell lysate from cultured cells, is prepared and fractionated by a method of choice. Separated proteins are digested with sequence-specific enzymes resulting in a mixture of peptides, which can be further fractionated if necessary. A final fractionation by reverse-phase chromatography (HPLC) separates and elutes peptides according to their hydrophobicity. The HPLC is directly coupled online to electrospray ionization, by which ionized peptides are injected into the mass spectrometer. Inside, peptide ions are fragmented to generate MS/MS spectra, which are then analyzed by mass spectrometry-specific data analysis-tools and subjected to database search engines. Picture taken from Steen & Mann (Steen and Mann, 2004).

1.3.2 Quantitative proteomics and label-free approaches

Besides the identification of many proteins out of a complex mixture, it is also crucial to obtain quantitative information about them and thus be able to accurately evaluate and differentiate between different conditions, for example a healthy and a diseased state.
Unfortunately, mass spectrometry (MS) is not quantitative on its own. Therefore, different relative quantification methods have been developed which are often based on stable isotope labeling. Chemical labeling methods range from reactions with light or heavy versions of an isotope tag (ICAT) over tandem mass tags (TMT) and dimethyl labeling, as well as derivatization of peptides to isobaric tags for relative and absolute quantitation (iTRAQ) – just to name a few (Bantscheff et al., 2012; Bantscheff et al., 2007; Ong and Mann, 2005). Metabolic isotope-based labeling methods such as stable isotope labeling with amino acids in cell culture (SILAC) are still the most accurate ones and therefore the gold standard for quantification (Li et al., 2017b). SILAC allows labeling of whole proteomes with amino acids that are labeled with stable heavy isotopes such as C13 or N15 (Ong et al., 2010).
Isotope labeling methods have the advantage of reduced MS analysis time because of their multiplexing capability, show high reliability and accuracy, but have the drawback of extra preparation steps and high costs. Most importantly, some sample types, such as primary cells or human clinical samples do only allow limited metabolic labeling.
In recent years, label-free quantification (LFQ) became the most popular method for relative quantification in discovery proteomics. Label-free quantification has the advantage that it is applicable to any kind of sample. The label-free approach for protein quantification exists already for a while, but only current improvements in mass resolution and accuracy of MS instruments together with advances in data analysis algorithms strongly increased the power and robustness of this method (Cox et al., 2014; Li et al., 2017b; Meissner and Mann, 2014).
Although, it is not possible to directly correlate the peak intensity of a measured peptide to its absolute amount, the acquired information can still be used for relative quantification between different measurements. For this, the most crucial requirements for reliable label-free quantification are uniform conditions during all experimental steps – from standardized sample handling to highly reproducible chromatographic separation.
In current algorithms for label-free quantification, peptide quantities can be determined at the MS level by integration of the signal from peaks of the eluting peptides (precursor ions). For this, the intensities of peptides are extracted by software using a narrow mass tolerance

window of a peptides mass to charge ratio *m/z* over time (extracted ion chromatogram). For comparisons of different samples, the chromatograms are aligned and the LFQ intensities of individual peptides are compared against each other. After normalization procedures to account for differences in sample loading, the determined peptide intensities are matched to their parent proteins and are used to calculate protein LFQ intensities. In this way, an arbitrary number of runs can be compared to each other. To increase the amount of peptide and protein quantifications, signals of peptides identified in one of the samples are compared to all the other samples on the basis of its m/z ratio and retention time within tight matching tolerances. (Aebersold and Mann, 2016; Cox et al., 2014; Cox and Mann, 2008, 2011).

1.3.3 Proteomics on the secretome

The most efficient way to identify substrates of membrane protease requires non-targeted quantification of protein cleavage products in the secretome. The secretome comprises all proteins that are released by cells – into body fluids or into the medium during cell culturing. In particular, endogenous protease levels in cell lines, primary cells, or even cerebrospinal fluid (CSF) are suitable for substrate identification. However, most of the commonly used cell lines and primary cells have to be cultured in the presence of serum or protein-containing supplements, which are highly abundant and interfere with the detection of low abundant secreted proteins. Previous studies used serum- or protein-free cell culture conditions to circumvent these limitations and several proteomic methods have been developed and optimized for these conditions (Muller et al., 2016). Unfortunately, serum-free culture conditions can cause cellular stress and are not compatible with many cell types making identification and quantification of secreted proteins in primary cells, such as neurons, impossible. Additionally, the activity of many membrane proteases is affected in the absence of serum (Eichelbaum et al., 2012). To quantitatively analyze secretomes, proteomic workflows need to enrich the low abundant secreted proteins. For this, several label-free methods exploit the glycosylation of transmembrane proteins.

Glycan structures on proteins are not only important for correct folding, but also facilitate trafficking and protect proteins from degradation. Glycostructures on plasma membrane proteins constitute the extracellular space and the surface quality of a cell. They are essential for cell survival and have crucial functions in a wide variety of extracellular activities, such as cell adhesion, antibody recognition, receptor multimerization, receptor-ligand binding, microorganism binding and may more. Nearly all surface proteins are predicted to be glycosylated, with N-glycosylation being the predominant modification (Bi and Baum, 2009; Elbein, 1991; Lis and Sharon, 1993; Rudd et al., 2001; Varki, 2017). In fact, according to Uniprot reviewed annotations, around 85% of single-span and 50% of multi-pass transmembrane proteins are known to be N-glycosylated (Herber et al., 2018). Hence, more and more studies on surface and secreted proteins utilize N-glycosylation for labeling, separation, and enrichment.

Methods for secretome analysis such as SPECS (serum protein enrichment with click sugars) have been developed (Kuhn et al., 2012). SPECS uses the click chemistry-suitable sugar derivate Ac4-ManNAz (tetra-acetylated N-azidomannosamine) to metabolically label only newly synthesized glycoproteins. Subsequently, click chemistry biotinylates the modified glycan structures and thus allows selective enrichment of glycoproteins in conditioned cell culture medium, containing serum protein. This method of ectodomain enrichment has been successfully used to identify substrates for several transmembrane proteases (Kuhn et al., 2015; Kuhn et al., 2012; Pigoni et al., 2016; Serdaroglu et al., 2017). A similar approach was developed where proteins are labeled with non-natural amino acids, such as azidohomoalanine (AHA) an azide-containing analog of methionine, which is incorporated into proteins and makes them susceptible to click chemistry-mediated labeling (Eichelbaum et

al., 2012). However, in contrast to labeling with azido-sugars, cellular toxicity has been observed as result of metabolic AHA labeling. As amino acid derivate, AHA is incorporated into the protein backbone and may influence their conformation. Altered proteome structure may thus lead to cellular toxicity (Muller et al., 2016). As mentioned before, azido-modified sugars are incorporated into external protein structures using SPECS and hence have limited effect on protein conformation. Nevertheless, both methods are well suited for secretome analysis under serum-containing conditions.
In addition to secretome analysis, SPECS has previously been used to enrich cellular glycoproteins (Kuhn et al., 2016), but was not able to distinguish between surface and intracellular proteins.

1.3.4 Proteomics on cell surface proteins

A classical approach to separate membranes and enrich cell surface proteins is based on subcellular fractionation by centrifugation (Stasyk and Huber, 2004). However, this simple technique only roughly distinguishes between membrane compartments, such as plasma membrane, Golgi and ER, and comes with limitations and co-purifies many proteins, which are associated to membranes through interactions with membrane proteins or tethered close to the membrane through cytoskeletal structures, but are not actually spanning the membrane. Transmembrane proteins have a high level of heterogeneity and e.g. contain one or multiple membrane spanning domains, whereas some don't have a transmembrane domain at all and are fixed to the membrane via a lipid anchor. All membrane proteins undergo the secretory pathway and are subjected to a variety of posttranslational modifications (PTMs). It is therefore technically challenging to extract, solubilize, and separate them all with just one universal technique (Josic and Clifton, 2007).
Specified methods isolate cell surface proteins by using electrostatic attachment of cationic colloidal silica to membranes (Mathias et al., 2011) or attachment of biotin through chemical labeling of all surface proteins or only glycosylated proteins followed by streptavidin pull-down and subsequent specific enrichment (Wisniewski, 2011). With respect to purity and highest yields of true plasma membrane proteins, however, studies still report conflicting results (Elschenbroich et al., 2010; Hormann et al., 2016; Weekens, 2010). Moreover, general biotinylation of lysine residues in surface proteins has the drawback of blocking tryptic digestion during sample preparation.
Similar to the methods based on N-glycan labeling, which were developed for the labeling and enrichment of secreted proteins, cell surface protein specific enrichment using N-glycosylation profits from the usually extensively glycosylated transmembrane protein ectodomains.
High purity is critical for determination of the cell surface proteome by mass spectrometry based proteomics and more recent techniques like cell surface capturing (CSC) and periodate oxidation and aniline-catalyzed oxime ligation (PAL) (Wollscheid et al., 2009; Zeng et al., 2009) involve chemical oxidation of glycans to aldehydes and a subsequent labeling step with a biotin-containing tag, which allows glycoprotein enrichment. Sugar oxidation on living cells helps to reduce unwanted labeling of intracellular proteins, but still is a chemical modification and might result in unwanted stimulation with consequent changes in cell homeostasis. Despite, CSC and PAL are two popular and suited approaches for proteomic analysis of the cell surface.
Unfortunately, they are not well compatible with analysis of the cell secretome, since highly abundant glycoproteins derived from serum in culture media would also be labeled and low-abundant secreted proteins would not be detected efficiently.

2 Aim of this work

Alzheimer's disease (AD) is the most common form of dementing neurodegenerative disorder worldwide and pathologically characterized by brain atrophy, cognitive decline, and memory loss. On molecular level, amyloid-β (Aβ) depositions and neurofibrillary tangles induce neurotoxicity and eventually result in death of neuronal cells. Although the molecular pathological mechanism is relatively well studied, there is no preventing treatment and much less a cure available.
Drug development is currently guided by the amyloid cascade hypothesis, according to which proteolytic processing of the amyloid precursor protein (APP) is a key process in driving the pathological progression of AD. Sequential APP processing by β- and γ-secretases releases the toxic Aβ peptide, which is prone to aggregation, forming the toxic Aβ-plaques. The three brain proteases a disintegrin and metalloprotease 10 (ADAM 10), beta-site APP cleaving enzyme 1 (BACE 1), and membrane-type 5 matrix metalloprotease (MT5-MMP) are all known to cleave the amyloid precursor protein (APP) in the brain. They therefore are directly involved in the molecular mechanism of AD by influencing the generation of proteolytic APP fragments and – in the case of ADAM10 and BACE1 – are targets in therapeutics and drug development. Stimulation of ADAM10 was shown to increase the non-toxic sAPPα fragment in the cerebrospinal fluid (CSF) of patients. BACE1-mediated APP cleavage is the rate-limiting step during Aβ generation and BACE1 inhibition almost completely abolishes Aβ production. This is why a number of BACE1 inhibitors are currently being tested in clinical trials as disease modulating agents. Yet, a few BACE1 inhibitors were recently terminated in Phase III clinical trials, because it did not succeed in lowering Aβ levels and/or showed non-mechanism based side effects. Raised concerns, based on the complex BACE1 knockout mouse phenotypes and the various physiological functions of the protease, seem therefore to be proven true - for the time being. These recent developments underline the necessity for additional drug targets to modulate disease progression. An alternative appeared with MT5-MMP, whose deficiency was beneficial for pathology outcome in an AD mouse model and resulted in reduced Aβ burden, less neuroinflammation, and cognitive improvement. A modulation or inhibition of MT5-MMP activity presents therefore a promising strategy in AD therapeutics.

The here presented study therefore addresses three major goals:

1. Validation of novel substrate candidates of ADAM10.
While ADAM10 is a protease with a broad range of functions, its substrates in the brain are only poorly described. Stimulation of ADAM10 activity could result in additional excessive cleavage of unknown substrates and lead to side effects. In the scope of a mass spectrometry-based identification of neuronal ADAM10 substrates, newly described substrate candidates will be investigated and validated by using an independent biochemical approach via Western blots.

2. Investigation of cell surface membrane composition upon pharmacological BACE1 inhibition.
After numerous novel BACE1 substrates have been identified and described in the past years, physiological BACE1 function is being elucidated more and more. A proteomic study investigated the neuronal secretome upon BACE1 inhibition, resulting in tremendous changes, leading to e.g. altered signaling between cells. This shows that BACE1 regulates the shedding of various membrane proteins and is involved in many cellular processes beyond APP-cleavage, accountable for the adverse effects upon drug treatment. Because the cell secretome is tightly coupled to cell membrane proteins, the second aim of this study is to use

mass spectrometry-based proteomics to investigate, if and how BACE1 inhibition changes the cell membrane protein composition.

3. Identification of MT5-MMP substrates and the proteases function in AD.
The third aim of this work is to analyze the physiological function and pathological involvement of MT5-MMP. To understand its mechanistic role in the brain, a secretome analysis of MT5-MMP knockout neurons will be performed to identify physiological substrates. Additionally, its role in AD will be investigated via proteomic CSF analysis of MT5-MMP knockout mice crossed with the AD- mouse model 5xFAD.

3 Material and Methods

3.1 Material and Reagents

In this study, following general equipment and material (Table 1) and reagents (Table 2) were used. Special material, reagents or buffers are listed – if applicable – together with the according application.

Table 1: General material and equipment.

Material	Manufacturer
Automated cell counter	Biorad
Cell culture dishes, plates, and flasks	Nunc
Centrifuge Megafuge 1.0	Hereaus
Falcon tubes	Sarstedt
Glass coverslips	Marienfeld
ImageQuant LAS-4000	Applied biosystems
Incubator	Heraeus
Microplate reader	Tecan
Nanodrop	Tecan
Pipette tips	Sarstedt
PVDF membrane (Immobilon-P)	Millipore
SDS-PAGE glasses, combs, casting chambers	Biorad
SDS-PAGE Mini Protean system	Biorad
STAGE-tip centrifuge	Sonation
Sterile cell culture hood	Heraeus
Sterile pipettes	Sarstedt
Syringe filter, 0.2/0.45µM (polyethersulfone)	VWR
Vivaspin diafiltration column	Sartorius Stedim Biotech
Wetblot transfer system	Biorad
Whatman paper	Macherey-Nagel

Table 2: General reagents.

Reagents	Manufacturer
Acetic acid	Merck
Acrylamid/Bis (37.5:1)	Serva Electrophoresis GmbH
Ammoniumpersulfate (APS)	Roche
B-27	Thermo Fisher Scientific
Biotin	Sigma
Bovine serum albumin (BSA)	Sigma
Bromphenol blue	Fluka
C3 (BACE inhibitor IV)	Calbiochem
Coomassie Brilliant Blue G	Sigma
Dimethylsulfoxide (DMSO)	Roth
Dithiotrethiol (DTT)	Sigma
DMEM	Gibco
DMEM Glutamax high-glucose	Gibco
ECL solution	GE Healthcare
Ethanol (80%)	Applichem
Ethanol absolute	Merck
Ethylenediaminetetraacetic acid (EDTA)	Sigma
Fetal Calf Serum (FBS)	Life Technologies
FluorSave	Calbiochem
Formic acid	Sigma

Glycine	Applichem
HBSS	Thermo Fisher Scientific
High-capacity streptavidin agarose beads	Thermo Fisher Scientific
Hoechst 33342	Life Technologies
Iodoacetamide	Sigma
Isopropanol	Merck
KCl	Merck
KH_2PO_4	Merck
KOH	Merck
L-cystein	Sigma
L-glutamine, 200mM	Life Technologies
Lipofectamine 2000	Life Technologies
Methanol (99.9%)	Sigma
NaH_2PO_4	Merck
NaOH	Sigma
Neurobasal	Thermo Fisher Scientific
Nitric acid	Merck
OPTI-MEM	Gibco
Papain	Sigma
Paraformaldehyde	Merck
Penicillin/Streptomycin antibiotic	Life Technologies
Phosphate-buffered saline	Gibco
Poly-D-Lysine (PDL)	Sigma
PrecisionPlus protein ladder	Biorad
Protease inhibitor	Sigma
Sodiumdeoxycholate	Sigma
Sodiumdodecylsulfate	Serva Electrophoresis GmbH
Streptavidin-dichlorotriazinylamino fluorescein	Dianova
Sulfo-dibenzylcyclooctyne-biotin	Jena Bioscience
TAPI	Abcam
TEMED (99%)	Roth
Tetra-acetylated N-azidomannosamine	Synthezised by laboratory of Stefan Bräse, KIT
Tris ultrapure	Applichem
Triton X-100	Merck
Trypsin, MS-grade	Promega
Trypsin-EDTA (0.05%)	Gibco
Tween-20	Merck
Urea	Merck
β-Mercaptoethanol	Roth

3.2 Cell culture

3.2.1 Immortalized cell lines and culture conditions

COS-7 and HEK293 cells were cultured in DMEM supplemented with 10 % FBS and 1 % Pen/Strep. Cell viability and confluence were regularly investigated under a light microscope. Cells were grown in dishes or flasks in humid environment at 37 °C and 5 % CO_2 in and incubator. At 70 - 90% confluence, cells were passaged. Passaging was performed under a sterile cell culture hood: culture medium was aspirated and cells were washed twice with PBS and incubated with 1-2 mL Trypsin-EDTA for 5 min to detach them from the surface and harvested in fresh culture medium. Cells were collected with a centrifugation step for 5 min at 1,000 x g at RT. The pellet was resuspended and cells were split and distributed to a new dish/flask in a ratio of 1:3, 1:5 or 1:10 depending on confluence and demand.

3.2.2 Freezing and thawing of cells

Immortalized cell lines were cryopreserved at -80 °C or in liquid nitrogen for long-term storage.

For freezing, 70 % confluent cells were washed and detached as during passaging. The cell pellet was resuspended in 1 mL of FBS containing 10 % DMSO as cryopreservative and gradually cooled down (1 °C/ min) in a styrofoam cooling device to -80 °C.

To thaw a frozen aliquot of cells, vial containing cells was quickly warmed in a 37 °C water bath and 1 mL cells were transferred to 9 mL of pre-warmed culture medium to dilute DMSO. Cells were collected with centrifugation for 5 min at 1,000 x g, resuspended in appropriate volume of culture medium, and transferred to a culture flask. After 12-24 h culture medium was replaced with fresh one to remove dead cells.

3.2.3 Generation of lentiviral particles

Lentiviral particles were produced by transient co-transfection of HEK293-T cells in 6-well plates or 10 cm dishes.

For transfection in 6-well plates (10 cm dishes) following amounts and reagents were used: 1.3 (30) µg of transfer vector containing the gene of interest, 0.75 (20) µg psPAX2 and 0.45 (10.8) µg pcDNA3.1(-)-VSVG, and 6.3 (136) µl Lipofectamine 2000. 2-3x10^6 HEK293T cells for a 6-well and 7-9x10^6 cells for a 10 cm dish were transfected in OPTIMEM solution and seeded on the according dish in OPTIMEM with 10 % FBS. The next day, medium was changed to 2 mL (6-well) or 10 mL (10 cm dish) packaging medium and cells were incubated at 37 °C. After 24 hours viral particles were harvested: packaging medium containing the lentiviral particles was collected and centrifuged (3000 x g, 15 minutes) to remove cellular debris. Cleared medium was sterile filtered through a 0.45 µm filter and lentiviral particles were concentrated via ultracentrifugation (OptimaTM XPN-100, Beckman Coulter) at 22.000 rpm at 4 °C for 2 hours using a swing-out rotor (SW28). The supernatant was carefully removed and the viral pellet was resuspended in 250 µl TBS-5. After incubation at 4 °C over night, viral particles were carefully resuspended and small aliquots of the concentrated virus suspension was stored at -80 °C until further use for transduction of cells.

Table 3: Media and reagents for production of lentiviral particles.

Medium/Reagent	
Packaging Medium	DMEM, 110 mg/l Na-Pyruvate, 10% FCS, 1% Non-essential amino acids, 1% P/S, 1 mM Sodium-butyrate
TBS-5	50 mM Tris-HCL pH 7.5, 130 mM NaCl, 10 mM KCl, 5 mM $MgCl_2$, 10 % (w/v) BSA

3.2.4 Stable transduction with lentiviral particles

3.2.4.1 Gene knockout using Cre recombinase

Lentiviral particles expressing codon-optimized Cre recombinase (iCre) (Shimshek et al., 2002) were generated as described in section 3.2.3.

Primary conditional ADAM10 knockout neurons were infected, extracted and cultured as described in section 3.4.3. On day in vitro (DIV) 5, neurons were infected 1:200 with concentrated iCre virus by addition of virus to the cell culture media.

3.3 Biochemistry

3.3.1 Lysis of cells

All steps of the following procedure were performed at 4 °C or on ice. If secreted proteins were subject of planned analyses, conditioned medium was collected and centrifuged at 4 °C for 5 minutes at 13,000 rpm in a tabletop microcentrifuge to get rid of cell debris. Supernatant was transferred to a new tube. Immediately after medium was taken off, cells were washed two time with 1x PBS and appropriate amount of lysis buffer (supplemented1:200 with freshly added 1x protease inhibitor) was applied. Cells were incubated for 15 min on ice, collected using a cell scraper, and transferred to a tube. To ensure a proper lysis, lysates were incubated another 10 min on ice followed by a 5 min centrifugation step at 4 °C and 13,000 rpm. Cleared cell lysate was subjected to BCA assay to determine protein concentration and stored at -20°C or used immediately for further analyses.

Table 4: Composition of cell culture buffers and reagents.

Buffer/Reagent	
PBS 10x	1.5 M NaCl, 162 mM Na_2HPO_4, 38 mM KH_2PO_4, 26 mM KCl, in ddH_2O
STET lysis buffer	50 mM Tris pH 7.5, 150 mM NaCl, 2 mM EDTA, 1% Triton (v/v), in ddH_2O
RIPA lysis buffer	10 mM Tris pH 8, 150 mM NaCl, 2 mM EDTA, 1% Triton (v/v), 0.1% SDS, 0.1% Sodium deoxycholate

3.3.2 Determination of protein concentration by bicinchoninic acid assay

The protein concentration was determined using the bicinchoninic acid assay (BCA)-Kit (Uptima) according to the manufacturer's instructions. Briefly, solution A and B were mixed in a ratio of 1:50. In a 96-well-plate format, 10 µl of protein-sample were incubated with 200µl of solution mix A+B and incubated for 30 min at 37 °C in an incubator (Heraeus). As reference, every assay was carried out alongside a predefined standard curve with known protein concentrations of BSA. Each sample was performed in duplicates. Spectral absorption was measured at 562 nm with a microplate plate reader (TECAN).

3.3.3 SDS-Polyacrylamide-gel electrophoresis

Sodium dodecyl sulfate polyacrylamide-gel electrophoresis (SDS-PAGE) is the most common method to separate protein mixtures, e.g. cell lysates, under denaturing conditions. Negatively charged proteins are separated according to their molecular weight inside a gel. Separation resolution depends on the polyacrylamide percentage of the gel and can be adjusted according to the protein of interest. In this study mostly 8 and 10 % polyacrylamide gels were used, unless otherwise noted. Gels were prepared manually with a thickness of 1.5 mm using the MiniProtean handcast system (Biorad).
For SDS-PAGE analyses, protein samples were mixed 3:1 with 4x SDS-sample buffer and boiled for 5 min at 95 °C. Equal amounts of proteins were loaded into stacking gel and concentrated at 80 V for approximately 30 min or until they reached the resolving gel, where they were separated with 120 V. A protein ladder was used as a reference. SDS-PAGE was performed using the Mini-Protean system (Biorad) and Tris-Gycine/SDS running buffer.

Table 5: Volume of reagents for 2 polyacrylamide gels for SDS-PAGE.

Reagent	4% stacking gel	8% resolving gel	10% resolving gel
Acrylamide 40%	1 mL	3.2 mL	4 mL
ddH2O	6.8 mL	8.8 mL	8 mL
Low-Tris buffer	-	4 mL	4 mL
High-Tris buffer	2.5 mL	-	-

APS 10%	60 µl	120 µl	120 µl
TEMED	30 µl	60 µl	60 µl

Table 6: SDS-PAGE buffer compositions and reagents

Buffer/Reagent	
4x protein sample buffer	0.25 M Tris/HCl pH 6.8, 8 % SDS (v/v), 40 % glycerol (v/v), 0.025 % bromophenol blue, 10% β-Mercaptoethanol, in ddH_2O
Tris-Glycine/SDS buffer	25 mM Tris Base, 192 mM Glycine, 0.1% SDS (v/v), in ddH_2O
Low-Tris buffer	1.5 M Tris pH 8.8, 0.4 % SDS (v/v), in ddH_2O
High-Tris buffer	0.5 M Tris pH 6.8, 0.4 % SDS (v/v), in ddH_2O

3.3.4 Western blot

For Western blot analysis proteins were separated with SDS-PAGE and transferred onto an isopropanol activated PVDF membrane. Blotting was performed using a submerged tank-blot system (Biorad). A bubble-free blotting sandwich was assembled on a perforated plastic cassette: Sponge pad, two layers of Whatman paper, SDS gel, PVDF membrane, two layers of Whatman paper, sponge pad (from cathode to anode). Blotting material was equilibrated/soaked in transfer buffer before assembly. The cassette containing the sandwich was inserted into the tank, filled with transfer buffer and a cooling device. Transfer was run for 70 minutes at 400 mA if up to two membranes were blotted or at 1 A if three or four membranes were blotted in parallel.

After the transfer the membrane was briefly washed in 1x PBS-Tween (PBS-T) and then blocked for 30 min at RT with 5 % milk in PBS-T on a horizontal shaker followed by two washing steps of 5 min with PBS-T. Primary antibodies against the protein of interest were then applied either 1 hour at RT or overnight at 4 °C depending on the antibody characteristics and incubated with gentle horizontal shaking. In the next step, the membrane was carefully washed 3 times with PBS-T for 5 min with gentle shaking followed by incubation with the appropriate secondary antibody for 1 hour at room temperature. Afterwards the membrane was again washed 4 times with 1x PBS-T for 5 min each step. All primary antibodies were diluted at the concentration advised from the manufacturer in 10 mL 1x PBS-T with 0.5 % BSA, 0.05 % (w/v) sodium azide. Secondary antibodies were diluted at a concentration of 1:10,000 or 1:5,000 in 10 mL 1x PBS-T with 0.5 % BSA.

Western blots were developed using enhanced chemiluminescence (ECL).

Table 7: Buffers and reagents for Western blot

Buffer/Reagent	
Transfer buffer	25 mM Tris, 192 mM Glycine, in ddH_20
PBS-T	0.05 % (v/v) Tween-20 in 1x PBS
Blocking solution	5 % (w/v) non-fat milk in PBS-T

3.3.4.1 Antibodies

Antibodies used in this study are listed in table 8.

Table 8: Primary and secondary antibodies

Primary antibody	Target	Provider
22C11	APP N-terminus	Millipore
2C11	APP C-terminus	In-house made

Anti-ADAM10	ADAM10	Millipore
Anti-Calnexin	Calnexin	Enzo/Stressgen
Anti-L1Cam	L1Cam	Altevogt
Anti-Neogenin	Neogenin	In-house made
Anti-NrCam	NrCam	Abcam
Anti-MT5-MMP	MT5-MMP	Rivera Lab

Secondary antibody	Target	Provider
Anti-mouse-HRP	Mouse-IgG	Promega
Anti-rabbit-HRP	Rabbit-IgG	Promega

3.3.5 Enhanced chemiluminescence

Protein signals were detected using enhanced chemiluminescence (ECL) method. The acquisition of signal is based on the oxidation of luminol catalysed by horseradish peroxidase (HRP) in the presence of peroxide, during which light is emitted. All secondary antibodies were conjugated to HRP. Luminescence was captured using the ImageQuant LAS4000. Signals were quantified using MultiGauge 3.0 software and Western blots were processed with Adobe Photoshop.

3.4 Animal related work

3.4.1 Mouse strains

Following mouse strains were used in this study:
Wildtype C57BL/6 wild type mice were obtained from the in-house animal facility or purchased from Charles River and used for wildtype primary neuronal cultures. Conditional ADAM10 knockout mice (Gibb et al., 2010). Two MT5-MMP knockout mice strains were used: 1. $Mmp24^{tm1Otin}$ (MGI:4365393) (Folgueras et al., 2009) were obtained from the laboratory of Isabella Farinas and used for SPECS experiments. 2. $Mmp24^{tm1Ski}$ (MGI:3028827) (Komori et al., 2004) were used for proteomic analysis of cerebrospinal fluid. Mice were maintained on a 12/12 h light-dark cycle with food and water *ad libitum*. All animal procedures were carried out in accordance with the European Communities Council Directive (86/609/EEC).

3.4.2 Mouse brain extraction and sub-dissection

Animals were euthanized by cervical dislocation or CO_2 and decaptiated. Skin was opened with a sagittal incision from neck to nose and moved to the sides. Next, a dorsal incision along the median axis of the head was performed to open the skull carefully. Using small pair of forceps, the skull bones were removed without touching the brain tissue. The brain without the brain stem was carefully liberated from the base of the skull using a spatula.
If necessary, the brain was sub-dissected on ice. First, the cerebellum was removed with a coronal cut behind the cerebrum using a scalpel. Additionally, left and right hemispheres were separated with a scalpel. Cortex was carefully dissected and hippocampus was removed, using a spatula. Dissected tissue was directly used for biochemistry or snap frozen in liquid nitrogen and stored at -80 °C until further processing.

3.4.3 Preparation of primary cortical neurons

Primary neuronal cultures were prepared at embryonic day 16.5 from wildtype and MT5 MMP knockout animals. Embryos were removed from uterus and collected in HBSS. Embryonic brains were isolated under a microscope and cleaned from meninges. Cortices

were dissected and collected in 5 mL fresh HBSS in a 15 mL falcon tube on ice. Each embryo was treated separately and genotyped in retrospect.
HBSS was removed and replaced by 2 mL of digestion medium. Tissue was enzymatically digested for 15 min at 37 °C (in the incubator). To stop the reaction, digestion medium was removed carefully and tissue was washed once with 5 mL dissociation medium. Using 2 mL of fresh dissociation medium the tissue was mechanically dissociated by pipetting up and down with first a 5 mL and then a 2 mL pipette. The cell suspension was transferred to a new tube avoiding not dissociated tissue pieces and centrifuged for 3 min at 700 rpm. Cells were resuspended in 10 mL fresh plating medium and seeded onto PDL-coated 10cm dishes (10-12x10^6 cells per embryo/dish). Cultures were incubated for 3 hours at 37 °C and 5 % CO_2 and medium was replaced carefully to culture medium. Neuronal cells were grown at 37 °C and 5 % CO_2.

Table 9: Media and solutions for neuronal cultures.

Medium	Composition
Digestion medium	9.7 DMEM Glutamax High Glucose, 0.01g L-Cystein, 200 U Papain (~300 µl), adjust pH to 7.4 with NaOH
Dissociation medium	DMEM Glutamax High Glucose with 10% FBS
Plating medium	DMEM Glutamax High Glucose with 10% FBS, 1% Pen/Strep
Culture medium	9.6 mL Neurobasal, 500 µM L-glutamine, 100 µl Pen/Strep, 200 µl B27

3.4.4 Collection of mouse cerebrospinal fluid (CSF) from cisterna magna

CSF was collected after Liu and Duff 2008 with adjustmens (Liu and Duff, 2008). Mice were anaesthetized using a Ketamine/Xylazine cocktail with a concentration of 10 mg/mL Ketamine and 5 mg/mL Xylazine and a dosage of 100 µl/10 mg bodyweight. Animals were fixed in a stereotaxic frame and position of the head was adjusted and fixed in an angle of approximately 130° between head and spine. Hair was parted and skin on the back of the head was vertically cut with a 1 cm long incision. Subcutaneous tissue and muscles above the cisterna magna were bluntly separated and fixed with retractors to open the field. If needed, position of the head was adjusted to increase or decrease the pressure inside the cisterna. A pulled and sharpened glass capillary connected to PEG-free sterile tubing was attached at the descending arm of the stereotaxic apparatus. Dura above the cisterna magna was punctured in a fixed angle of 45° and CSF was collected slowly by application of minimal negative pressure through the tubing. At the end of collection, capillary was retracted with simultaneous release of negative pressure and CSF was transferred into a clean protein loBind tube. After centrifugation for 10 min at 3000 x g at 4 °C CSF was aliquoted à 5 µl in protein Lobind tubes and frozen on dry ice. Samples were stored at -80 °C.

3.4.5 Transcardial perfusion and fixation

Tubing for perfusion was pre-flushed with buffer, so that the perfusion system was air bubble-free. Mice were anaesthetized using a Ketamine/Xylazine cocktail with a concentration of 10 mg/mL Ketamine and 5 mg/mL Xylazine and a dosage of 10 µl/mg bodyweight. Anaesthetized and unresponsive mice were positioned laying on the back and stabilized by fixing the fore and hind paws. A vertical incision along the sternum and a lateral incision just below the thorax were used to separate skin and subcutaneous muscle. Holding and lifting the xiphoid process with a forceps, the diaphragm was carefully cut along the thorax to open the cardiothoracic cavity. Two vertical incisions through the ribs to the claviculae were done to open the thorax. Holding the xiphoid process and carefully lifting the sternum away, any

tissue connected to the heart was separated. The thorax was flipped open and fixed, so that the heart was exposed. A short 23 gauge needle connected to a perfusion pump was inserted a few millimeters into the posterior end of the left ventricle and fixed. The perfusion pump was started and simultaneously a small incision into the right atrium was created as outlet for the perfusion fluids. Animals were perfused with a constant flow rate with PBS for approximately 2-4 min until liver was blood-free.
If animals were fixed during perfusion procedure, the pump was stopped and tubing was transferred to 4 % PFA solution avoiding air bubbles in the tubing. Animals were perfused with fixative for another 5 min.
After perfusion, tissue of interest was dissected.

3.5 Sample preparation methods for mass spectrometry

3.5.1 Secretome protein enrichment with click sugars

Secretome protein enrichment with click sugars (SPECS) was performed on conditioned cell culture supernatant (SN) of primary neurons from MT5-MMP wildtype and knockout neurons, which were prior subjected to metabolic labeling with ManNAz for 48 h. 20 mL of SN was concentrated on a vivaspin diafiltration column with a 30 kDa cut off via centrifugation until retentate was reduced to approximately 0.5 mL. Flow through (FT) was discarded and retentate was washed 2 times by adding 20 mL of autoclaved ddH_2O and centrifuging down to 0.5 mL. In the next step metabolically labelled proteins were biotinylated via click reaction. For this, 2 µl of 50 mM DBCO-PEG-Biotin was diluted in 0.5 mL autoclaved ddH_2O with 0.2% formic acid and added to the retentate (f.c. DBCO-PEG-Biotin 100 nM). Click reaction was performed overnight at 4 °C. The next day, concentrated and biotinylated proteins were washed 3 times by adding 20 mL of autoclaved ddH_2O and centrifuging down to 0.5 mL. In the first washing step 1-2 mL of 1 M Tris pH 7.4 was added to neutralize the sample. After the washes, 0.5 mL retentate was resuspended in 10 mL 2 % SDS in PBS and transferred to a polyprep column containing 300 µl of PBS-washed high capacity streptavidin beads. Samples were run over streptavidin beads by gravity flow and FT was collected and reloaded once to maximize binding. Followed by 2 washing steps with 10 mL 2 % SDS, beads were taken up in 2x 500 µl 2 % SDS and transferred to a reaction tube. Beads were collected by 1 min centrifugation at 1000 rpm and SN was removed. Remaining liquid was aspirated with a Hamilton syringe. Dry beads were stored at -20 °C or directly used for SDS-PAGE fractionation and subsequent in-gel digestion.

3.5.2 Surface-spanning protein enrichment with click sugars

Surface-spanning protein enrichment with click sugars (SUSPECS) was performed on primary wildtype neuronal cultures treated with the BACE inhibitor C3 and vehicle (DMSO). Primary neurons were prepared and cultured as described in section 3.4.3. $20x10^6$ neurons were grown in one T-175cm flask and two flasks were used for one condition. On day in vitro (DIV) 7, culture medium was replaced with new culture medium supplemented with 50 µM ManNAz and neurons were treated with 2 µM C3 or the according amount of DMSO. ManNAz-labeling and inhibitor/control-treatment was performed for 48h in the incubator. In the next step, medium was removed and cells were washed twice with PBS (cell culture grade, Gibco). Immediately after, ManNAz-labeled proteins were biotinylated by click chemistry using 50 µM sulfo-dibenzylcyclooctyne-biotin (DBCO-biotin) in 2 mL PBS per T-175 cm flask for 2 h at 4 °C. Cells were washed twice with PBS and lysed in 4 mL of STET supplemented with proteinase inhibitor per T-175 cm flask. Lysates of 2 flasks containing the same condition were pooled, cleared by centrifugation, and sterile filtered using a 0.45 µM syringe filter. 300 µl of high-capacity streptavidin agarose beads were transferred into a

polyprep column and washed twice with 10 mL 2 % SDS in 1x PBS. Pooled lysate wash run over the polyprep column containing streptavidin beads by gravity flow. Flow through was collected and reloaded to increase binding of proteins. Beads were washed two times with 10 mL of 2 % SDS in 1x PBS and then transferred using two times 500 µl of 2 % SDS in 1x PBS to a 0.5 mL Eppendorf tube. All liquid was removed with a Hamilton syringe and beads were boiled for 5 min at 95 °C in 150 µl 4x sample buffer supplemented with 8 M urea and 3 mM biotin to elute the proteins. Eluted proteins were collected using a Hamilton syringe and directly loaded onto a 10 % polyacrylamide gel and separated by SDS-PAGE.

3.5.3 SDS-PAGE fractionation of mass spectrometry samples

Complex samples were fractionated via 1-dimensional SDS-PAGE for subsequent mass spectrometric analysis. Streptavidin bead-bound biotinylated proteins were eluted from beads by adding 140 µl of 1x-sample buffer containing 8 M urea and 3 mM biotin. Submerged beads were boiled 5 min at 95 °C and eluted proteins were taken up with a Hamilton syringe. For each sample, the complete 140 µl were loaded and separated in a 10 % gel. Samples of one experiment were always separated on the same gel to minimize variation (SPECS: WT and KO, SUSPECS: DMSO and C3). SDS-PAGE was run with 60 V for stacking and 100 V for resolving gel until the loading dye just ran out of the gel.

3.5.4 Staining and destaining of SDS-PAGE gels

After SDS-PAGE and prior to in-gel digest, gels were stained with Coomassie Brilliant blue staining solution for 15 min with gentle horizontal shaking. Subsequently, gels were destained with horizontal shaking in destaining solution two times for 30 min and overnight to visualize proteins.

Table 10: Solutions for Coomassie staining and destaining

Buffers/reagent	
Coomassie Brilliant blue staining solution	0.025 % (w/v) Coomassie Brilliant blue, in 10 % acetic acid (v/v) in MS-grade H_2O
Coomassie Brilliant blue destaining solution	10 % acetic acid (v/v) in MS-grade H_2O

3.5.5 In-gel digest

The whole lane of separated protein was fractionated in 14 fractions to reduce the level of complexity. In SPECS experiments this step also removed the remaining amount of BSA originating from the neuronal culture medium. Gel cutting was performed at a PCR cabinet. Both lanes (SPECS: WT and KO, SUSPECS: DMSO and C3) were cut with a sterile scalpel at equal heights in 14 horizontal slices so that equal fractions from both conditions contain proteins of equal molecular weight. Slices were further cut into 1x1x1 mm small cubes and transferred to a polypropylene 96-well plate with conical bottoms. One well contained all cubes from one fraction.

In-gel digest was performed after Shevshenko et al. (Shevchenko et al., 2006). All solutions were prepared freshly for each procedure. Gel cubes were dehydrated in 3-4 dehydration cycles. In each cycle 150 µl ACN was added per well and incubated for 10 min at RT with gentle horizontal rotation. Liquid was removed from well and new ACN was added. When cubes were completely dehydrated and white, 50 µl of 10 mM DTT was added for 30 min incubation at 55 °C to reduce and denature proteins. Samples were allowed to cool down to RT and dehydration was repeated. In the next step, 75 µl (or enough to cover the gel pieces) of 55 mM was added to alkylate free cysteine residues and incubated for 20 min in the dark.

Samples were again dehydrated and 150 ng trypsin was added per fraction/well and incubated on ice for 30 min. If solution was absorbed, enough trypsin buffer was added to cover gel pieces and left on ice for another 90 min. After 90 min, if needed ABC was added to cover gel pieces. The 96-well plate was covered with a lid, carefully sealed with parafilm on the sides, and transferred to an incubator. Protein digestion with trypsin was performed at 37 °C overnight. The next day, peptides were extracted. During 3-4 extraction steps liquid from one well was pooled and collected in one protein loBind tube. In each extraction step, 100 µl of peptide extraction buffer was added per well and incubated for 15 min at RT with gentle horizontal rotation. Extraction was performed until gel pieces were completely dehydrated and collected peptides were dried with vacuum centrifugation. Peptides were stored at -20 °C or directly reconstituted in appropriate volume of 0.1% FA in H_2O for LC-MS/MS analysis.

Table 11: Buffers and reagents for in-gel digest

Buffer/Reagent	
ABC (ammonium bicarbonate)	100 mM ABC, in MS-grade H_2O
DTT (dithiothreitol)	10 mM DTT, in 100 mM ABC
IAA (iodoacetamide)	55 mM IAA, in 100 mM ABC
ACN (acetonitrile)	100 % ACN, MS-grade
Trypsin	MS-grade
Trypsin buffer	10 mM ABC, in 10% ACN in MS-grade H_2O
Extraction buffer	1:2 ratio 5% FA : ACN

3.5.6 In-solution digest of cerebrospinal fluid

5 µl CSF containing approximately 1.5 – 2.0 µg protein were denatured with 0.5 % sodium deoxycholate (SDC) in 250 mM ABC and reduced with 2 µl 10 mM DTT for 30 min at room temperature. Free cysteine residues were alkylated with 2 µl of 55 mM IAA for 30 min in the dark and remaining IAA was quenched with another incubation of 2 µl 10 mM DTT for 30 min. Proteins were digested with 0.1 µg LysC for 3h followed by 0.1 µg trypsin over night at room temperature. Digestion was stopped by acidification (pH < 2.5) with 150 µl 0.1 % and 8 µl 8% FA and SDC was precipitated for 20 min at 4 °C and removed by centrifugation for 10 min at 16.000 x g at 4 °C. Further, peptides were purified using stop and go extraction (STAGE) –tips (Rappsilber et al., 2007).

Table 12: Buffers and reagents for in-solution digest

Buffer/Reagent	
DTT, IAA, trypsin	See table 10
ABC	250 mM ABC, in MS-grade H_2O
SDC (sodium deoxycholate)	0.5 % (X/v) in 250 mM ABC
LysC	MS-grade
ACN	60 % ACN, in MS-grade H_2O

3.5.7 STAGE-tip based sample clean-up

Stop and go extraction (STAGE) –tips were prepared manually and used to desalt, purify, and concentrate digested peptide samples for LC-MS/MS analyses.

A conventional sterile pipet tip (200 µl) was stuffed with one (or more, if necessary) disks of C18 (octadecyl carbon chain bonded to porous silca) embedded in PTFE (polytetrafuoroethylene) material. The C18 material was stenciled out of a lager unit (Empore) with the blunt needle tip of a Hamilton syringe and released tightly into a sterile pipet tip by using a plunger. It has hydrophobic features and allows binding of peptides in an

aqueous solution with a binding capacity of approximately 5 µg per disk. Peptides can be released with non-polar organic solvents such as acetonitrile.

Clean-up was performed according to Rappsilber et al. (Rappsilber et al., 2007). In brief, STAGE-tips were conditioned with 100 µl methanol (HPLC grade) and well equilibrated with 0.1 % formic acid (FA) in HPLC grade H_2O. Liquid was forced through the tip by using a STAGE-tip centrifuge (Sonation, Germany). Peptides were loaded onto C18 material and washed 4x with 100 µL 0.1 % FA. Washed peptides were stored on STAGE-tips at -80 °C or directly eluted with 60 % acetonitrile (ACN) and 0.1 % FA directly into 0.5 mL protein Lobind tubes (Eppendorf). Vacuum centrifugation was used to dry the samples and remove ACN. Dried peptides were dissolved in an appropriate volume of 0.1 % FA by mixing and sonicating and subjected to LC-MS/MS analysis.

3.6 High performance liquid chromatography and mass spectrometry

3.6.1 High performance liquid chromatography (HPLC)

Experiments were performed on an Easy nLC-1000 (Thermo Proxeon) setup, which was coupled online via a nano electrospray source (Thermo Proxeon) equipped with a column oven (Sonation) to a LTQ Velos Orbitrap Pro or a Q-Exactive Mass Spectrometer (Thermo Scientific).
Peptides were separated on an analytical column (in-house-packed C18 column, 75 µm x 30 cm, ReproSil-Pur 120 C18-AQ, 1.9 µm, Dr. Maisch GmbH).
Peptide separation was performed using binary gradients of water (solvent A) and acetonitrile (solvent B) containing 0.1 % formic acid. A binary gradient of 75 min duration was used for analysis of MT5-MMP knockout secretome and BACE1 surface experiments on 30 cm columns: 0 min, 2% B; 3:30 min 5% B; 48:30 min, 25% B; 59:30 min, 35% B; 64:30 min, 60% B. A longer gradient of 120 min was used for MT5-MMP knockout/5xFAD CSF and BACE2 glia secretome analysis on 30 cm columns: 0 min, 2% B; 2:00 min, 5% B; 92:00, 25% B; 112:00 min, 35% B; 121:00 min, 60% B; 123:30 min, 95% B; 138:30, 95% B. At the end of the gradient, the column was washed with 95% solvent B, before the column was equilibrated again and the next sample was loaded.

3.6.2 In-house-packing of analytical columns

Empty nano-capillary-emitter columns were purchased in 30 cm length and an inner diameter of 75 µm (FS360-75-8-N-S-C30, New Objective) and packed with C18 beads with a diameter of 1.9 µm (ReproSil-Pur 120 C18-AQ, 1.9 µm, Dr. Maisch GmbH).
Beads were washed three times with HPLC grade acetone, sonicated in fresh acetone for 1 min, and transferred into a 2 mL flat-bottom glass vial containing a small PTFE-coated magnetic stirrer. The glass vial containing the bead slurry was placed into the packing unit (SP-400 packing unit, coupled to a CE-005 high pressure adapter kit, Nanobaume). An empty column was fixed in the lid and packing unit was closed tightly. Everything was put onto a magnetic stirrer and packing was performed at 650 rpm stirring using technical nitrogen and pressure of up to 200 bar. Packed columns were allowed to air dry and inspected by eye for continuous filling.

3.6.3 LC-MS/MS mass spectrometry measurements: LTQ Velos Orbitrap Pro

The LTQ Velos Orbitrap is a hybrid mass spectrometer from Thermo Fischer Scientific. It incorporates the LTQ Velos™ dual cell linear ion trap and the Orbitrap™ analyzer. The mass

spectrometer setup is a high performance LC-MS/MS system and combines rapid ion trap data acquisition with high mass accuracy through the orbitrap mass analyzer (www.thermofisher.com).
Full MS spectra were acquired using a top-10 method at a resolution of 60,000, which means, in one acquired MS spectrum inside the orbitrap, the ten most intense peptide ions were chosen for collision-induced dissociation (CID) within the ion trap. The automatic gain control target value for full-MS spectra was set to 1,000,000. During CID the isolation width for the precursor ion was set to 2 m/z. The automatic gain control target value for MS/MS acquisition was set to 10,000. A dynamic exclusion of 90 sec was applied for CID acquisition, in order to avoid unnecessary fragmentation of previously MS/MS fragmented precursor ions. Molecules with a charge state of one were excluded from fragmentation, since they usually represent common contaminants, but not peptides. Monoisotopic precursor selection was chosen and only ions were selected for fragmentation, if the isotopic pattern had a typical peptide pattern enabling calculation of the charge state of the measured m/z.
This instrument was used to measure samples of the BACE1-inhibition cell surface and BACE2 glia secretome analysis as well as for the MT5-MMP secretome analysis.

3.6.4 LC-MS/MS mass spectrometry measurements: Q-Exactive HF

The Q-Exactive HF (high field) from Thermo Fisher Scientific is an orbitrap mass spectrometer, in which both MS and MS/MS spectra are acquired in the orbitrap mass analyzer. A linear quadrupole serves as mass filter. The Q-Exactive HF is equipped with improved ion optics via quadrupole segmentation and achieves double the scan rate at almost the same resolution, compared to other Q-Exactive instrument models. (www.thermofisher.com).
Full MS spectra were acquired at a resolution of 120,000 and the top fifteen intense precursor ions were chosen for fragmentation. The automatic gain control target was set to 3,000,000 and MS/MS spectra were recorded at a resolution of 15,000 with the automatic gain control target value set to 100,000. The mass window for precursor ion selection was 1.6 m/z. Higher-energy C-trap dissociation fragmentation was performed with normalized collisional energy of 26 % and a dynamic exclusion of 120 sec was applied. Molecules with the charge state one or six and higher were excluded from fragmentation and monoisotopic precursor selection was enabled.
This instrument was used for measurements of MT5-MMP knockout/5xFAD CSF experiments.

3.7 Data analysis and statistical evaluation of mass spectrometry data

Database search and label-free quantification was performed with the freely available software MaxQuant (version 1.5.5.1, www.maxquant.org). Trypsin was defined as protease. Following settings were chosen for MaxQuant analysis: Carbamidomethylation of cysteines was defined as fixed modification and oxidation of methionines and N-terminal acetylation of proteins were defined as variable modifications. The allowed number of missed cleavages for peptide identification was set to 2. Following reviewed Uniprot databases were used for database searches: 1. For SPECS experiments: Mus musculus reviewed canonical database, downloaded 26.08.2015, 16,725 protein entries; 2. For CSF analyses: Mus musculus reviewed canonical database including mutated human APPsw/PS1, downloaded 11.01.2017, 16,845 protein entries. First search option was enabled with a precursor and fragment mass tolerance of 20 ppm. For the main search, a mass deviation of 4.5 ppm was allowed for precursor ions and of 20 ppm and 0.5 Da for fragment ion masses recorded in the orbitrap and ion trap, respectively. A false discovery rate (FDR) of less than 1 % was defined for proteins and

peptides by using a target and decoy library (concatenated forward and reverse database) including a database of common protein contaminants. Label free protein quantification required at least two ration counts of unique peptides.
Data analysis was done with the software Perseus and Microsoft Excel using label-free quantification (LFQ) intensity values. Proteins were considered identified and quantitatively evaluated, if they were detected with at least two unique peptides in at least three experiments of each sample group, unless stated otherwise. LFQ-intensities were log2-transformed and ratios between sample groups were calculated. For SPECS experiments, statistical evaluation was done with a one-sample t-test (μ_0=0) with a significance threshold of p=0.05. The p-value was corrected for FDR (5 %) by application of multiple hypothesis testing-criteria according to Benjamini-Hochberg. For proteomic CSF analysis, a two-sided Student's t-test was applied to evaluate significant changes. A permutation-based false discovery rate estimation was used in addition to the t-test (FDR=0.05, s0=0.1).
Functional classification of quantified proteins was done using reviewed Uniprot annotations for subcellular locations and keywords and Gene Ontology based protein annotations through evolutionary relationship (PANTHER).

4 Results

4.1 Validation of novel ADAM10 substrate candidates

The following results have been included in the publication *Systematic substrate identification indicates a central role for the metalloprotease ADAM10 in axon targeting and synapse function* in the journal *eLife* (Kuhn et al., 2016).

In preliminary work, Dr. P.H. Kuhn (Neuroproteomics, German Center for Neurodegenerative Diseases and Technische Universität München; *P.H.K. is now affiliated with the Institute of Pathology, Technische Universität München*) systematically identified 91, mostly novel ADAM10 substrate candidates in primary neurons using label-free high-resolution mass spectrometry and the 'secretome protein identification with click sugars' (SPECS) method. Primary murine neuronal cultures, wildtype or ADAM10-deficient, were analyzed for levels of proteolytically secreted ectodomains, which resulted in the discovery of previously unknown neuronal ADAM10 substrate candidates.
Selected substrates (APP and L1Cam) and substrate candidates (NrCAM and Neogenin1) were further investigated in this thesis and validated by Western blot in ADAM10-deficient neurons.

4.1.1 NrCam and Neogenin1 are novel ADAM10 substrates

In the scope of the identification of 91 new ADAM10 substrate candidates using SPECS and mass spectrometric analyses, selected substrates and substrate candidates were chosen for further validation via quantitative Western blotting in primary mouse neurons.
Primary conditional ADAM10 knockout neurons were transduced on DIV 5 with Cre virus for recombination and knockout of ADAM10. A virus coding for GFP was used as transduction control. To additionally investigate a potential overlap between ADAM10 and BACE1 substrate cleavage, ADAM10-deficient neurons were treated with the BACE inhibitor C3 for 48 h. Conditioned neuronal supernatant (SN) and neuronal lysates were subjected to SDS-PAGE and analyzed by Western blot (Figure 7). Chosen proteins were selected according to the mass spectrometry discovery experiment and antibody availability and showed following reduction in the ADAM10-deficient secretome: NrCAM 70±6 %, Neogenin1 60±11 %, L1Cam 41±2 %. Soluble APP did not show a significant decrease upon ADAM10 knockout, because APP is predominantly cleaved by BACE1 in neuronal cell cultures, which show a high BACE1 expression (Kuhn et al., 2016).
Cre manipulation of conditional ADAM10 knockout neurons resulted in gene excision and thus absent expression of ADAM10 (Figure 6A, ADAM10). Investigation of APP processing showed that soluble APP (sAPP-α and -β) fragments are very slightly, but not significantly reduced in the SN of ADAM10-deficient neurons (Figure 7, 22C11, Cre) compared to GFP-control. At the same time APP levels were accordingly not significantly increased in the total cell lysate (2C11, Cre). Inhibition of BACE1 in addition resulted in a strong significant reduction of sAPP by 71±2 % (22C11, Cre+C3) and a strong 6.8-fold accumulation of APP in the lysate (2C11, Cre+C3). Thus, APP shedding is mainly driven by BACE1 but not ADAM10 in primary neuronal cell cultures. The soluble ectodomain of the newly identified substrate candidate NrCAM was significantly reduced to 30±6 % remaining level in the media of ADAM10-deficient neurons (NrCam SN, Cre). NrCAM full-length protein levels were significantly increased 2-fold in the total lysate (NrCam Lys, Cre). Additional inhibition of BACE1 mildly enhanced the reduction of soluble NrCAM in the SN to 20±7 % remaining (NrCam SN, Cre+C3), but also mildly reduced accumulation of full-length levels to 1.8-fold (NrCam Lys, Cre+C3). Neogenin1 (NEO1) showed a similar behavior: ADAM10 knockout

greatly reduced ectodomain shedding by 60±11 % and resulted in a 2.4-fold accumulation, however not significant, in the total lysate (Neogenin1 SN+Lys, Cre). BACE1 inhibition in ADAM10-deficient neurons led to an even stronger reduction of soluble NEO1 by 87±3 % and significant 2.6-fold increase inside the cell (Neogenin1 SN+Lys, Cre+C3).
L1CAM is an already established substrate of ADAM10 (Maretzky et al., 2005), but also known to be cleaved by BACE1 (Zhou et al., 2012). It therefore served as a positive control. As shown by Western blot, soluble L1CAM ectodomain was reduced by 41±2 % in the SN of neurons, when ADAM10 was no longer present (L1Cam SN, Cre). This reduction was significantly enhanced, if in addition to ADAM10, BACE1 was inhibited (14±5 % remaining) (L1Cam SN, Cre+C3). Both proteases affected the full-length levels in the total lysate, which increased by 43±15 % (L1Cam Lys, Cre) and 33±13 % (Cre+C3), but these changes did not meet the significance criteria.

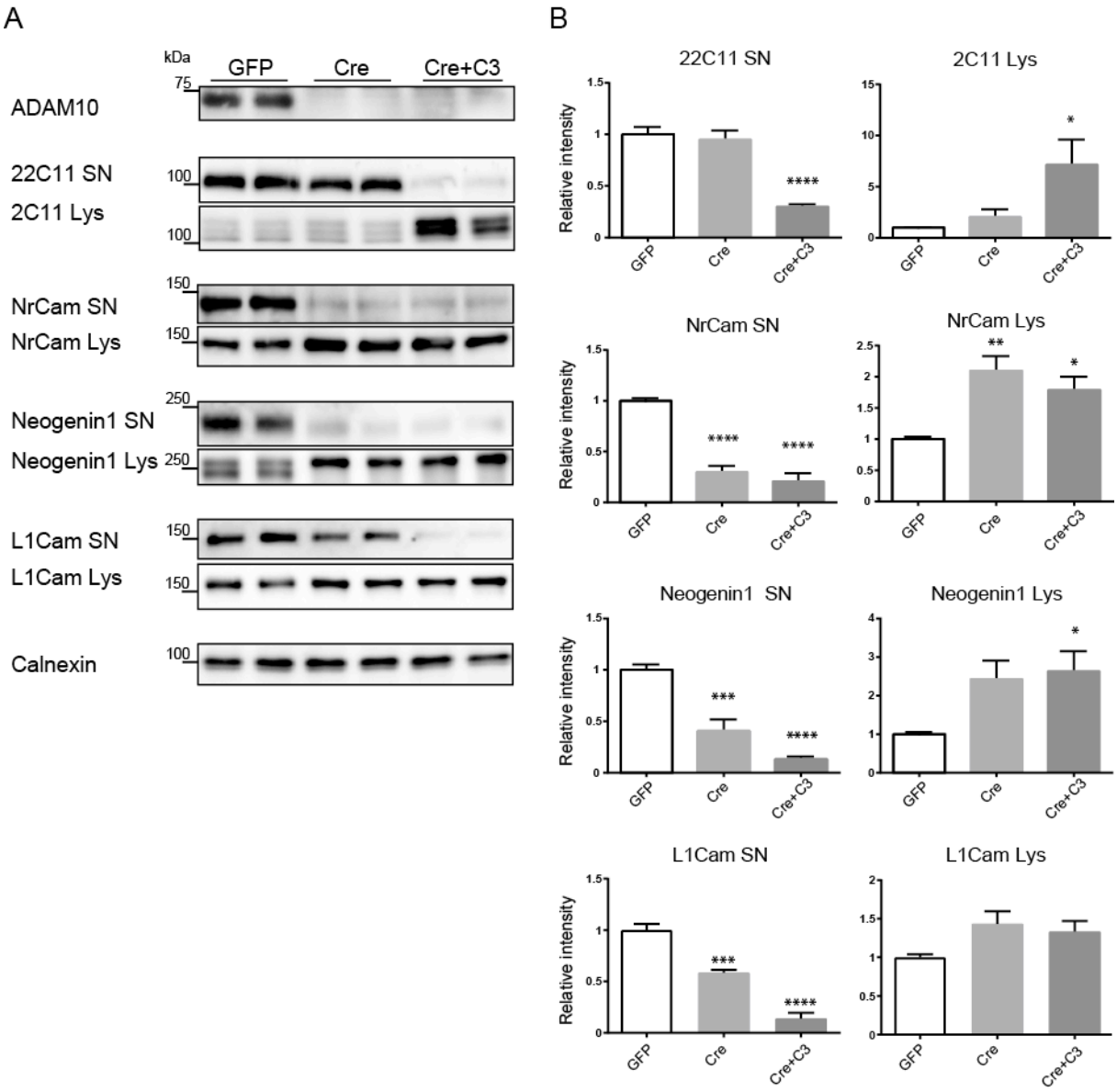

Figure 7: Additive effect of BACE1 inhibition in ADAM10 conditional knockout neurons.
A) Conditional ADAM10 knockout primary neurons were transduced with Cre virus to knock out ADAM10 expression. Control neurons were transduced with a virus containing GFP instead of Cre recombinase. In addition, neurons were treated with the BACE inhibitor C3 or DMSO as control and the proportions of ADAM10 and BACE1 cleavage of potentially common substrates was investigated by Western blot. Cre

treatment results in depletion of mature ADAM10, whereas control virus-infected neurons (GFP) show clear presence of the protease (ADAM10). Neuronal cell culture supernatant and total lysates were investigated for protein changes of shed and full-length forms. **B)** Western blot quantification of n=4; Signal intensities were normalized to calnexin and ratios of treated over ctrl (Cre/GFP; Cre+C3/GFP) were statistically evaluated using a one-way ANOVA and significance criteria of p=0.05. Bar graphs show values of the mean ± standard error of the mean (SEM) (SN=conditioned supernatant, Lys=Cell Lysate).

In summary, two newly identified substrate candidates NrCAM and NEO1 were validated as physiological ADAM10 substrates and point towards a function for ADAM10 in neurite outgrowth and regulation of axon targeting.

4.2 Analysis of the neuronal cell surface membrane protein-composition after pharmacological BACE1 inhibition

The following results are published in the journal *Molecular and Cellular Proteomics* with the title *Click chemistry-mediated biotinylation reveals a function for the protease BACE1 in modulating the neuronal surface glycoproteome* (Herber et al., 2018).

4.2.1 Surface-spanning protein enrichment with click sugars - establishing a new method for the specific labeling of cell surface membrane proteins

In 2012, the secretome of primary mouse neurons was investigated using the SPECS method upon BACE inhibition and revealed over 30 BACE substrate candidates (Kuhn et al., 2012). However, pharmacological inhibition of BACE most likely also strongly affects the cell surface proteome of neurons. Therefore the method ***SU****rface-****S****panning* ***P****rotein* ***E****nrichment with* ***C****lick* ***S****ugars* (SUSPECS) was developed to allow investigation of the surface membrane proteome without "contaminating" proteins of other membrane compartments. Similar to SPECS, the method exploits the fact that around 90% of the transmembrane proteins are N-glycosylated (Herber et al., 2018) and facilitates the separation and enrichment of glycosylated transmembrane surface proteins for subsequent analysis with a variety of downstream applications.

To specifically target N-glycosylated transmembrane proteins, the modified sugar tetra-acetylated N-azidomannosamine (Ac_4-ManNaz) was used. When metabolized by cells, Ac_4-ManNaz is converted to N-azido-sialic acid and incorporated into the glycans of newly synthesized proteins. As sialic acid is a terminal sugar moiety, the modified N-azido-sialic acid is easily accessible and represents a click chemistry-suitable target (Mende et al., 2016). Hence, labeled proteins were subsequently biotinylated via copper-free strain-promoted alkyne-azide Click Chemistry reaction with sulfo-dibenzylcyclooctyne (DBCO)-biotin (Laughlin and Bertozzi, 2007). The biotinylated alkyne (sulfo-DBCO-biotin) carries a sulfo-group, which provides the molecule with increased hydrophilic properties. It therefore should not permeate the hydrophobic cell membrane and only react with azide group-containing molecules outside of the cell. In addition, the reaction is performed at 4 °C to prevent/minimize endocytotic take up of sulfo-DBCO-biotin (Figure 8).

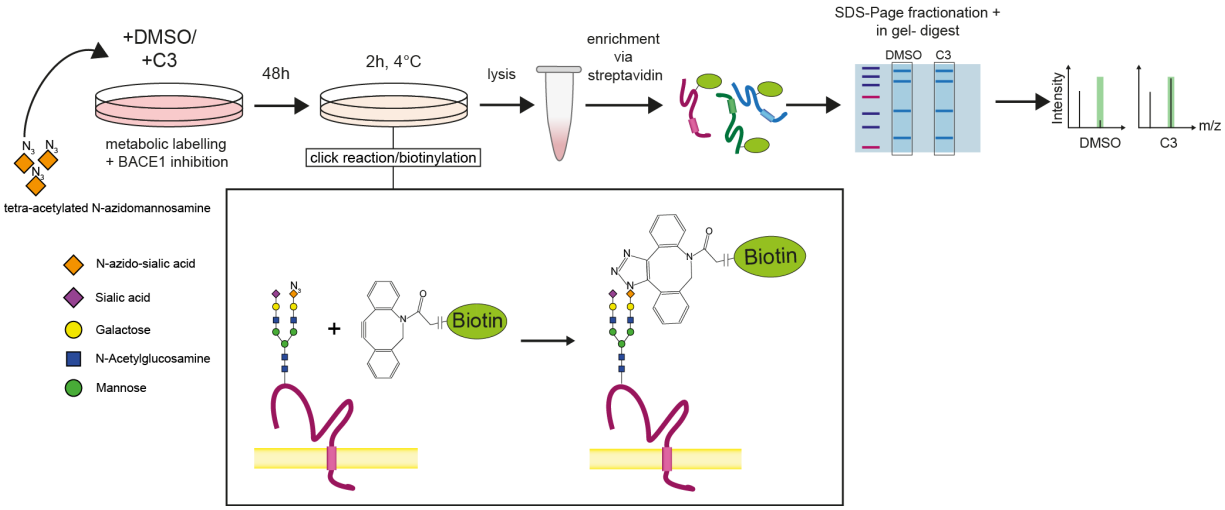

Figure 8: Workflow of SUSPECS method.
Cells were metabolically labeled in culture by supplementing the medium with tetra-acetyl N-azidoacetylmannosamine (Ac4-ManNAz). In parallel, cells were treated with BACE inhibitor (C3) or control (DMSO). Cells metabolized Ac4-ManNaz and incorporated the modified sugar into glycan structures of newly synthesized proteins as terminal N-azido-sialic acid. Click chemistry-mediated biotinylation was performed 48 h later for 2 h at 4 °C: The alkyne group of the sulfo-dibenzylcyclooctyne-biotin conjugate (DBCO) covalently reacted with the azide group of the azido-sialic acids of glycoproteins in the cell membrane (inset box). Biotinylated glycoproteins were enriched and purified with streptavidin-beads and separated via 1D-SDS-PAGE. After fractionation, in-gel digested proteins were analyzed by mass spectrometry using label-free quantification. (Herber et al. 2018)

To test this crucial requirement for specific surface transmembrane protein-labeling, biotinylated proteins were visualized by immunofluorescence. COS-7 cells were subjected to metabolic labeling of newly synthesized proteins with Ac_4-ManNaz and click chemistry-mediated biotinylation with sulfo-DBCO-biotin. After fixation and permeabilization of cells, fluorescein-conjugated streptavidin (streptavidin-dichlorotriazinylamino fluorescein (DTAF)) determined the localization of biotinylated proteins. Cell nuclei were stained with Hoechst (Figure 9). Confocal microscopy showed a clear cell surface staining with no obvious signal in the cytoplasm or intracellular organelles, such as the endoplasmic reticulum (ER) and Golgi, where glycosylation takes place (Figure 9A and B). Cells cultured without Ac_4-ManNAz did not show any streptavidin-DTAF positive signal (Figure 9B, lower panel), indicating the specificity of the fluorescent signal for biotinylated proteins. In addition, the absence of streptavidin-DTAF signal in Ac_4-ManNAz-free cells proves the selectivity of the click reaction. A magnified representation at different z-positions (bottom, mid, and top plane) through the cell confirmed a plasma membrane staining (Figure 9B). The bottom plane showed punctuated staining within the cell representing the cell's focal adhesion contacts to the surface and filamentous staining at the cell border depicting filopadia (Figure 9B, arrowheads). Signal in the magnified mid plane showed a clear rim with the nucleus in the middle. Notably, no cytoplasmic staining was observed, being in line with a cell surface staining. The signal gathered in the top plane is in agreement with the described staining pattern of the plasma membrane.
Concluding the results gained by the immunofluorescent readout, metabolic labeling with Ac_4-ManNAz in combination with click chemistry-mediated biotinylation using sulfo-DBCO-biotin selectively enabled targeting of glycosylated transmembrane proteins at the cell surface.

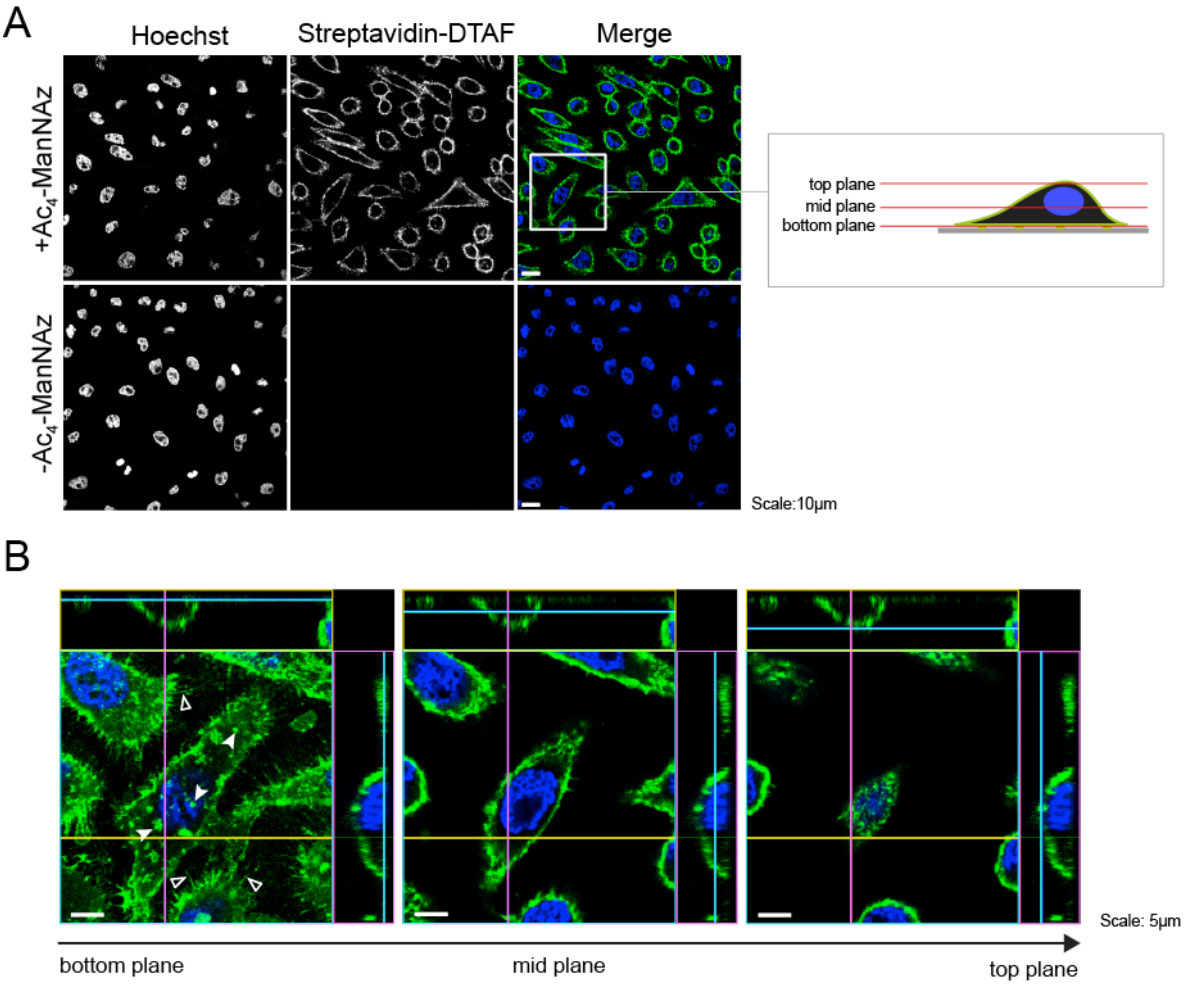

Figure 9: SUSPECS labels cell surface membrane proteins.
COS-7 cells were cultured with Ac4-ManNAz and subjected to click chemistry-mediated biotinylation with sulfo-DBCO-biotin. Fluorescein-conjugated streptavidin (streptavidin-DTAF, green) was used to detect biotinylated glycoproteins, nuclei were stained with Hoechst dye (blue). **A)** Cells cultured with Ac4-ManNAz showed a clear streptavidin-DTAF signal on the cell surface, no fluorescent signal was detected in the cytoplasm or internal structures of the cells (upper panel). Culturing cells without Ac4-ManNAz did not result in streptavidin-DTAF signal (lower panel). Scale bar: 10 µm. **Inset:** Schematic representation of three confocal planes shown in (B) with a higher magnification. **B)** The bottom plane shows streptavidin-DTAF signal (green) visualizing contact sites between the cells and the glass coverslip, such as focal adhesions (filled arrowheads) and filopodia (clear arrowheads). The mid plane is a magnification of cells as shown in (A): Streptavidin-signal around the cells represents the biotinylated proteins located in the cell surface. Nuclei are shown in blue. No streptavidin-signal was detected in the cytoplasm. The top plane demonstrates staining at the plasma membrane. Scale bar: 5 µm. (Herber et al. 2018)

4.2.2 SUSPECS enriches and identifies transmembrane glycoproteins at the neuronal cell surface

Surface-spanning protein enrichment with click sugars (SUSPECS) was applied to neuronal primary cultures, which were treated with the BACE inhibitor C3 or vehicle (DMSO) to investigate putative changes in the membrane protein composition after pharmacological BACE1 inhibition. The method involves LC-MS/MS analysis after labeling and enrichment of transmembrane proteins to provide a wide-ranged and explorative readout of the application. Primary neuronal cultures were prepared and subjected to metabolic labeling, BACE1 inhibitor and control treatment was administered and after 48 h cell surface proteins were biotinylated via click chemistry. After cell lysis, biotin-tagged proteins were captured

with streptavidin agarose, fractionated using SDS-PAGE and subjected to proteolytical in-gel digestion for subsequent LC-MS/MS analysis (Figure 8).
First, the general suitability of SUSPECS was assessed before protein changes depending on BACE1 inhibition were investigated. In 6 independent experiments, each comprising two conditions (C3-treated and DMSO-treated), the analysis yielded 4389 identified proteins. To increase the confidence of identifications, following criteria were set: 1) a protein had to be identified with at least two unique peptides and 2) a protein had to be identified in at least 3 out of 12 samples. Applying these requirements reduced the number to 3957 consistent protein identifications. Even though the method labels glycoproteins and was designed to extract transmembrane proteins, overall identified proteins did also contain non-glycosylated and non-transmembrane proteins. These nonspecifically enriched proteins might have been co-purified during the streptavidin enrichment either due to non-specific biotin labeling with sulfo-DBCO-biotin, their putative interaction with glycosylated or membrane proteins, or their unspecific binding to the beads. To circumvent such false positive extracted proteins, only glycosylated transmembrane proteins were included in the further analysis. For this, proteins were filtered according to reviewed Uniprot annotations. Uniprot is a database comprising protein sequence and functional information (www.uniprot.org). Comparing the SUSPECS-identified proteins to the Uniprot keyword 'glycoprotein' and the subcellular location terms for being a single-span membrane protein of type I, II, III or IV, as well as GPI-anchored and multi-pass membrane protein resulted in 691 proteins. The majority was represented by single-span type I membrane (40%) or multi-pass membrane proteins (45%) followed by single-span type II membrane (9%) and GPI-anchored proteins (5%). Two proteins were categorized as single-span type III membrane proteins and one as single-span type IV membrane protein. For five proteins double annotations were found and so they were separated into according categories (TM1/GPI, TM1/TM2, and TM1/Multi pass) (Figure 10A).
Although implementing these specifications reduced the number of proteins to a large extent, at the same time the reliability of the dataset was strongly increased. Hence, the 691 glycosylated transmembrane and GPI-anchored proteins were functionally classified according to Gene Ontology annotations using the *Protein Annotation through Evolutionary Relationship* (PANTHER)-tool (Mi et al., 2013). Proteins divided into functional categories of transporters (18.20%), receptors (17.57%), hydrolases (16.11%), transferases (8.79%), and signaling molecules (6.07%) among other categories (33.26%), which included cell adhesion molecules, extracellular matrix proteins and defense/immunity proteins (Figure 10B). The subcategorized groups represent proteins, which are known – according to Uniprot – to be located at the (neuronal) cell surface and therefore demonstrate the validity of SUSPECS as a method to investigate cell surface proteins. Moreover, a broad range of physiological functions could be assigned to the extracted transmembrane proteins.

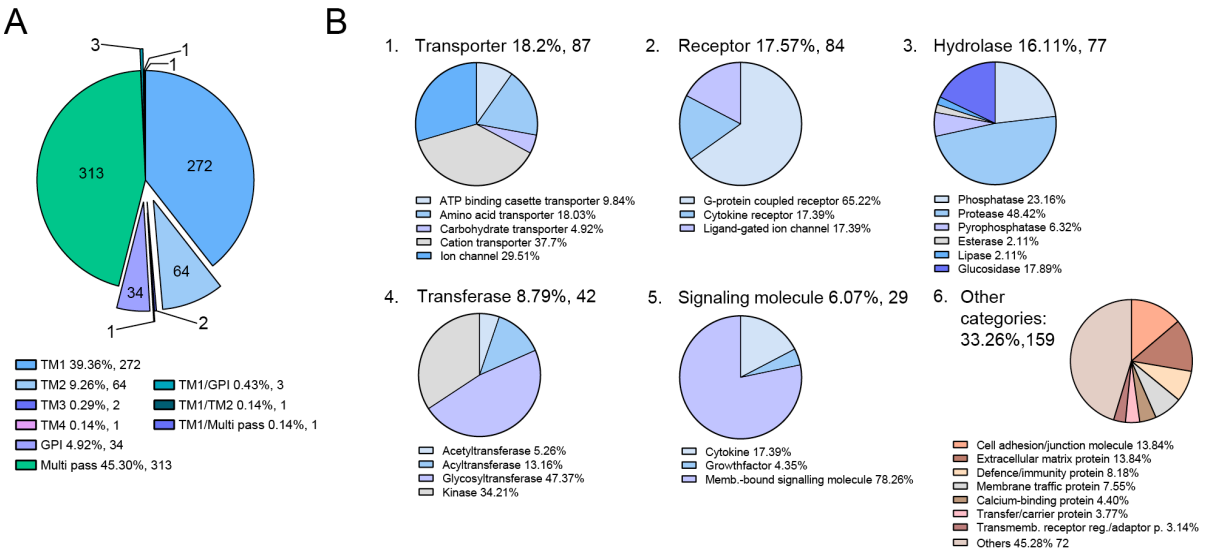

Figure 10: Topology and protein classification of identified transmembrane glycoproteins.
A) Identified glycosylated transmembrane proteins (691) were categorized using Uniprot 'subcellular locations': shown are single-pass type I membrane proteins (TM1), single-pass type II membrane proteins (TM2), single-pass type III membrane proteins (TM3), single-pass type IV membrane proteins (TM4), GPI-anchored (GPI) and multi-pass membrane proteins (Multi pass). Double annotations were separated into separate categories. **B)** PANTHER (protein annotation through evolutionary relationship) classification of identified proteins. Total number of proteins in each class is given and their percentage relative to all classified proteins that were functionally annotated in PANTHER. Note that individual proteins may fall into multiple functional classes in PANTHER. Sub-categorization of the 5 main protein classes as well as an overview of the remaining other categories is shown as pie charts under each class. Relative percentages of functional classes in each category are given below the pie charts.(Herber et al., 2018)

The Quantitative Analysis of Regulated Intramembrane Proteolysis (QARIP)-tool was used to assign all detected peptides to the according protein sequence (Ivankov et al., 2013). This analysis directly indicates whether an identified peptide originates from the extracellular, intracellular, or transmembrane part of a protein. SUSPECS-identified peptides were derived from both extracellular and intracellular protein domains (Figure 11). Transmembrane domains consist of hydrophobic amino acids and rarely contain tryptic cleavage sites, which makes them unlikely to be detected by LC-MS/MS analysis. However, in this analysis 20 multi-pass proteins showed peptides, which contained a few amino acids originating from the transmembrane region (Figure 11).
For three known BACE1 substrates (CHL1, L1CAM, and APLP1) peptides mapped to the juxta-membrane region and were found to indeed span the cleavage site for BACE1 (Figure 11). This was not surprising, since in 6 of 12 samples BACE1 proteolytic activity was inhibited. However, detection of these cleavage site-spanning peptides happened only in a few experiments and was not sufficient for differential quantification.

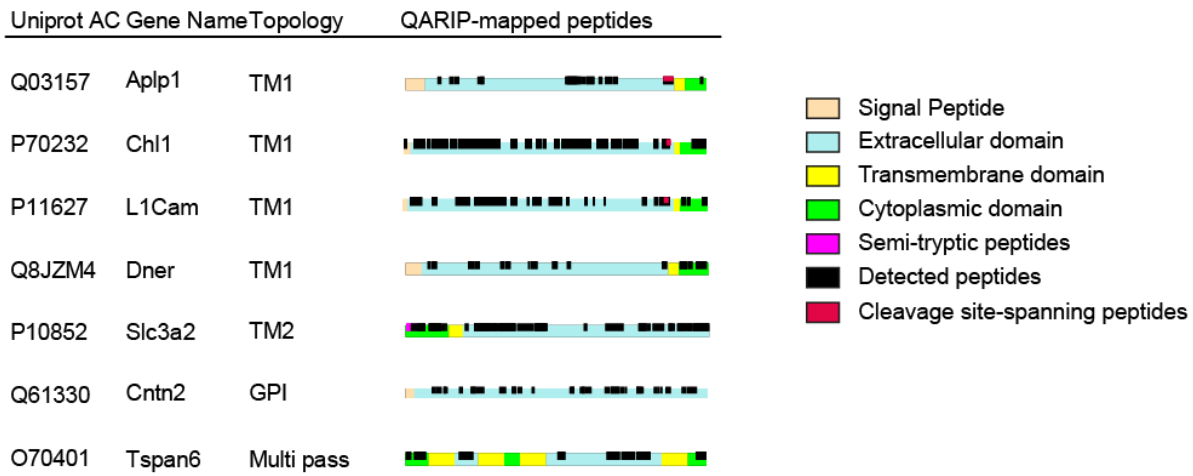

Figure 11: QARIP mapping of identified peptides.
Identified peptides were mapped to protein sequences using the QARIP-server. Protein domains and peptides are indicated by different colors (see legend). Selected proteins representative for different membrane topologies are shown: single-pass type I membrane proteins (TM1), single-pass type II membrane proteins (TM2), Glycosylphosphatidylinositol-anchored (GPI), Multi-pass membrane protein (Multi-pass). Identified peptides are shown as black bars and locate to the extracellular (light blue) and the cytoplasmic (green) domains. Semi-tryptic peptides are shown in magenta. The same accounts for the TM2 and the multi-pass proteins. Signal peptide and GPI-anchor are shown in beige. For the proteins APLP1, CHL1, and L1CAM peptides spanning the BACE1-cleavage site were identified and are shown as red bar. (Herber et al., 2018)

4.2.3 Loss of BACE proteolytic activity changes the protein composition of neuronal surface membranes

SUSPECS labelling and enrichment was performed on primary neurons, which have been treated with the inhibitor C3 or DMSO as vehicle control. Six biological replicates were analyzed by label-free quantification LC-MS/MS and indicate clear alterations in protein levels of plasma membrane proteins after pharmacological inhibition of BACE.
In order to be more accurate, only proteins that were identified and relatively quantified in both conditions (C3 and DMSO) in at least three experiments were considered for statistical evaluation. This resulted in 471 transmembrane glycoproteins. BACE preferably cleaves proteins with transmembrane type 1 and GPI-anchored topologies (Hemming et al., 2009) and mainly these proteins were expected to show increased or not changed protein levels upon BACE1 inhibition. Altered abundance of apparent non-substrates would result from and point towards secondary effects caused by BACE1 inhibition.
As expected, a majority of changed proteins were type 1 transmembrane and GPI-anchored proteins (45.2%) (Figure 12, blue dots), but still some single-span proteins with type 2 (8.5%, Figure 12, black dots) and type 3 (<1%, 1 protein, Figure 12, red dot) topology could be detected. Proteins with multiple transmembrane domains constituted the largest part of identified proteins (46.1%, Figure 12, grey dots). Overall, total of 106 transmembrane proteins showed significant changes of surface levels when applying a Student's t-test with p=0.05 as significance criterion. The abundance of six proteins was decreased upon BACE inhibition opposed to 100 accumulated proteins.
The statistical evaluation with the Student's t-test (p=0.05) was corrected for multiple hypothesis testing according to Benjamini-Hochberg using a 5 % false discovery rate (FDR) (Diz, 2011). 21 proteins met the stringent corrected significance criteria of q=0.0022 (Figure 12) and 16 of the 21 proteins were single-span transmembrane proteins (including GPI-anchored) (Table 13). In addition to single-span transmembrane proteins also multi-pass membrane proteins showed altered protein abundance after multiple hypotheses correction:

three had increased (LMBRD1, TSPAN6, TTYH3) and two (SCL38a3, UBAC2) decreased levels upon BACE1 inhibition (Figure 12).
Seven proteins showed a strong enrichment of more than 2-fold, of which six were single-span transmembrane type 1 (TM1) or GPI-anchored proteins, and more importantly, established and known BACE1 substrates: APLP1, CNTN2, CHL1, SEZ6, SEZ6L1, and APP (Dislich et al., 2015; Li and Sudhof, 2004; Pigoni et al., 2016; Vassar, 1999; Zhou et al., 2012). The seventh protein PLD3 is a single-span transmembrane type 2 (TM2) protein and controversially studied in AD (Cruchaga et al., 2014; Fazzari et al., 2017; Satoh, 2014). Three proteins accumulated to a lesser extent, between 1.5 and 2-fold. These moderately accumulated proteins are the before-mentioned multi-pass membrane proteins LMBRD1, TSPAN6, and TTYH3. Finally, nine proteins showed a mild increase in protein level of up to 1.5-fold. Among these mildly enriched proteins, another BACE1 substrate (L1CAM) and substrate candidate (TMEM132a) were identified (Hemming et al., 2009; Kuhn et al., 2012; Zhou et al., 2012). The remaining proteins in this mildly enriched category were mainly TM1 proteins (PODXL2, PTK7, CADM2, ROBO1, CNTN6) and one TM2 protein (SLC3a2) and represent putative BACE1 substrates, but accumulation could also be derived by secondary effects of BACE inhibition. In addition, the analysis also identified BACE1 substrate candidates, which did not change significantly and are only mildly or not changed, such as SEZ6L2 (Dislich et al., 2015; Hemming et al., 2009; Kuhn et al., 2012; Stutzer et al., 2013), LRRN1, GLG1, and NTM (Kuhn et al., 2012) (Figure 12).
Taken together, pharmacological BACE1 inhibition resulted in proteomic changes in neuronal cell surface membranes, which ranged from very mild to strong effects. Moreover, not only BACE1 substrates were affected, but also proteins, which are unlikely to be proteolytically cleaved by BACE1.

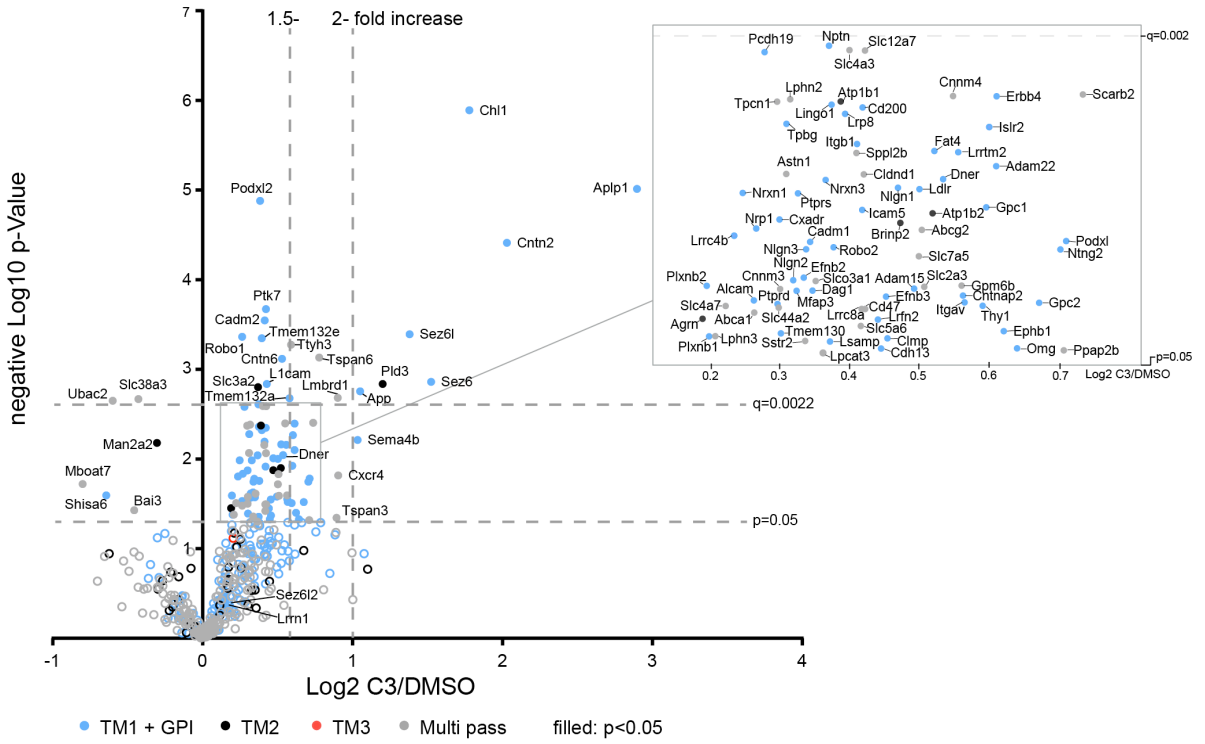

Figure 8: Pharmacological BACE1 inhibition selectively changes the neuronal surface glycoproteome.
Proteomic changes of glycosylated transmembrane proteins upon BACE1 inhibition visualized in a volcano plot. Dots and circles illustrate 471 quantified proteins. Blue: transmembrane type I and GPI-anchored proteins (TM1+GPI), black: transmembrane type II proteins (TM2), red: transmembrane type III (TM3) proteins, and gray: multi-pass membrane proteins (Multi pass). The log2 fold change of LFQ-intensity ratios (Log2 C3/DMSO) was plotted against the negative log10 the p-value (One-sample t-test). Filled dots represent proteins

with a p-value <0.05 (lower horizontal dashed line); Open circles are proteins with a p-value >0.05. Benjamini-Hochberg correction was applied to control for FDR with 5 % and is indicated by the upper dashed line (q=0.0022). 106 proteins have a p-value <0.05 and 21 proteins meet the FDR significance criteria of q<0.0022. Vertical dashed lines indicate a fold change of 1.5 and 2. Magnified box shows changes of proteins between p=0.05 and q=0.0022 up to a 1.74-fold increase. (Herber et al., 2018)

4.2.4 BACE1 inhibition significantly alters surface levels of only a subset of its known substrates

A subset of established BACE1 substrates, namely APLP1 (Li and Sudhof, 2004), CNTN2 (Dislich et al., 2015), CHL1 (Zhou et al., 2012), SEZ6 and SEZ6L (Pigoni et al., 2016)) showed a very strong accumulation of more than 2-fold in C3 treated neurons: the strongest increase of 7.5-fold was detected for amyloid precursor-like protein 1 (APLP1) levels. A 4-fold accumulation was observed for contactin-2 (CNTN2) followed by neural cell adhesion molecule L1-like protein (CHL1), which increased 3.4-fold in protein level. Seizure protein 6 (SEZ6) and its homolog seizure 6-like protein (SEZ6L) showed a positive change of 2.9- and 2.6-fold, respectively. The amyloid precursor protein (APP) (Vassar, 1999) increased to a moderate level of 2-fold expression. In contrast to that, other known BACE1 substrates like neural cell adhesion molecule L1 (L1CAM) (Zhou et al., 2012) and substrate candidates like transmembrane protein 132A (TMEM132a) (Hemming et al., 2009; Kuhn et al., 2012), Roundabout homolog 1 (ROBO1) (Hemming et al., 2009), Neurexin 1 (NRXN1) and Neuroligin 1 and 2 (NLGN1,2) (Kuhn et al., 2012) and Delta and Notch-like epidermal growth factor-related receptor (DNER) (Kuhn et al., 2012; Stutzer et al., 2013) showed a rather mild increase. For example L1CAM levels accumulated 1.3-fold and DNER levels 1.5-fold.

Application of a 5 % FDR cut-off increased the overall confidence of the dataset. However at the same time, this stringency introduced so-called false negative hits (Drachmann, 2008). The identified accumulated proteins, which were Student's t-test significant, but did not meet the Benjamini-Hochberg criteria, include such false negative hits and might still be BACE-dependent. Overall, 85 TM1 and GPI anchored proteins were enriched with p>0.05 but q<0.002 (Figure 12) and still represent potential BACE1 substrates. In line with this, the proteins NLG1, NLG2, NRXN1, and DNER were detected in this category and have been already proposed to be BACE1 substrate candidates (Kuhn et al., 2012; Stutzer et al., 2013). Worth mentioning, the surface levels of substrate candidates such as SEZ6L2 and LRRN1 were not significantly affected by BACE1 inhibition.

In summary, BACE1 inhibition altered the surface levels of its substrates in an irregular manner. Some substrates showed very strong effects of accumulation (more than 2-fold, e.g. APLP1), while others were only affected mildly (less than 1.5-fold, e.g. L1CAM). Putative substrates, such as DNER showed mild enrichment with less confidence or no enrichment in the case of SEZL2. The unequal accumulation dynamics of BACE1 substrates and substrate candidates indicate a differential regulation of transmembrane proteins by BACE1 proteolytic activity.

Table 13: Significantly changed single-pass membrane proteins and GPI-anchored proteins.
False discovery rate-corrected, significant proteins are sorted by their effect size (C3/DMSO). Proteins are shown with their Uniprot accession number (Uniprot AC), their topology, change in surface levels detected upon BACE1 inhibition over control (LFQ intensity ratio C3/DMSO). Proteins described as BACE1 substrates in literature are highlighted in blue (Herber et al. 2018).

Uniprot AC	Gene name	Protein name	Topology	LFQ intensity ratio C3/DMSO	p-value
Q03157	Aplp1	Amyloid precursor-like protein 1	Type 1	7.45	9.72E-06
Q61330	Cntn2	Contactin-2	GPI	4.08	3.88E-05
P70232	Chl1	Close homolog of neural cell adhesion molecule L1	Type 1	3.43	1.29E-06
Q7TSK2	Sez6	Seizure protein 6	Type 1	2.88	1.38E-03
Q6P1D5	Sez6l	Seizure 6-like protein	Type 1	2.60	4.06E-04
O35405	Pld3	Phospholipase D3	Type 2	2.30	1.45E-03
P12023	App	Amyloid beta A4 protein (APP)	Type 1	2.07	1.76E-03
Q922P8	Tmem132a	Transmembrane protein 132A	Type 1	1.49	2.11E-03
Q9JMB8	Cntn6	Contactin-6	GPI	1.44	7.61E-04
P11627	L1cam	Neural cell adhesion molecule L1	Type 1	1.35	1.46E-03
Q8BKG3	Ptk7	Inactive tyrosine-protein kinase 7	Type 1	1.34	2.13E-04
Q8BLQ9	Cadm2	Cell adhesion molecule 2	Type 1	1.33	2.85E-04
Q6IEE6	Tmem132e	Transmembrane protein 132E	Type 1	1.31	4.50E-04
Q8CAE9	Podxl2	Podocalyxin-like protein 2	Type 1	1.30	1.32E-05
P10852	Slc3a2	4F2 cell-surface antigen heavy chain	Type 2	1.29	1.57E-03
O89026	Robo1	Roundabout homolog 1	Type 1	1.20	4.33E-04

4.2.5 Secondary effects of BACE1 pharmacological inhibition

A majority of transmembrane surface proteins that were identified upon inhibition of BACE1 proteolytic activity with C3 were apparent non-substrates. 46.1 % of the proteins displayed in Figure 12 were multi-pass (Figure 11, grey dots) and 8.5 % were type 2 membrane proteins (TM2) (Figure 12, black dots). After correcting for multiple hypotheses with a false discovery rate of 5 %, five proteins with multi-pass and two with TM2 topology still showed a significant change in abundance (Table 14). For the multi-pass proteins accumulation and reduction of surface levels was observed. The three proteins LMBRD1, TSPAN6, and TTYH3 showed an intermediate extent of accumulation ranging from 1.5-fold (TTYH3) over 1.7-fold (TSPAN6) to 1.8-fold (LMBRD1), while SLC38a3 and UBAC2 decreased to 0.7-fold and 0.6-fold, respectively. Proteins with multiple transmembrane domains have not been observed to be processed by BACE1 and are unlikely to be direct protease substrates. Their alteration is therefore most possibly happening due to secondary effects of BACE1 inhibition. The TM2 proteins PLD3 and SLC3a2 both increased on the cell surface to 2.3-fold and 1.3-fold, respectively. In contrast to multi-pass proteins with more than one transmembrane domain, BACE1 is already known to cleave the TM2 protein ST6GAL1, suggesting that proteins with type 2 topology can be processed by BACE1 as well (Kitazume et al., 2001).

Table 14: False discovery rate-significant BACE1 non-substrates changed upon BACE1 inhibition. Proteins, which are unlikely or unknown to be proteolytically processed by BACE1, but show FDR-significant change of surface protein levels, are sorted by their effect size (C3/DMSO). Uniprot accession number (Uniprot AC), their topology, change in surface levels detected upon BACE1 inhibition over control (C3/DMSO) and their significance strength as p-value.

Uniprot AC	Gene name	Protein name	Topology	LFQ intensity ratio C3/DMSO	p-Value
O35405	Pld3	Phospholipase D3	TM2	2.29	1.45E-03
Q8K0B2	Lmbrd1	Probable lysosomal cobalamin transporter	Multi	1.86	2.07E-03
O70401	Tspan6	Tetraspanin-6	Multi	1.71	7.37E-04
Q6P5F7	Ttyh3	Protein tweety homolog 3	Multi	1.50	5.32E-04
P10852	Slc3a2	4F2 cell-surface antigen heavy chain	TM2	1.29	1.57E-03
Q9DCP2	Slc38a3	Sodium-coupled neutral amino acid transporter 3	Multi	0.74	2.15E-03
Q8R1K1	Ubac2	Ubiquitin-associated domain-containing protein 2	Multi	0.65	2.24E-03

In summary, inhibition of BACE1 proteolytic activity affected proteins, which are unlikely to be BACE1 substrates and led to significant changes of their protein levels in the neuronal cell surface membrane. Most likely, these changes represent secondary effects of BACE1 inhibition.

4.2.6 Surface and secreted levels of BACE1 substrates are differentially regulated

SPECS analysis of the secretome previously showed that not all substrates are cleaved by BACE1 to the same extent (Kuhn et al., 2012). Similar to the surface analysis with SUSPECS in this study, SPECS was performed on cultured primary neurons treated with the BACE inhibitor C3 or DMSO as control. For some substrates, BACE1 inhibition almost completely abolished shedding of the proteins' ectodomains into the supernatant, such as SEZ6L, SEZ6, and APLP1. For other substrates, the reduction of ectodomain shedding was less prominent, because they were cleaved by other proteases in addition to BACE1: APP, CNTN2, and DNER are also processed by ADAM10 and therefore inhibition of BACE1 cleavage only resulted in a mild reduction of secreted ectodomains.

To investigate, the correlation between protein levels at the cell surface and their according proteolytically released fragments, data from SPECS and SUSPECS (as described in section 4.2.4) was evaluated in a meta-analysis. Effect sizes of surface increase and decrease in the sectretome after BACE1 inhibition were compared (Figure 13).

The six BACE1 substrates, which increased strongest upon C3 treatment, were APLP1, CNTN2, CHL1, SEZ6, SEZ6L, and APP (7 – 2-fold increase). However only four of them also showed a prominent decrease in the secretome: SEZ6L, SEZ6, and APLP1 were almost completely absent (4 % SEZ6L, 8 % SEZ6, and 11 % APLP1 remaining) and CHL1 was reduced to 35 % compared to the control (Figure 13). In contrast to that, CNTN2 showed only a reduction of cleavage down to 64 % in the secretome, though the full length protein accumulated more than 4-fold at the surface. A likewise, but less drastic, trend was seen for APP, which showed an accumulation of 2-fold in the membrane after BACE1 inhibition, but a reduction of ectodomain shedding by only 33 % (67 % remaining). An opposite effect was observed for the mildly increased substrate L1CAM (1.35-fold), which was decreased by 79 % in the secretome (21 % remaining). Similar to L1CAM, also the BACE1 substrate candidates GLG1, LRRN1, and NTM showed no reasonable correlation between changes in the secretome and at the cell surface. Their full-length levels at the cell surface did not reveal

a significant alteration and showed almost no or only a very mild increase of 1.1 – 1.18-fold. However, their ectodomains were reduced in the range of 67 – 79 % in the secretome.
Proteins that were defined as *unchanged* in the secretome by Kuhn et al. mainly showed only a mild change at the surface, such as PODXL2, TMEM132E, PTK7, and ROBO1 (1.2 – 1.34-fold increase). However, for some proteins, such as GPC1 and ADAM22, an accumulation of more than 1.5-fold was observed at the surface.
Taken together, this analysis showed that BACE1 substrates are differentially affected by BACE1 inhibition in regards to their full-length levels on the cell surface and secreted ectodomain levels in the secretome.

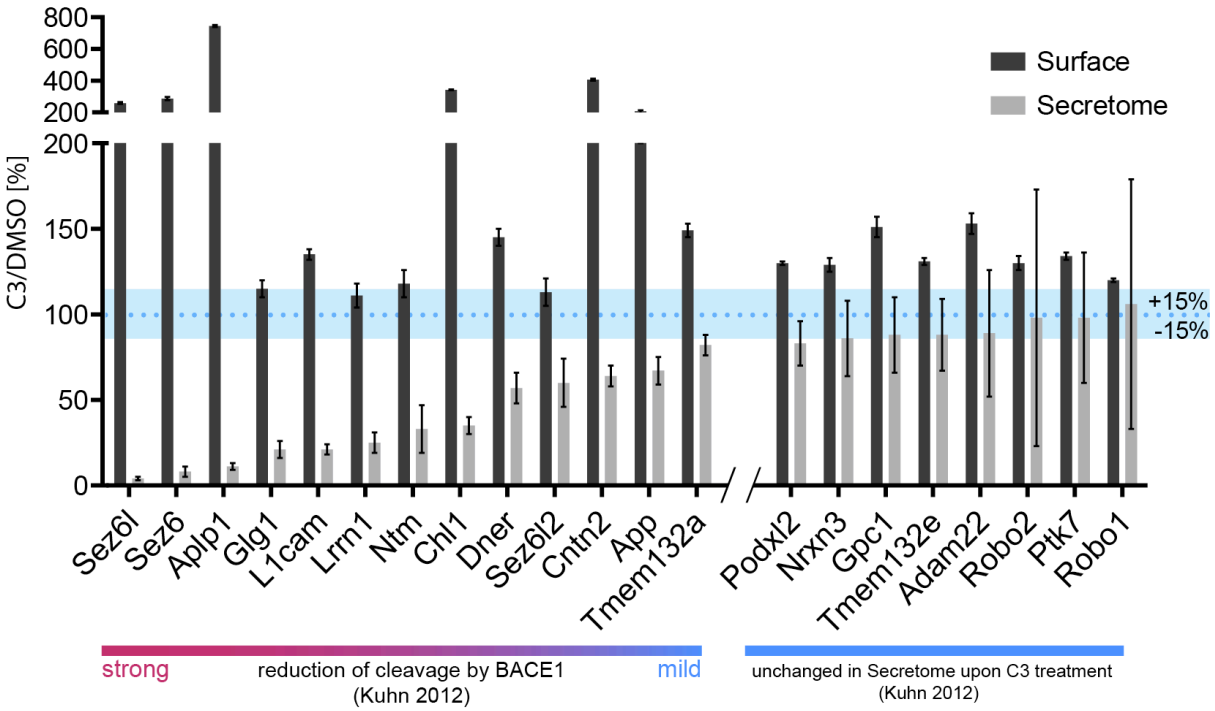

Figure 93: Meta-analysis of changes in surface proteome and secretome after BACE1 inhibition.
Protein abundance changes on the cell surface after BACE1 inhibition (as shown in Figure 12) were compared to their changes in the secretome (Kuhn et al., 2012) for all BACE1 substrates and substrate candidates. Proteins are sorted from a strong reduction in the secretome (light grey bars) to a mild reduction and no change (arbitrary criteria of ± 15 %, blue bar; blue dotted line indicates 100 % protein level in control conditions) and compared to their protein level on the surface (dark grey bars). (Herber et al., 2018)

4.2.7 A combination of secretome and surface proteome analysis can improve substrate identification of proteases

Investigating the secretome has the advantage of identifying direct substrates of a protease (Muller et al., 2016). However, it also comes with certain drawbacks: One being that a substrate can be cleaved by more than one protease. A compensatory effect due to loss of cleavage by one protease can lead to an up-regulated processing by another protease, as it was shown for ADAM10 and BACE1 and their common substrate APP (Colombo et al., 2013). Hence, the secretome provides valuable information, if the proteolytic effects are very strong or have high substrate-protease selectivity. Therefore, some BACE1 substrates might have been missed by SPECS, because their ectodomain levels were not (strongly enough) reduced, due to such compensatory mechanisms. Additionally, some substrates might be shed to a very low extent and their ectodomains were just below detection limit in secretome analysis.

Moreover, during the SPECS sample preparation procedure, serum albumin is still highly abundant. Therefore, the BSA band has to be cut out and discarded before the in-gel digestion procedure, resulting in the loss of proteins, which are running at a similar molecular weight in the SDS-PAGE. In SUSPECS sample preparation, cells are washed with PBS prior to biotin labeling which almost completely removes albumin and might therefore compensate for the loss of information in SPECS analysis. Additionally, the abundance of many proteins in the secretome might be below detection limit, but could be well identified at the cell surface.
Indeed, upon BACE1 inhibition in primary neurons, SUSPECS identified a significant accumulation (+ >30 %) in the surface for 29 proteins, which were not significantly reduced (- >30 %) in the secretome (Figure 14). 18 of these proteins, such as CNTN-6, ERBB4 or CD200, have not been detected in the secretome analysis and may therefore represent additional novel BACE1 substrates. The other way around, SPECS identified 17 proteins, with significant reduction in the secretome that did not significantly accumulate during SUSPECS analysis. Seven of these 17 proteins were identified exclusively with SPECS analysis. However, substrates that were strongly affected by the loss of BACE1 cleavage, such as APLP1, CHL1, SEZ6, SEZ6L, and APP, were identified in both analyses (Figure 14). A combination of SPECS and SUSPECS may therefore provide substrate information, which would be incomplete by only applying one of the two methods.

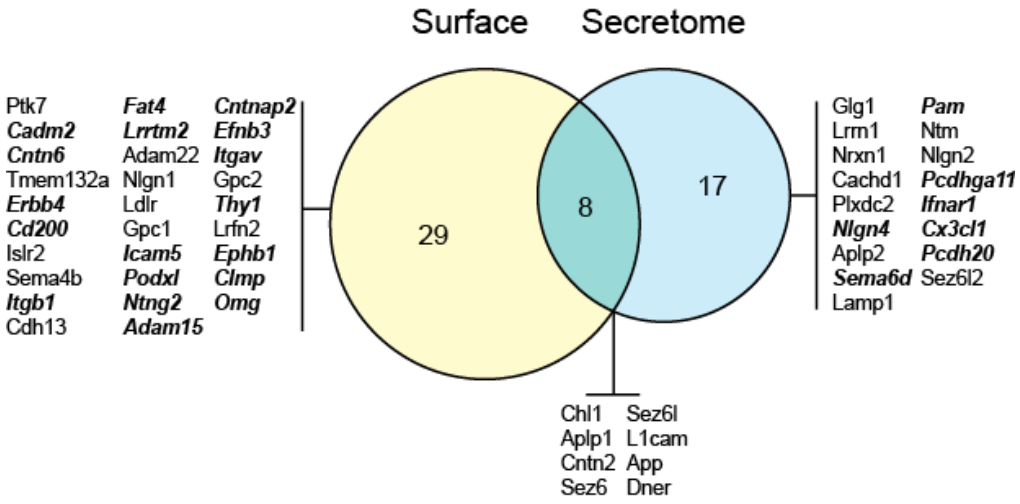

Figure 14: Substrate candidates identified in surface and secretome analysis of BACE1 inhibited neurons. Substrate candidates, i.e. filtered glycosylated transmembrane proteins, of SUSPECS (surface) and SPECS (secretome) analyses were overlapped. Proteins were included, if they met the criteria of 1) significant change ($p<0.05$) and 2) change of +30 % in surface, -30 % in secretome. Substrate candidates, which were exclusively identified in only one of the analyses, are printed in ***bold italic.***

4.3 BACE2-deficient secretome changes of primary glia cultures with BACE1 knockout-background

Following data was originally published in the journal *Life Science Alliance* under the title *BACE2 distribution in major brain cell types and identification of novel substrates* (Voytyuk et al., 2018b).

In the scope of a collaborative study with I. Voytyuk (Department of Neurosciences, Katholieke Universitet Leuven, Belgium) BACE2 substrates were identified using BACE1 knockout primary glial cells, which were treated with the unselective BACE1 and BACE2

inhibitor Compound J (CpJ) or vehicle. To this aim, exclusive BACE2 substrates should be identified in a background of BACE1 knockout.
Samples were received from the collaborator, processed according to secretome enrichment with click sugars (SPECS) procedure, and analyzed with LC-MS/MS. Label-free quantification yielded 246 proteins identified with at least two unique peptides in three biological replicates (3 samples CpJ-treated and 3 samples vehicle treated) (Figure 15). Subsequent data analysis matching for Uniprot annotations identified 191 glycoproteins (Figure 15A, B). The majority of identified proteins was annotated to be secreted and membrane-type proteins, which consisted mainly of GPI-anchored and transmembrane type I and type II proteins (Figure 15B, C). Of the 246 relatively quantified proteins, 16 showed a significant change in protein abundance (Figure 15A, red dots and circles), but only six proteins decreased and are therefore likely to be proteolytic BACE2 substrate candidates. Four of the six decreased proteins showed a reduction of 30 % or more (Figure 15, red filled dots): VCAM1 (20 % remaining), DNER (27 % remaining), FGFR1 (52 % remaining), and PLXDC2 (65 % remaining). Further, all four proteins are transmembrane type I proteins and present large extracellular domains. A QARIP analysis revealed that the identified peptides for VCAM1, DNER, FGFR1, and PLXDC2 mapped exclusively to their ectodomains, which provides evidence for the proteolytic secretion of these proteins (Figure 15D).

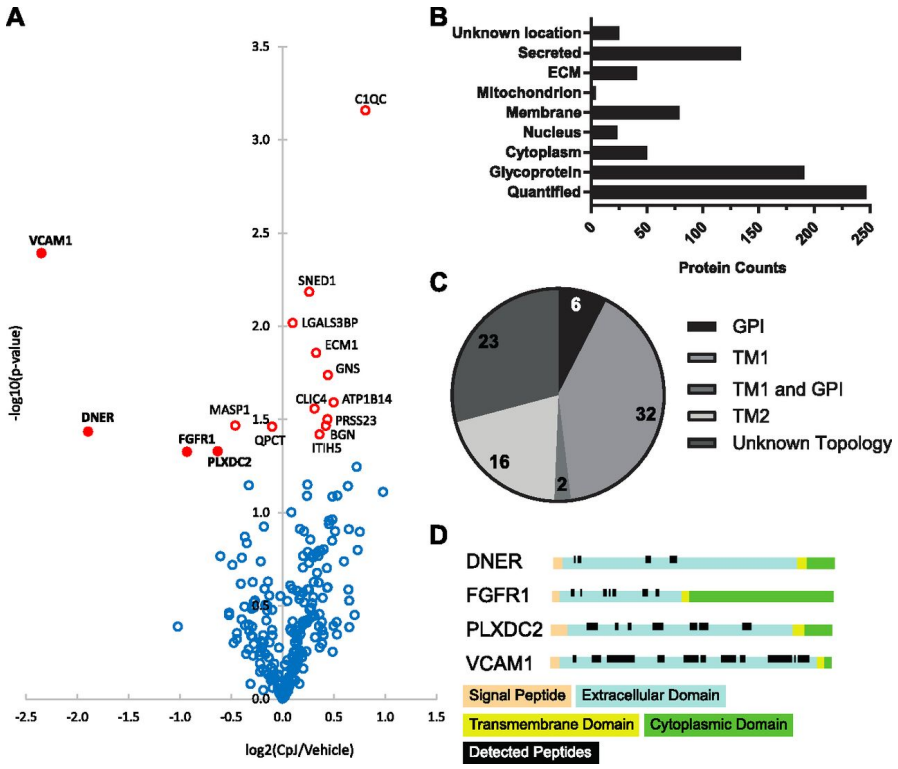

Figure 15: Changes in the secretome of BACE1 knockout glia upon BACE2 inhibition.
A) Proteomic analysis of BACE1 knockout glia treated with the BACE1/2 inhibitor CpJ or vehicle (n=3). For identified proteins (246 proteins), the negative log10 of the p-value was plotted against the log2 transformed LFQ-intensity ratio (CpJ/vehicle). Student's t-test criteria were applied and significant proteins with $p<0.05$ are visualized in red (16 proteins). Proteins labeled in **bold** showed a reduction of more than 30 % (4 proteins) **B)** Categorization of identified proteins according to reviewed Uniprot annotations using subcellular location-terms and glycosylation-keywords. **C)** Topology of identified transmembrane proteins according to reviewed Uniprot annotations. **D)** QARIP analysis of DNER, FGFR1, PLXDC2, and VCAM1: identified peptides (black boxes) mapped exclusively to the proteins' extracellular domains (blue stretch).(Voytyuk et al., 2018b)

4.4 MT5-MMP substrate identification – a proteomic approach

Recently, membrane-type 5 matrix metalloprotease (MT5-MMP) was demonstrated to cleave APP, generating a small proteolytic fragment (Aη-α) with detrimental impact on neuronal activity (Willem et al., 2015). At the same time, MT5-MMP deficiency was shown to have beneficial effects on Alzheimer's disease (AD) pathology, gliosis, and inflammation (Baranger et al., 2016b). Especially the letter findings and the function of MT5-MMP as APP-cleaving enzyme put the protease in position as potential therapeutic target for AD.
To understand the (patho-)physiological involvement of MT5-MMP a broad proteomic approach was used in this thesis to identify substrates in neurons.

4.4.1 Neuronal secretome does not significantly change upon MT5-MMP knockout

Secretome protein enrichment with click sugars (SPECS) allows enrichment and purification of secreted and shed proteins inside cell culture supernatants (Kuhn et al., 2012). Through the comparison of proteolytically active to inactive conditions with downstream mass spectrometric analysis, it allows identification and quantification of substrate repertoires of membrane bound proteases. A shed substrate – detectable in normal conditions – will be no longer detected in the protease-deficient secretome due to loss of shedding.
To determine the MT5-MMP-dependent secretome, primary MT5-MMP knockout neurons were compared to wildtype littermates. Mice heterozygous for the MT5-MMP knockout allele were mated in order to obtain wildtype and knockout animals in the same F1 generation. Primary neuronal cultures were extracted on embryonic day 16.5 from cortex including hippocampus. Cortices from embryos were kept separated for neuron preparations and genotyped after the extraction using embryonic tissue. Day *in vitro* (DIV) 5 neuronal cultures were subjected to metabolic Ac_4-ManNAz labeling and supernatant was collected 48 hours later. SPECS usually requires $40x10^6$ cells per condition, however, to compare littermates and still have as much material as possible, two embryos were combined for one condition resulting in approximately $20x10^6$ cells. Conditioned media obtained from two neuronal cultures with the same genotype were pooled in order to collect enough material for subsequent secretome analysis (Figure 16A). After collection of supernatants, Western blot analysis was used to confirm the absence of MT5-MMP protein in neuronal cultures (Figure 16B).

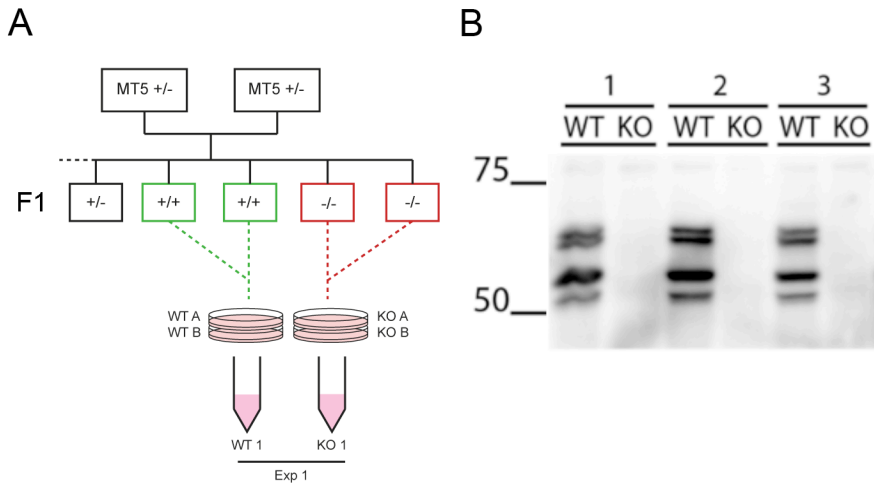

Figure 16: MT5-MMP SPECS experiments.
A) Mouse mating scheme for MT5-MMP SPECS experiments. Mice heterozygous for MT5-MMP-deficiency (MT5+/-) were mated. MT5-MMP wildtype (MT5+/+) and MT5-MMP knockout (MT5-/-) littermates in the F1

generation were used for experiments. Conditioned medium from 2 neuronal cultures was pooled. **B)** Representative Western blot analysis and validation of MT5-MMP deletion in neuronal cultures. In contrast to MT5-MMP knockout (KO), wildtype (WT) samples show a clear protein signal. Band pattern indicates different maturation states of the protease.

Conditioned media were prepared according to the SPECS procedure and subjected to SDS-PAGE fractionation with subsequent in-gel tryptic digest. Secretome samples were measured with LC-MS/MS and label-free protein quantification was performed using MaxQuant.
Overall, MT5-MMP secretome analysis identified 944 proteins with at least 2 unique peptides (UPs). To increase the confidence of the dataset, proteins were considered for quantification, if they were identified in both conditions (MT5 WT and KO) in at least 3 out of 5 experiments, which yielded 295 proteins (Figure 17). In secretome analyses, proteins do not necessarily have to be identified in both conditions to be quantified: A substrate, which is exclusively shed by one protease, would no longer be detected upon loss-of-cleavage (MT5 KO) and therefore only be detected in the control group (MT5 WT). However, analysis of the MT5-MMP secretome did not result such exclusive substrates.
Although SPECS metabolically labels glycan structures and utilizes glycosylation during enrichment, the number of totally identified proteins may be higher and also contain non-glycoproteins and secreted proteins. These proteins may have bound unspecifically to the high capacity streptavidin beads or were potentially co-purified due to their interaction with glycoproteins. Therefore, proteins were considered for quantification, if they were annotated and reviewed as 'glycoprotein' in the Uniprot database. This criterion resulted in 198 relatively quantified glycoproteins (Figure 17). In other words, 67.1 % of all quantified proteins were glycosylated. The remaining 97 proteins may still be glycoproteins, but not yet described as such. Since reviewed annotations have been applied as filter criteria, they therefore did not meet the requirements.

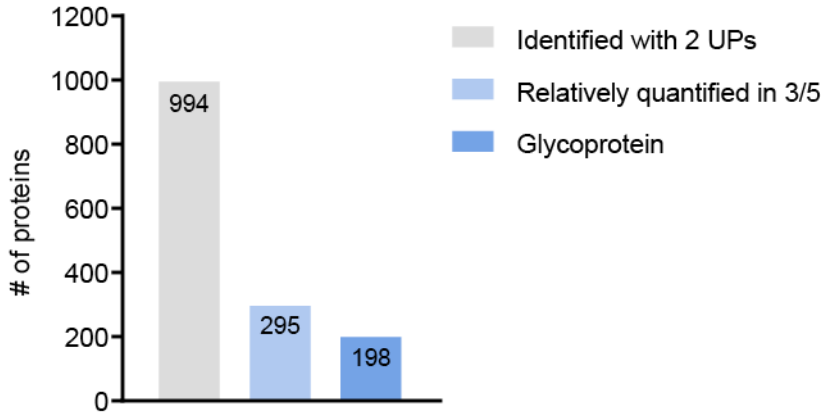

Figure 17: Identified MT5-MMP secretome proteins.
Analysis yielded in 994 proteins that were identified with at least 2 unique peptides (UPs) (grey) of which 295 were present in both conditions (MT5 WT and KO) in at least 3 out of 5 experiments and were relatively quantified (bright blue). Of these 295 quantified proteins, 198 (67.1 %) are annotated as glycoproteins (dark blue) according to Uniprot keywords.

To further categorize the glycoproteins, they were classified using reviewed Uniprot annotations according subcellular location terms (Figure 18A). Proteins fell into following categories: Cytoplasm (10 proteins), nucleus (9 proteins), membrane (138 proteins), mitochondrion (2 proteins), secreted (66 proteins), and for 4 glycoproteins localization was unknown. Some glycoproteins had more than one annotation and fell into two or more classes. Noteworthy, the majority of quantified glycoproteins was annotated as membrane

proteins and contained a transmembrane domain (Figure 18B). Figure 18B shows the membrane orientation of transmembrane glycoproteins. The majority were type I proteins (81 proteins), followed by 23 proteins with type II orientation. 16 proteins were anchored in the membrane via a GPI-anchor and 8 proteins had two or more transmembrane domains (multi-pass). For 12 proteins no membrane orientation other than being 'membrane-spanning' was annotated (unknown).

The LFQ intensities of the 198 quantified glycosylated proteins were used to calculate the ratio of relative protein abundance in MT5 KO and MT5 WT samples and differences were tested for statistical significance using a Student's t-test with significance criteria of p=0.05 (Figure 18C, lower dashed line). Results were visualized in a volcano plot (Figure 18C). Surprisingly, none of the identified proteins showed significant reduction. Only one protein (ST6GAL2) showed a significant accumulation of 0.6-fold. To test for possible false positive results, the dataset was subjected to multiple hypotheses testing according to Benjamini-Hochberg with a false discovery rate (FDR) of 5 %. After adjusting the significance threshold to q=0.00036 (Figure 18C, upper dashed line), ST6GAL2 did no longer meet the significance criteria and is therefore likely to be a false positive hit.

In summary, though secretome analysis yielded a reasonable number of total and glycosylated identified proteins, changes in the secretome of MT5-MMP knockout neurons were very mild and overall not significant.

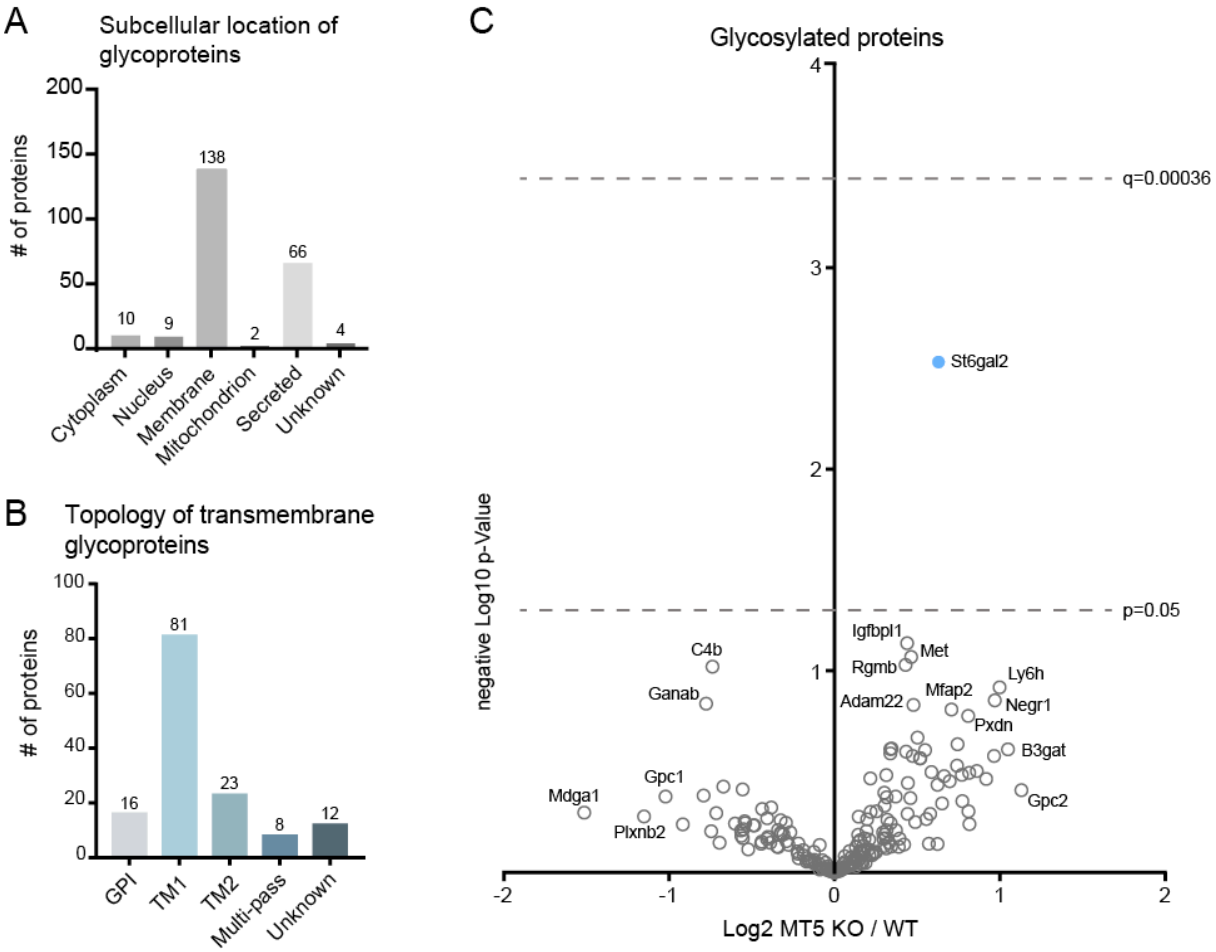

Figure 18: Analysis and quantification of MT5-MMP-dependent secretome.
A) Subcellular location of quantified glycoproteins according to reviewed Uniprot annotations. Cytoplasm: 10 proteins, nucleus: 9 proteins, membrane: 138 proteins, mitochondrion: 2 proteins, secreted: 66 proteins, unknown: 4 proteins. Note that proteins may fall into two or more categories. **B)** Within the 138 proteins

annotated to the membrane (A) 81 showed transmembrane type I (TM1) and 23 type II (TM2) orientation. 16 proteins were GPI-anchored (GPI) and 8 proteins had two or more transmembrane domains (multi-pass). 12 proteins were annotated to be 'mambrane-spanning' without further classification (unknown). (2 proteins were annotated as both TM1 and GPI) **C)** Proteomic changes in the secretome of MT5-MMP knockout neurons compared to wildtype. Fold-change (Log2 MT5 KO/WT ratios) of relative protein abundance was plotted against the negative Log10 of the p-value. ST6GAL2 was the only protein to be Student's t-test significant, but did not remain significant after FDR correction according to Benjamini-Hochberg. Lower dashed line marks the significance threshold of p=0.05. Statistical significance was tested with Student's t-test; significance criteria p=0.05. Benjamini-Hochberg corrected significance threshold of q=0.00036 (upper dashed line).

4.4.2 Proteomic analysis of mouse cerebrospinal fluid of MT5-MMP knockout in the background of an Alzheimer's disease mouse model

Depletion of MT5-MMP in mice did not lead to developmental abnormalities or apparent histological defects in the nervous system (Komori et al., 2004). However, in pathological conditions the knockout of MT5-MMP displays clear phenotypes: The protease is involved in neuronal plasticity after sciatic nerve injury (Komori et al., 2004) and is important in the peripheral nervous system, where it mediates an inflammatory response to interleukin-1 beta (IL-1β) and tumor necrosis factor-alpha (TNF-α) (Folgueras et al., 2009). Moreover, in the context of Alzheimer's disease (AD) MT5-MMP-deficiency was shown to ameliorate the pathological outcome resulting in reduced Aβ-burden, less neuroinflammation, and cognitive benefits (Baranger et al., 2016b).

To approach the role and involvement of MT5-MMP in the brain under physiological and pathological conditions, a mass sprctrometry based proteomic analysis of mouse cerebrospinal fluid (CSF) was performed. For this, MT5-MMP knockout and wildtype animals were crossed to the AD mouse model 5xFAD. 5xFAD mice carry five mutations, which are known to cause familial AD (Oakley et al., 2006). CSF was collected from wildtype animals (WT) (n=8), MT5-MMP knockout (MT5 KO) (n=8), 5xFAD (n=10), and double transgenic 5xFADxMT5-MMP KO (5xFAD-MT5 KO) (n=9) animals at 7 months of age and analyzed with LC-MS/MS after tryptic digestion. The chosen age represents a symptomatic time point, at which 5xFAD mice show advanced Aβ plaque deposition, gliosis, cognitive deficits, and impaired long-term potentiation (LTP) (Kimura and Ohno, 2009; Oakley et al., 2006). CSF is topologically equivalent to the extracellular space. Secreted proteins and extracellular protein domains derived from proteolytic ectodomain shedding of all brain cells are released into it and CSF therefore represents the *in vivo* secretome of the whole brain. Rather than cell type-specific substrates, proteomic CSF analysis can elucidate global changes in a preserved network of different cell types *in vivo*.

The analysis of CSF by LC-MS/MS yielded 1535 identified proteins with at least 2 unique peptides. Proteins were considered for further quantification, if they have been detected in at least three samples of each genotype. This requirement resulted in 1147 quantified proteins in the 5xFAD CSF, 968 quantified proteins in the double transgenic 5xFAD-MT5 KO CSF, 954 identified proteins in the MT5 KO CSF and 966 identified proteins in WT CSF. Among the 1535 identified proteins, 1195 were detected in at least three samples of one or more genotypes (Figure 19A). Those proteins were considered as consistently identified and were matched against the reviewed subcellular location database of Uniprot (Figure 19B). The majority of quantified proteins was annotated to be membrane type or secreted proteins: 408 membrane type proteins and 386 secreted ones. However, also a number of proteins had cytoplasmic origin (320 proteins). For 177 proteins, no annotation regarding their subcellular localization was found (unknown). Only few proteins were annotated to be located in the nucleus (117 proteins) or mitochondria (47 proteins) (Figure 19B).

The CSF analyses by mass spectrometry yielded a high number of protein identifications with reproducible and reliable quantifications among the four genotypes. In the following, the four conditions will be compared to each other.

A

	5xFAD	5xFAD-MT5 KO	MT5 KO	WT
Total IDs min. 2UPs	1535			
IDs in min. 3 samples	1195			
IDs in min. 3 samples	1147	968	954	966

B

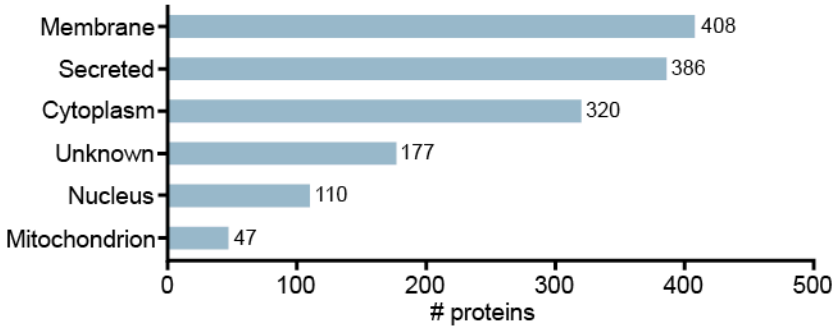

Figure 19: Mass spectrometric analysis of cerebrospinal fluid (CSF).
5xFAD mice were crossed to MT5-MMP knockout (MT5 KO) animals and CSF was collected from all resulting genotypes at 7 months of age. **A)** LC-MS/MS analysis of the four sample groups 5xFAD (n=10), double transgenic 5xFAD-MT5 KO (n=9), MT5 KO (n=8), and wildtype animals (WT, n=8) identified 1535 proteins with at least two unique peptides. 1195 proteins were identified in at least 3 samples within at least one genotype and are regarded as overall quantified. Within the separate sample groups 1147 proteins were quantified in at least three 5xFAD samples, 968 proteins at least three 5xFAD-MT5 KO samples, 954 in at least three MT5 KO, and 966 in at least three WT samples. **B)** 1195 identified proteins were compared Uniprot database reviewed annotations and categorized according to their subcellular location. Proteins fell into following categories: Membrane (408), secreted (386), cytoplasm (320), unknown (no annotation available, 177), Nucleus (110), and mitochondrion (47). Note that for some proteins more than one annotation is deposited.

4.4.2.1 MT5-MMP knockout only mildly affects the CSF protein composition under physiological conditions

To assess the effects MT5-MMP knockout has on the protein composition of the CSF, MT5-MMP knockout (MT5 KO) CSF was compared to wildtype (WT) CSF. Proteins were considered identified, if they were detected with at least 2 unique peptides. As further requirement for relative quantification, proteins had to be identified in at least three samples in both sample groups, i.e. 3 MT5 KO samples and 3 WT samples. Applying these criteria, 908 proteins were relatively quantified in both groups. Label-free quantification (LFQ) intensity values were log2-transformed and changed protein abundance was calculated by forming the ratio between LFQ intensity means of MT5 KO and WT. The significance of proteins with changed abundance was evaluated using a Student's t-test (p=0.05) and corrected for a false discovery rate of 5 % (FDR=0.05, s0=0.1). In addition, significance was defined depended on the effect size of the change by an arbitrary cut off of s0=0.1. S0 is an artificial value within the group variance. It controls the relative importance of the t-test p-value and the difference between the means of the sample groups. At s0=0 only the p-value matters, while at s0=non-zero the difference of means plays a defined role (Tusher et al.,

2001). Figure 20 shows the differences of the 908 relatively quantified proteins between MT5 KO and WT CSF.
Among 83 t-test-significant proteins, only one protein Cerebellin1 (CBLN1) showed FDR-significant reduction of 53 % upon MT5-MMP knockout (Figure 20 and table 15).

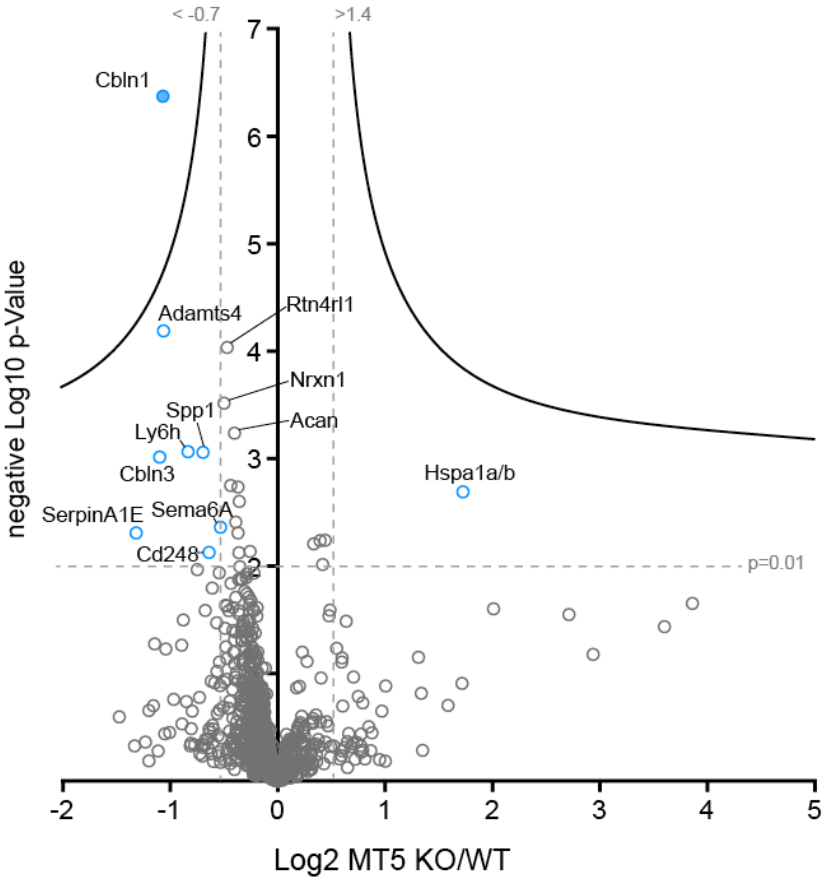

Figure 20: Proteomic changes in the CSF of MT5-MMP knockout mice.
Proteins in the CSF of MT5-MMP knockout (MT5 KO, n=8) animals were compared to CSF of wildtype (WT, n=8) animals. Overall, 908 proteins were relatively quantified. For 24 proteins, abundance changed significantly ($p<0.01$) and they are depicted above the horizontal dashed line. 9 proteins had a log2 fold-change of at least ± 0.5 (blue circles). 1 of the 9 proteins is significant after correction for false discovery rate (FDR) (filled blue circle). Black hyperbolic curves represent significance criteria of a FDR of 5 % and effect size requirement s0=0.1.

Correction for FDR stringently filters for high significance and strongly depends on the reproducibility of the quantification within a sample group. In other words, if the quantification of samples varies slightly, proteins are very likely to be categorized as false hits by FDR correction. In addition to CBLN1, which was changed with highest significance (48 % remaining protein), 21 proteins showed significant changes with a p-value of <0.01 (Figure 20, horizontal dashed line): Cerebellin3 (CBLN3) and a disintegrin and metalloproteinase with thrombospondin motifs 4 (ADAMTS4) showed a similar level of reduction (47 and 48 % remaining, respectively). Lymphocyte antigen 6H (LY6H) was reduced to a remaining protein level of 56 % and Osteopontin (SPP1) was decreased to 62 % in comparison to WT. Among the ten most significantly changed proteins (Table 15), the remaining five showed a decrease in the range of 29 % to 22 %: Neurexin1 (NRXN1) protein levels were reduced to 71 %, Reticulon-4 receptor-like 1 (RTN4RL1) showed 72 % remaining protein. Cell adhesion molecule 2 (CADM2) was decreased to 74 % in MT5 KO CSF compared to WT. Aggrecan

core protein (ACAN) and Cadherin-10 (CDH10) showed 76 % and 78 % of the WT protein level unpon MT5 KO. One protein, the Heat shock 70 kDa protein 1A/B (HSPA1A/B), showed a strong 3.3-fold increase (Figure 20).
Overall, only one protein Cerebellin-1 (CBLN1) showed highly confident reduction in the CSF of MT5-MMP knockout mice and was significant after FDR testing. However, several other proteins were changed in abundance and meet significance criteria of $p<0.01$ and therefore represent putative targets of MT5-MMP. Although, several proteins were significantly changed (Table 15), the effect of reduction was not strong enough to meet the strict criteria of multiple hypothesis correction.

Table 15: Proteins changed in CSF of MT5 KO compared to WT.
The 10 most significantly changed (t-test) proteins in CSF upon MT5-MMP knockout are listed and sorted by effect size (LFQ intensity ratio MT5 KO/WT). Uniprot accession numbers (Uniprot AC) and p-value are given for each protein. FDR significant proteins are marked with a '+'.

Uniprot AC	Gene name	Protein name	LFQ intensity ratio MT5 KO/WT	p-Value	FDR significant
Q9JHG0	Cbln3	Cerebellin-3	0.47	9.68E-04	
Q9R171	Cbln1	Cerebellin-1	0.48	4.25E-07	+
Q8BNJ2	Adamts4	A disintegrin and metalloproteinase with thrombospondin motifs 4	0.48	6.45E-05	
Q9WUC3	Ly6h	Lymphocyte antigen 6H	0.56	8.59E-04	
P10923	Spp1	Osteopontin	0.62	8.70E-04	
Q9CS84	Nrxn1	Neurexin-1	0.71	3.06E-04	
Q8K0S5	Rtn4rl1	Reticulon-4 receptor-like 1	0.72	9.22E-05	
Q8BLQ9	Cadm2	Cell adhesion molecule 2	0.74	1.78E-03	
Q61282	Acan	Aggrecan core protein	0.76	5.78E-04	
P70408	Cdh10	Cadherin-10	0.78	1.83E-03	

4.4.2.2 CSF of 5xFAD mice shows a clear increase of Alzheimer's disease-related proteins

Next, the CSF of the Alzheimer's disease (AD) mouse model 5xFAD was investigated using mass spectrometry-based proteomics to 1) assess the CSF changes in the AD-background and 2) be able to detect the influence of MT5-MMP in AD in further experiments. Therefore, proteomic changes in the CSF of 5xFAD were compared to healthy wildtype animals (WT). The requirements were set like in the other CSF experiments: Proteins with at least two unique peptides were considered identified and had to be quantified in at least three samples of each group. Applying these criteria resulted in 951 relatively quantified proteins between 5xFAD (n=10) and WT (n=8) CSF samples.
All relatively quantified proteins and their statistical evaluation are visualized in a volcano plot (Figure 21).
Four proteins showed an increase in the 5xFAD CSF in comparison to WT after FDR correction. Two of these proteins were tremendously increased (over 35-fold): human amyloid precursor protein (hsAPP) and Neurofilament medium polypeptide (NEFM). Transgenic 5xFAD mice carry the mutated human gene variant of APP and thus, not surprisingly, hsAPP showed the highest increase in 5xFAD CSF, where protein levels were 46-fold higher in comparison to WT. In fact, hsAPP was identified in nine 5xFAD samples and only in two WT samples. The two WT samples, in which hsAPP was identified, showed a

one order of magnitude lower LFQ intensity of the protein (average LFQ intensity of $1.03x10^7$) compared to 5xFAD (average LFQ intensity $4.76x10^8$). Therefore, most likely the high amount of hsAPP peptides on the analytical HPLC-column during 5xFAD sample runs led to residual elution of those peptides during WT sample analysis. However, although hsAPP was only 'detected' in two and not the required three samples in the WT sample group, it was intentionally not excluded from quantifications in order to demonstrate the validity of the AD model. Noteworthy, murine APP (mAPP), which was equally well detected in both sample groups, does not significantly change in abundance. This and the fact that proteins were identified based on *unique peptides* shows that the detected soluble APP species in CSF are derived from transgenic hsAPP.

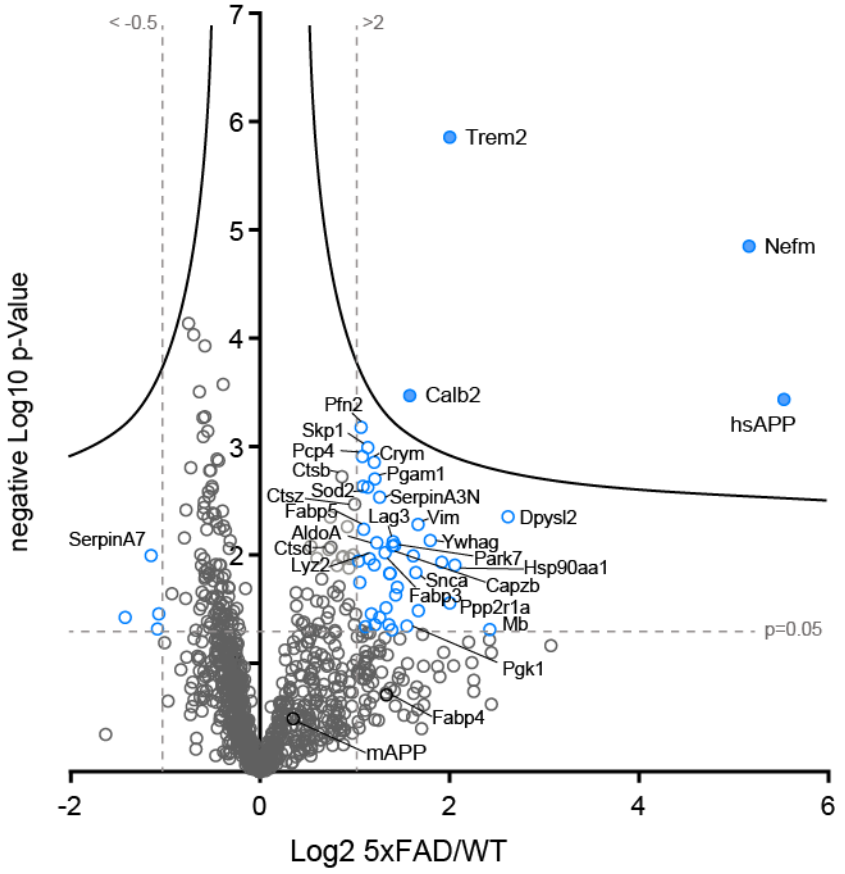

Figure 21: Proteomic changes in the CSF of 5xFAD mice.
Proteins in the CSF of 5xFAD mice (5xFAD, n=10) were compared to wildtype (WT, n=8) CSF. The negative log10 transformed p-values (two-sided Student's t-test) are plotted against the log2 transformed LFQ intensity ratios indicating an increase or decrease of protein abundance and the significance of the effect. After statistical evaluation 183 proteins showed a significant change and are located above the horizontal dashed line ($p<0.05$). Proteins with changed abundance of log2 fold change of ±1 (vertical dashed lines) are depicted as blue circles. Filled blue circles show FDR-significant changed proteins. Black lines represent a false discovery rate of 5 % (s0=0.01).

The same was true for the second-most increased protein NEFM (also called NFM), which showed a 35-fold accumulation. This protein was as well identified in only 2 WT samples with a much lower LFQ intensity, but included in relative quantifications, because its close relation to and interaction with Neurofilament light polypeptide (NEFL or NFL) (Lépinoux-Chambaud and Eyer, 2013; Petzold, 2005), which was found to be increased in CSF and blood and proposed as marker for neurodegenerative disease progression in mouse models (Bacioglu et al., 2016). Here, NEFL and the heavy variant NEFH (Neurofilament heavy

polypeptide, NFH) were both abundantly detected in the 5xFAD sample group, but were below detection limit in the WT sample group.
The other two significantly increased proteins were Triggering receptor expressed on myeloid cells 2 (TREM2) and Calretinin (CALB2), which showed a 4- and 3-fold increase, respectively. In line with the other two strongly accumulated proteins, hsAPP and NEFM, also TREM2 has an established connection to AD and neurodegeneration and was demonstrated to be increased in CSF of patients (Henjum et al., 2016; Heslegrave et al., 2016; Ulrich and Holtzman, 2016).
Including the four FDR-significant proteins hsAPP, NEFM, TREM2, and CALB2, 183 proteins showed t-test significant change with a p-value <0.05. Table 16 lists 15 proteins, which showed the strongest changes in the CSF of 5xFAD compared to WT. Among the 183 significant proteins three cathepsins, CTS-D, CTS-B, and CTS-Z, showed increased abundance of 1.68-, 1.82-, and 1.99-fold. Cathepsins have already been shown to play critical roles in induction of AD pathology and inflammation (Allan et al., 2017; Di Domenico et al., 2016; Keren-Shaul et al., 2017; Schuur et al., 2011; Wu et al., 2017). Also α-synuclein (SNCA) and its receptor Lymphocyte-activation gene 3 (LAG3) were accumulated in 5xFAD CSF 3.13- and 2.64-fold, respectively, and are linked to progression of neurodegeneration (Mao et al., 2016). Moreover, high levels of α-synuclein were detected in CSF of AD patients (Chiasserini et al., 2017; Wang et al., 2015). Additionally, proteins such as the fatty acid binding proteins 3 and 5 (FABP 3 and 5) showed increased abundance of 2.5-fold and 2.1-fold, respectively. These two proteins were either demonstrated to be upregulated in CSF of AD patients (FABP3) (Chiasserini et al., 2017; Chiasserini et al., 2010) or shown to be involved in blood-brain barrier regulation (FABP5) (Pan et al., 2016).
Taken together, the CSF of 5xFAD animals showed an increase of pathology associated proteins and validates the symptomatic stage with progressed disease mechanisms.

Table 16: Significantly changed proteins in 5xFAD CSF compared to WT.
Proteins with a p<0.05 are sorted according to their effect size (LFQ intensity ratio 5xFAD/WT) and the 15 strongest changes are shown. Four proteins met the stringent FDR criteria of 5% and s0=0.1 (indicated with a + in the last column).

Uniprot AC	Protein name	Gene name	LFQ intensity ratio 5xFAD/WT	p-Value	FDR significant
P05067	APP *human*	APP	46.27	3.65E-04	+
P08553	Neurofilament medium polypeptide	Nefm	35.82	1.41E-05	+
O08553	Dihydropyrimidinase-related protein 2	Dpysl2	6.15	4.43E-03	
P04247	Myoglobin	Mb	5.38	4.89E-02	
P07901	Heat shock protein HSP 90-alpha	Hsp90aa1	4.16	1.24E-02	
Q76MZ3	Serine/threonine-protein phosphatase 2A 65 kDa regulatory subunit A alpha isoform	Ppp2r1a	4.01	2.77E-02	
Q99NH8	Triggering receptor expressed on myeloid cells 2	Trem2	4.01	1.39E-06	+
Q61316	Heat shock 70 kDa protein 4	Hspa4	3.78	1.17E-02	
P61982	14-3-3 protein gamma	Ywhag	3.48	7.31E-03	
P62908	40S ribosomal protein S3	Rps3	3.19	3.27E-02	
P20152	Vimentin	Vim	3.18	5.23E-03	
O55042	Alpha-synuclein	Snca	3.13	1.45E-02	
Q7TQI3	Ubiquitin thioesterase OTUB1	Otub1	3.07	1.02E-02	
Q08331	Calretinin	Calb2	2.99	3.38E-04	+
P09411	Phosphoglycerate kinase 1	Pgk1	2.93	4.53E-02	

4.4.2.3 MT5-MMP knockout changes the CSF protein composition under pathological conditions

Finally, the effect of MT5-MMP-deficiency on the CSF proteome was investigated in the pathological 5xFAD background. For this, CSF of double transgenic 5xFAD mice deficient for MT5-MMP (5xFAD-MT5 KO, n=9) was compared to CSF of 5xFAD mice (n=8). As for prior CSF analysis, proteins needed to be identified with at least two unique peptides in at least 3 samples of each genotype, which resulted in 943 relatively quantified proteins (Figure 22). Overall, for 205 proteins a significantly changed abundance was detected ($p<0.05$, Figure 22, proteins above dashed horizontal line). Changes in the proteome were further evaluated by introducing a threshold of a minimum log2 fold change of ± 1 and correcting for FDR of 5 % with s0=0.1 (Figure 22, blue circles and filled dots). A total of 95 proteins showed a strong effect of changed abundance and met the set criteria (blue circles) and 56 proteins were significantly changed in 5xFAD-MT5 KO CSF after FDR correction compared to 5xFAD CSF (blue filled dots).

Two proteins showed an FDR-significant increase, whereas 54 showed a decrease in protein level. The two increased proteins were Mast/stem cell growth factor receptor Kit (KIT, 1.64-fold) and (Pro-) Neuropeptide Y (NPY, 1.87-fold).

Table 17 lists 15 proteins with the strongest effects of reduction and $p>0.05$. Among the significantly reduced proteins, Tubulin beta-4B chain (TUBB4B) was the one with highest reduction with only 6 % of the protein level in 5xFAD CSF, followed by Glycogen phosphorylase (PYGM), which was reduced to 7 %, Transitional endoplasmic reticulum ATPase (VCP) with a remaining level of 8 % and Apolipoprotein B (APOB), which was reduced to 9 %. Retinal dehydrogenase 2 (ALDH1A2), Glutamine synthetase (GLUL), Hemoglobin subunit alpha (HBA), Retinol-binding protein 1 (Rbp1), mitochondrial ATP synthase subunit beta (ATP5B), Vimentin (VIM), Heat shock protein HSP 90-alpha (HSP90AA1) were reduced in 5xFAD-MT5 KO CSF to 11-15 % of the protein levels in 5xFAD CSF. The two last proteins, VIM and HSP90AA1, were both detected among the strongest significant changes in the CSF of 5xFAD/WT and 5xFAD-MT5 KO/5xFAD (Figures 21 and 22; Tables 16 and 17) and showed a significant increase in the CSF of 5xFAD, whereas they were significantly decreased in CSF upon MT5-MMP knockout in 5xFAD animals. However, the majority of proteins, which were significantly increased in 5xFAD CSF in comparison to WT, such as hsAPP, TREM2, NEFM, CALB2, CTS-Z/B/D, LAG3, SNCA and FABP3/5 were not detected to be changed upon MT5-MMP-deficiency in the 5xFAD background.

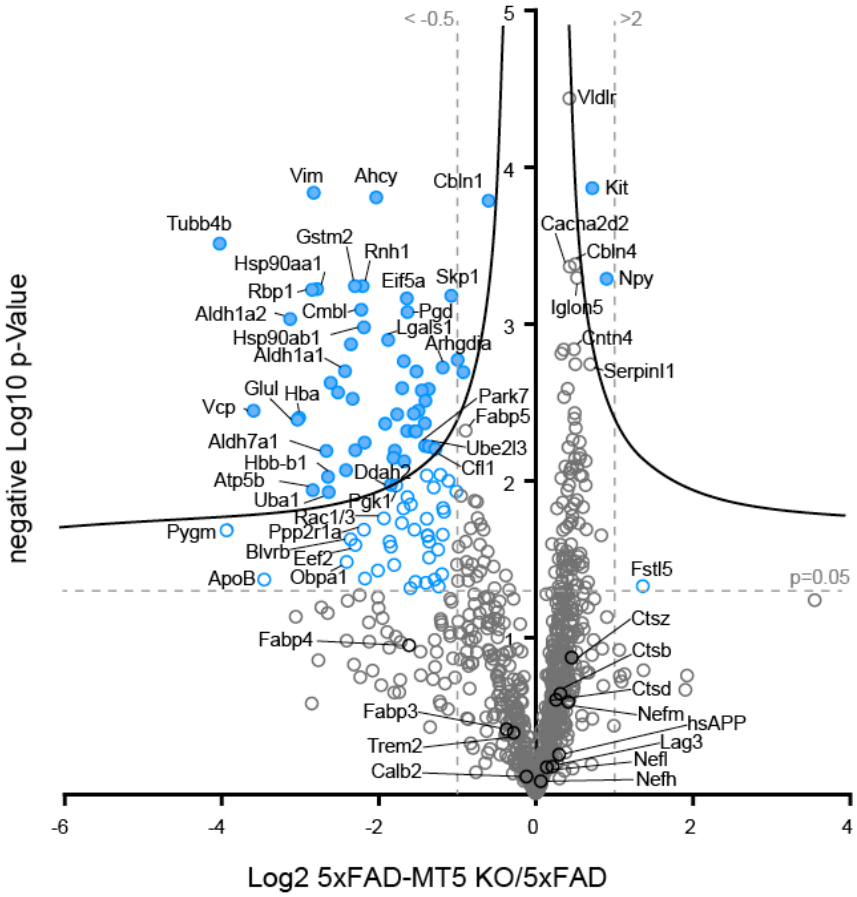

Figure 22: Proteomic changes in the CSF of MT5-MMP-deficient 5xFAD transgenic mice.
Proteins in the CSF of 5xFAD-MT5 KO mice (n=9) were compared to 5xFAD (n=8) CSF. The negative log10 of the p-values (two-sided Student's t-test) is plotted against the log2 transformed LFQ intensity ratios indicating an increase or decrease of protein abundance and the significance of the effect. Proteins depicted in blue (circles or filled dots) showed a log2 fold change of ± 1 (vertical dashed lines) and a p-value of <0.05 (horizontal dashed line, blue circles). Filled blue dots represent proteins that were significant after FDR correction. Black curves represent a FDR of 5 % (s0 = 0.1).

Overall, the absence of MT5-MMP in 5xFAD animals had an effect on protein composition of the CSF and 56 proteins were changed with high confidence, most of which showed a reduction of protein level in comparison to 5xFAD CSF. Only a few of the proteins, which were increased in 5xFAD CSF compared to WT CSF (Figure 21), did not show a significant change upon MT5-deficiency.

Table 17: Significantly changed CSF proteins upon MT5-MMP knockout in the background of 5xFAD. Listed are the 15 proteins (p<0.05), which showed the strongest reduction in protein abundance sorted by their effect size.

Uniprot AC	Protein name	Gene name	LFQ intensity ratio 5xFAD-MT5 KO/5xFAD	p-Value	FDR significant
P68372	Tubulin beta-4B chain	Tubb4b	0.06	3.06E-04	+
Q9WUB3	Glycogen phosphorylase	Pygm	0.07	2.05E-02	
Q01853	Transitional endoplasmic reticulum ATPase	Vcp	0.08	3.56E-03	+
E9Q414	Apolipoprotein B	Apob	0.09	4.26E-02	
Q62148	Retinal dehydrogenase 2	Aldh1a2	0.11	9.27E-04	+
P15105	Glutamine synthetase	Glul	0.12	4.07E-03	+
P01942	Hemoglobin subunit alpha	Hba	0.12	3.94E-03	+
Q00915	Retinol-binding protein 1	Rbp1	0.14	6.05E-04	+
P56480	ATP synthase subunit beta, mitochondrial	Atp5b	0.14	1.14E-02	+
P20152	Vimentin	Vim	0.14	1.45E-04	+
P07901	Heat shock protein HSP 90-alpha	Hsp90aa1	0.15	5.97E-04	+
Q9DBF1	Alpha-aminoadipic semialdehyde dehydrogenase	Aldh7a1	0.16	6.45E-03	+
P02088	Hemoglobin subunit beta-1	Hbb-b1	0.16	9.42E-03	+
Q02053	Ubiquitin-like modifier-activating enzyme 1	Uba1	0.16	1.18E-02	+
P45376	Aldose reductase	Akr1b1	0.16	2.37E-03	+

4.4.2.4 Increased proteins in 5xFAD/WT CSF are significantly downregulated upon MT5-MMP knockout

A preliminary comparison of the 15 most strongly changed significant proteins in the two CSF proteomes of 5xFAD/WT and 5xFAD-MT5 KO/5xFAD showed that the two proteins VIM and HSP90AA1 were affected in opposite directions: both proteins showed an increase of 3.18- and 4.16-fold in 5xFAD CSF in comparison to WT CSF, whereas upon MT5-MMP knockout in 5xFAD animals, the protein abundance of VIM strongly decreased to 14 % and HSP90AA1 strongly decreased to 15 % of 5xFAD level. Therefore, such a comparison was carried out with the proteins in both datasets, which met the criteria of a log2 fold change of +/- 1 and p<0.05 or FDR-significance. In other words, proteins, which were significantly increased by at least 2-fold or significantly decreased by minimum 50 % and proteins with FDR-significant changes. These criteria resulted in 49 proteins in the 5xFAD/WT dataset and 96 in the 5xFAD-MT5 KO/5xFAD dataset. An overlap of these proteins yielded 16 common proteins between the two analyses (Figure 23).

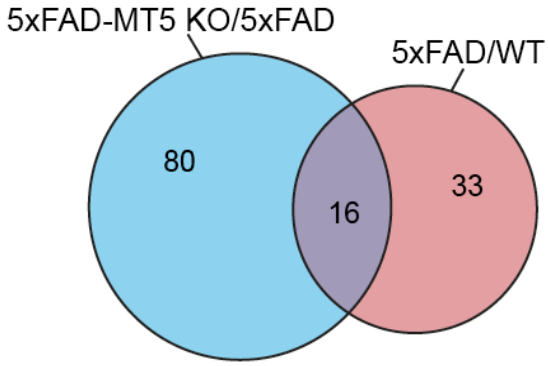

Figure 23: Overlap of significantly changed proteins in 5xFAD/WT CSF and 5xFAD-MT5 KO/5xFAD CSF. Proteins regulated in both datasets with a minimum log2 fold-change of +/-1 and $p<0.05$ and FDR-significant proteins were compared and yielded an overlap of 16 proteins, which met the set criteria in both experiments.

Further, the extent of the changes of the 16 common proteins was investigated and listed in Table 18. Interestingly, all of the common proteins showed an increase in 5xFAD CSF compared to WT CSF and were reduced upon MT5-MMP knockout in the 5xFAD background.
Therefore, these 16 proteins very likely reflect changes, which are directly or indirectly mediated by MT5-MMP-deficiency and might be involved in the beneficial changes MT5-MMP deficiency has in on AD pathology.

Table 18: Common significantly changes proteins in 5xFAD/WT CSF and 5xFAD-MT5 KO/5xFAD CSF. 16 Proteins were found to be significantly regulated in both, CSF of 5xFAD compared to WT and CSF of 5xFAD-MT5 KO compared to 5xFAD. All of the common proteins were increased in the 5xFAD/WT CSF and a knockdown of MT5-MMP in the 5xFAD background resulted in a strong reduction of these proteins.

Uniprot AC	Protein name	Gene name	5xFAD/WT	5xFAD-MT5 KO/5xFAD
P20152	Vimentin	Vim	3.18	0.14
P07901	Heat shock protein HSP 90-alpha	Hsp90aa1	4.16	0.15
Q9WTX5	S-phase kinase-associated protein 1	Skp1	2.20	0.47
Q62048	Astrocytic phosphoprotein PEA-15	Pea15	2.26	0.39
P17182	Alpha-enolase	Eno1	2.16	0.37
P68254	14-3-3 protein theta	Ywhaq	2.70	0.36
P99029	Peroxiredoxin-5, mitochondrial	Prdx5	2.32	0.38
Q61316	Heat shock 70 kDa protein 4	Hspa4	3.78	0.32
Q99LX0	Protein deglycase DJ-1	Park7	2.68	0.38
P68037	Ubiquitin-conjugating enzyme E2 L3	Ube2l3	2.40	0.39
P18760	Cofilin-1	Cfl1	2.07	0.41
P62259	14-3-3 protein epsilon	Ywhae	2.58	0.46
P09411	Phosphoglycerate kinase 1	Pgk1	2.93	0.29
Q11011	Puromycin-sensitive aminopeptidase	Npepps	2.73	0.44
P70349	Histidine triad nucleotide-binding protein 1	Hint1	2.51	0.38
Q76MZ3	Serine/threonine-protein phosphatase 2A 65 kDa regulatory subunit A alpha isoform	Ppp2r1a	4.01	0.22

4.4.2.5 Computational database analysis of significantly changed proteins in 5xFAD-MT5 KO CSF

To further analyze the inflicted changes in the CSF caused by MT5-MMP deficiency in 5xFAD mice, a bioinformatic approach was used to describe the affected proteins. The 56 FDR-significantly changed proteins (Figure 22) were matched against reviewed Uniprot annotations in order to gain more information about their subcellular location (Figure 24A). The majority of proteins (50) were of cytoplasmic origin. 13 proteins were annotated to localize to the nucleus and 12 were known to have membrane localization. 8 proteins were described as mitochondrial and 5 were known to be secreted into the extracellular space (Figure 24A). Due to several isoforms and multiple functions of proteins, 22 proteins had more than one annotated localization and therefore fell into multiple categories (Supplementary data 1). The 12 membrane proteins were further investigated to describe their membrane topology (data not shown), but only one protein was annotated to be a single-span transmembrane protein: the Mast/stem cell growth factor receptor Kit (Kit), which was increased in 5xFAD-MT5 KO CSF (Figure 22 and table 17). Among the remaining membrane-annotated proteins, one protein – Protein deglycase DJ-1 (Park7) – was described to localize to the plasma membrane as a lipid-anchored protein upon palmitoylation. Most of the other proteins, which were annotated to the membrane, were peripheral membrane proteins and only associated to the membrane due to interaction with transmembrane proteins. Hence, they were in addition annotated to be cytoplasmic (8 of 12 proteins), nuclear (5 of 12 proteins), mitochondrial (2 of 12 proteins) or secreted (2 of 12 proteins).

In order to evaluate the change in CSF protein composition caused by MT5-MMP knockout in 5xFAD mice, the 56 significantly altered proteins were functionally classified according to Gene Ontology (GO) annotations using the *Protein Annotation through Evolutionary Relationship* (PANTHER)-tool (Mi et al., 2013) (Figure 22B). The proteins were categorized into following protein classes: Oxidoreductase (28 %), hydrolase (12 %), nucleic acid binding (10 %), signaling molecule (8 %), ligase (8 %), enzyme modulator (6 %), transfer/carrier protein (4 %), transferase (4 %), transporter (2 %), cell adhesion molecule (2 %), calcium-binding protein (2 %), isomerase (2 %) and lyase (2 %). This classification provides information about the molecular activities of the single gene products and might point towards a protein class regulated by MT5-MMP.

In the next step, significantly changed proteins were clustered according to their biological processes involvement to allow an assessment of the biological alterations MT5-MMP knockout has in the 5xFAD background (Figure 24C, left panel). Proteins were annotated to function in metabolic processes (25 proteins), cellular processes (24 proteins), responses to stimuli (12 proteins), general biological regulation (6 proteins), organization and biogenesis of cellular components (4 proteins), multicellular processes (4 proteins), localization (3 proteins), developmental processes (2 proteins) and immune system processes (2 proteins). The three most abundant biological process-categories were sub-classified and are shown in the right panel (box) of Figure 24C. The general classification of ‘cellular processes’ divided into the two categories cell communication (10 proteins) and Cell cycle (6 proteins) (1. GO BP cellular process, Figure 24C, box). Proteins involved in ‘metabolic processes’ (MP) could be sub-classified into primary MPs (20 proteins, lower level primary MPs: carbohydrate MP, cellular amino acid MP, lipid MP, nucleobase-containing compound MP, protein MP, tricarboxylic acid cycle), catabolic process (9 proteins), nitrogen compound MP (7 proteins), generation of precursor metabolites and energy (5 proteins), phosphate-containing compound MP (4 proteins), biosynthetic process (4 proteins), co-enzyme MP (1 protein), and sulfur compound MP (1 protein) (2. GO BP metabolic process, Figure 24C, box). The third most represented biological process-category was made of proteins, which are involved in ‘response to stimuli’ and their sub-classification is shown in Figure 24C, box: 3. GO BP response to stimulus: The 12 proteins in this category were involved in responses to stimuli in

behavior (1 protein), cellular defense (1 protein), abiotic and extracellular stimuli (each 1 protein), and response to stress stimuli (8 proteins). A detailed list of the proteins in the single categories is available in the supplementary data 2 and 3 section.
A computational approach with Gene Ontology annotations was used to define protein classes and classify biological processes of the significantly changed proteins in CSF of 5xFAD animals upon MT5-MMP knockout. A clustering into biological processes was used to determine the pathways and larger processes, in which multiple of the identified proteins are involved and active. In other words, this analysis was used to describe molecular activities and involvement of MT5-MMP deficiency-dependent changes in the AD brain.

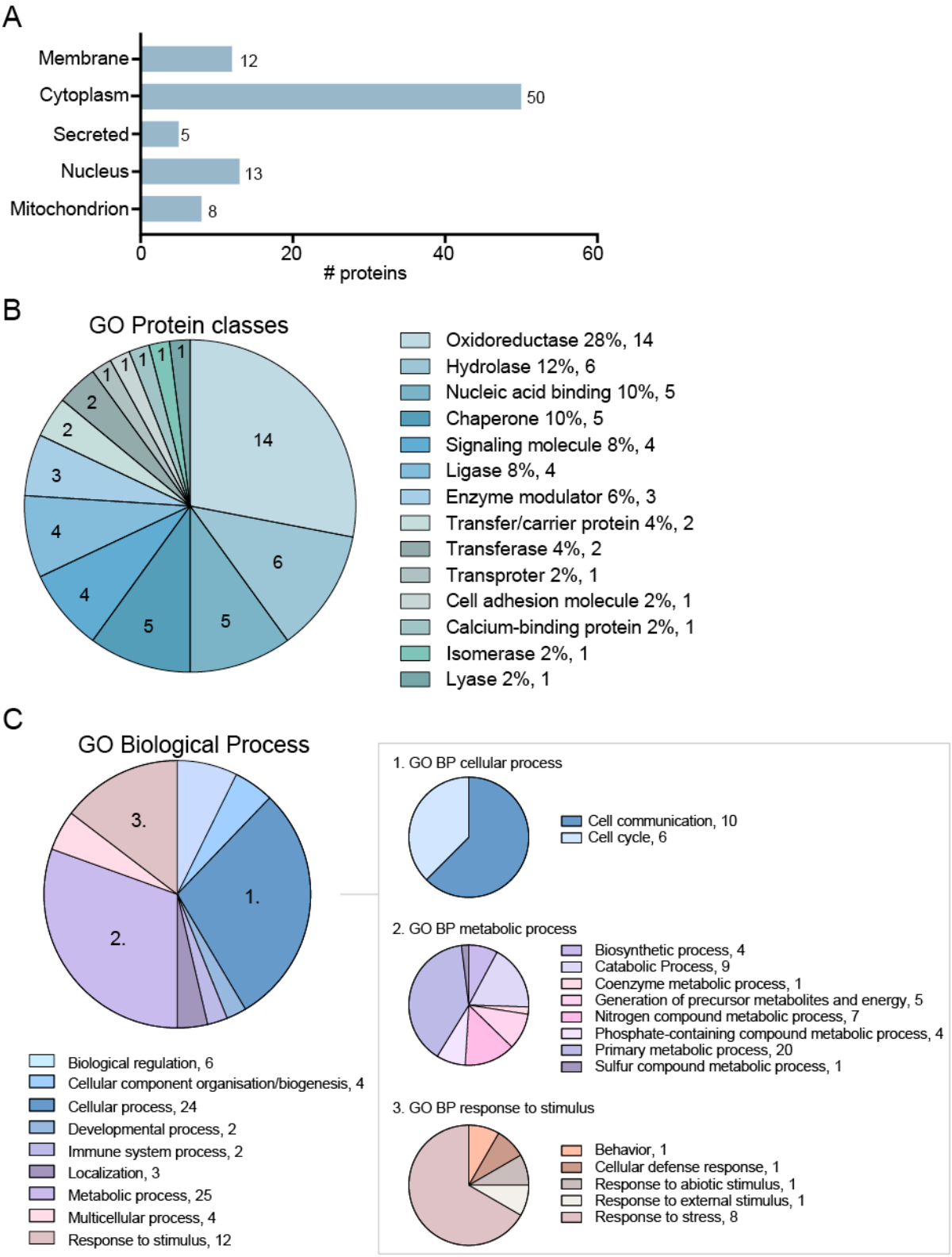

Figure 24: Bioinformatic analysis of significantly changed proteins in CSF of 5xFAD animals upon MT5-MMP knockout. A) Subcellular location of significantly changed proteins according to reviewed Uniprot annotations: Cytoplasm (50 proteins), nucleus (13), membrane (12), mitochondrion (8), secreted (5). Among the membrane-annotated proteins, only 1 was known to be membrane-spanning and 1 was annotated as lipid-anchored protein. **B)** Functional classification using the PANTHER annotation tool categorized the proteins into following protein classes: The proteins were categorized into following protein classes: Oxidoreductase (28 %), hydrolase (12 %), nucleic acid binding (10 %), signaling molecule (8 %), ligase (8 %), enzyme modulator (6 %), transfer/carrier protein (4 %), transferase (4 %), transporter (2 %), cell adhesion molecule (2 %), calcium-binding protein (2 %), isomerase (2 %) and lyase (2 %). **C)** Left panel: Proteins were clustered according to their

involvement in biological processes. The three most abundant categories were ‘cellular processes’ (24 proteins), ‘metabolic processes’ (25 proteins), and ‘response to stimulus’ (12 proteins) and were further sub-classified (**box**). A detailed list of the proteins in the single categories is available in the supplementary data section. GO=Gene Ontology; Protein classes in B are given with relative percentages and protein numbers; Biological processes and subcategories in C are given with protein numbers.

5 Discussion

5.1 New ADAM10 substrates in the brain implicate a central role in neurite outgrowth

ADAM10 is a ubiquitously expressed protease and regulates numerous processes during development and diseases by ectodomain shedding of its substrates (Saftig and Lichtenthaler, 2015; Saftig and Reiss, 2011). A well-studied substrate is Notch, which requires cleavage by ADAM10 for signaling in development and differentiation (Pan and Rubin, 1997). Notch signaling is, among other functions, important for embryogenesis, and the development of different tissue and organs such as the central nervous system, the endocrine and the cardiovascular system (Chiba, 2006; Luxan et al., 2016; Pierfelice et al., 2011). Additional substrates are known for different tissues. Cleavage of the amyloid precursor protein (APP) in neurons attributes a central role to ADAM10 in treatment strategies for Alzheimer's disease (AD). As ADAM10-mediated APP cleavage counteracts the generation of the toxic amyloid-β (Aβ) peptide, stimulation of its activity is one of the main approaches in drug development (Saftig and Lichtenthaler, 2015). In fact, the already approved drug Acitretin was demonstrated to increase sAPPα levels in cerebrospinal fluid of patients with mild to moderate AD (Endres et al., 2014). At the beginning of the here presented study, only little was known about ADAM10 physiological functions in the brain, because embryonic lethality of ADAM10 knockout mice complicated its investigation in the central nervous system. Generation of a conditional knockout mouse line and the identification of additional substrates, implicated an important role for the protease in embryonic brain development and homeostasis of neuronal networks into adulthood, but the mechanisms of action remain largely unclear.

In preliminary work to the here presented study, Dr. P.H. Kuhn carried out an unbiased proteomic approach using mass spectrometry to identify neuronal ADAM10 substrates: Secretome analysis of conditional ADAM10-deficient primary neurons described 91 novel substrate candidates of ADAM10, of which several were chosen for further validation with an independent analysis method in this study.
After ADAM10-deficiency was introduced in primary neuronal cultures, protein levels of selected substrate candidates were analyzed by Western blot (WB). A successful knockout of ADAM10 after Cre virus treatment was demonstrated through an absence of WB signal for ADAM10. The total of soluble proteolytic fragments of APP (sAPPα and sAPPβ) was almost not affected by loss of ADAM10 activity in neurons, whereas APP full-length protein levels increased very mildly, but not significantly. When, in addition to ADAM10-deficiency, BACE1 activity was inhibited with C3, shedding of APP was dramatically reduced and the full-length protein accumulated in the cells. These results are in line with common knowledge of BACE1 being the predominant sheddase of APP in neurons and ADAM10 being rather responsible for APP cleavage in non-neuronal tissues and cell lines (Seubert et al., 1993; Sisodia et al., 1990; Weidemann et al., 1999). Besides APP, L1CAM is another known ADAM10 substrate and also known to be involved in neuronal cell adhesion, migration, and neurite outgrowth (Gutwein et al., 2003; Maretzky et al., 2005). In both the prior performed proteomic analysis as well as in Western blot analysis of ADAM10-deficient neurons, soluble secreted L1CAM displayed a reduction of 40 %, indicating that the majority of shedding in neurons might be mediated by another protease. Indeed, blocking BACE1 cleavage on top of ADAM10 mostly abolished L1CAM shedding. This is in agreement with previous reports, showing that BACE1 is prevalently responsible for L1CAM cleavage in neuronal cells (Kuhn et al., 2012; Zhou et al., 2012).
Two novel substrate candidates Neuronal cell adhesion molecule (NrCAM) and Neogenin1 (NEO1) displayed a similar reduction in the supernatant of ADAM10-deficient neurons (70

and 60 %, respectively), clearly indicating that ADAM10 activity is to a major extent responsible for the shedding of these two proteins. Moreover, the reduction observed in the biochemical approach correlated well with the proteomic approach, underlining the quantitative integrity of label-free proteomics. Soluble NrCAM showed 67 % reduction in the secretome (Kuhn et al., 2016) and 70 % by Western blot analysis. For soluble NEO1, protein level decreased by 65 % in secretome (Kuhn et al., 2016) and 60 % and Western blot analysis. Both proteins were only mildly affected by BACE1 and loss of activity showed an additive effect of reduction for NEO1 (87 % reduction if ADAM10 and BACE1 were not active) in Western blot analysis. In fact, in a previous work, NrCAM showed no changes in the secretome of BACE-deficient neurons, showing that BACE1 does not shed NrCAM (Kuhn et al., 2012). The same study reported also shedding of NEO1 as 'unaltered' upon BACE1 inhibition. However, soluble Neogenin1 levels were reduced mildly by 10 % upon C3 treatment, being in line with the here observed mild additive effect of BACE1 inactivity in ADAM10-deficient neurons.

The here investigated known and novel ADAM10 substrates L1CAM, NrCAM, and NEO1 are all involved or implicated in neurite outgrowth and axon guidance in the brain of mice (L1CAM, NrCAM) or mice and zebrafish (NEO1) and therefore implicate a putative central role for ADAM10 in these critical neuronal mechanisms. Moreover, ADAM10-mediated L1CAM shedding was shown to affect neuronal adhesion, migration, and outgrowth (Maretzky et al., 2005). For NEO1 a study in zebrafish showed that knockdown of NEO1 enhanced aberrant dorsal axon projection in embryos (Gao et al., 2012). In mouse, NEO1 was demonstrated to be important in axonal pathfinding of thalamocortical projections (Braisted et al., 2000). A knockout of NRCAM resulted in mistargeted guidance of axons in frontal olfactory bulb and to the visual cortex (Demyanenko et al., 2011; Heyden et al., 2008). The NRCAM-deficient phenotype of misled axonal growth in the olfactory bulb was also copied by a knockout of the protein CHL1, which is cleaved by ADAM10, but also by BACE1. However, the study excluded an identical molecular guidance mechanism for these axon misguidances, since the two proteins (CHL1 and NRCAM) are differentially expressed. CHL1 expression is located to fibers incoming from the nasal epithelium, whereas NRCAM expression is exclusively seen in the target region of axons (Heyden et al., 2008). Thus, ADAM10 might regulate axon guidance in the target region of neuronal projections from the nasal epithelium to the olfactory bulb via the cleavage of NrCAM. Loss of NrCAM or ADAM10-mediated shedding could result in a repulsive effect of olfactory axons and lead to the observed targeting defects.

Indeed, after NrCAM was validated as ADAM10 substrate in the here presented work, ADAM10-deficient mice were examined for similar axon target defects in the olfactory bulb. Investigations resulted in a phenocopy of the NrCAM knockout-mediated guidance defects proving that ADAM10 regulates axon targeting in the olfactory bulb via NrCAM cleavage. The results of this study are published in the study "Systematic substrate identification indicates a central role for the metalloprotease ADAM10 in axon targeting and synapse function" (Kuhn et al., 2016).

5.2 The therapeutic potential of BACE1 might be limited by its physiological substrates

The protease BACE1 has a central role in current drug development for Alzheimer's disease (AD) and a number of pharmaceutical companies focus on BACE1 inhibition as therapeutic approach. However, BACE1 inhibitors have to be anticipated with caution, as was pointed out

by recent development, in which the most advanced BACE1 inhibitors in clinical trials were terminated early in Phase III, because of lack of positive effects and observed side effects (Egan et al., 2018; Janssen, 2018; Kennedy et al., 2016). Additionally, up to now all BACE1 inhibitors in clinical trials also inhibit BACE2 to a similar extent which raises the concerns of mechanism based side effects (Bennett et al., 2000; Farzan et al., 2000). In fact, such side effects have already been observed in BACE inhibitor treated patients (Kennedy et al., 2016). This emphasizes how important it is to understand the physiological and pathological mode of actions of proteases in order to predict and prevent adverse effects during therapeutic BACE1 inhibition.
Over the last years, extensive proteomic discovery-based approaches investigated changes due to BACE-deficiency or overexpression in the secretome or the whole cell lysate (or CSF and brain homogenates *in vivo*) (Dislich et al., 2015; Hemming et al., 2009; Hogl et al., 2013; Kuhn et al., 2012; Stutzer et al., 2013; Zhou et al., 2012), but were not selective enough to detect such consequent changes specific to the cell surface. The here presented study set out to investigate this unexplored field and thus contribute to BACE1 research.

5.2.1 The new SUSPECS workflow reliably identifies a broad range of functional surface proteins and is suited for analysis of BACE1-deficient primary neurons

To be able to exclusively enrich, identify, and quantify the cell surface proteome of BACE1-inhibited neurons, some technical limitations had to be overcome.
The two most common strategies for labeling and analysis of surface transmembrane glycoproteins are cell surface capturing (CSC) and periodate oxidation and aniline-catalyzed oxime ligation (PAL) (Wollscheid et al., 2009; Zeng et al., 2009). Both methods use a two-step chemical labeling: First, surface glycoproteins are chemically oxidized and then labeled with a biotin-containing reagent. To specifically enrich membrane proteins, PAL and CSC target N-glycosylation for labeling and use PNGase F digestion after tryptic digest, which releases specific peptides containing the targeted N-glycosylation sites. By this, both methods are able to reduce the sample complexity and increase protein identification, but with the drawback of obtaining only few peptides per protein. As this is a disadvantage for quantitative proteomics, the here presented study intended to specifically enrich cell surface proteins and to analyze all peptides after tryptic digestion to achieve reliable relative label-free protein quantification.
To this extent, a new method named SUSPECS (surface-spanning protein enrichment with click sugars) was established to technically allow specific labeling and enrichment of surface proteins for subsequent analysis with mass spectrometry. It was intended to be applicable to living cultures, such as primary cells, and to be compatible with the use of serum or other protein containing supplements, to facilitate a combination with secretome analysis.
After optimization and validation of the cell surface labeling, SUSPECS was applied to BACE1-inhibited primary neurons and used to assess consequent alterations in the cell surface protein composition using mass spectrometry-based protein label-free quantification.
A first evaluation, determined the efficiency and applicability of SUSPECS for mass spectrometry-based analysis. Overall, almost 700 transmembrane and GPI-anchored glycoproteins were identified in at least three replicates, which makes SUSPECS comparable to CSC in terms of protein identifications (Wollscheid et al., 2009). Moreover, a majority (44.2 %, 306 proteins) of these proteins were transmembrane type I and GPI-anchored proteins, which are likely to contain BACE1 substrates, since BACE1 preferably cleaves proteins with these membrane topologies (Hemming et al., 2009; Kuhn et al., 2012). However, a high percentage of the identified proteins was represented by multi-pass proteins (45.3 %, 313 proteins), which have more than one transmembrane domain. Additionally, also transmembrane type II, III and IV proteins were identified. The variety of membrane protein orientation among the identified proteins shows that SUSPECS allows an unbiased labeling

and enrichment of common transmembrane proteins. A functional categorization of the SUSPECS-identified proteins, demonstrated a broad coverage of protein classes, such as transporters, receptors, hydrolases, transferases, and cell adhesion molecules among others.
In summary, with SUSPECS a new method was established, to specifically modify newly synthesized, glycosylated proteins and allow directed biotinylation at the cell surface, which can be used to selectively purify and enrich transmembrane proteins from the cell surface. Further, SUSPECS can be combined with label-free mass spectrometry, which showed reproducible quantification of several hundred transmembrane proteins. The workflow easily extracted a broad functional variety of proteins from the surface membrane, ranging from receptors over signaling molecules to cell adhesion molecules, making it applicable to study diverse biological questions. Moreover, SUSPECS can be combined with secretome analysis in the same experiment and is compatible with serum-containing supplements, which broadens its utility.

5.2.2 BACE1 inhibition changes the protein composition of neuronal cell surface membranes and results in high accumulation of selected substrates

Surface-spanning protein enrichment with click sugars (SUSPECS) was applied to evaluate the proteome of neuronal surface membranes upon pharmacological inhibition of BACE1 with the common inhibitor C3 (Stachel et al., 2004). Although C3 inhibits also the close homolog BACE2, the investigated effects are accountable to BACE1 inhibition, since BACE1 and not BACE2 is the predominantly expressed form in neurons (Bennett et al., 2000; Vassar, 1999; Voytyuk et al., 2018b).
A mass spectrometric approach using label-free quantification consistantly relatively quantified 471 transmembrane glycoproteins demonstrating that BACE1 inhibition selectively remodels the cell surface proteome of primary neurons. Some proteins strongly accumulated upon loss of BACE1-mediated cleavage, for others the effect was less pronounced. Observed alterations of protein levels could be categorized into strong (> 2-fold), moderate (between 1.5 and 2-fold), and mild (< 1.5-fold) increase and the strongest changes were detected for six proteins, which are the known BACE1 substrates APLP1, CHL, CNTN2, SEZ6, SEZ6L, and APP (2-7-fold) (Dislich et al., 2015; Pigoni et al., 2016; Vassar, 1999; Zhou et al., 2012). For these substrates, an accumulation in total lysates of murine neurons upon BACE1 inhibition and membrane fractions of BACE1 knockout brains was already reported and therefore emphasizes the integrity of the here presented study results. Additionally, this observation led to the assumption that BACE1 controls the cell surface protein levels of its substrates as a general mechanism (Gautam, 2014; Kuhn et al., 2012; Pigoni et al., 2016; Zhou et al., 2012). However, this possibility has not yet been tested for the numerous additional substrates. Moreover, BACE1, which has an acidic pH optimum, does not cleave its substrates at the cell surface, but mainly in the early endosomes and partially also in the trans-Golgi network (Hook et al., 2002; Vassar, 1999). In contrast to other strongly accumulated substrates, the established BACE1 substrate L1CAM (Zhou et al., 2012) showed only a mild increase (1.3-fold) at the cell surface, which has not been reported until now.
Noteworthy, not all known BACE1 substrates showed a pronounced accumulation at the cell surface. Some well-known substrates and substrate candidates such as L1CAM, TMEM132a, ROBO1, DNER, LRRN1 and SEZ6L2 accumulated only mildly or not at all. The cleavage of those proteins might be compensated by another protease such as ADAM10, as it was shown for APP (Colombo et al., 2013). Alternatively, BACE1 could also only cleave a small proportion of those proteins, which could lead to strong differences for the shed ectodomains in the secretome but to minor changes of the related cell surface levels. Though APP showed a 2-fold accumulation, the increase was relatively weak compared to APLP1, whose abundance was increased 7-fold. Indeed, it is known for several other BACE1 substrates, such as CHL1, L1CAM or DNER that they can also be cleaved by ADAM10 (Gutwein et al.,

2003; Kuhn et al., 2016; Kuhn et al., 2010; Maretzky et al., 2005). Additionally, cell surface levels of other BACE1 substrates were mildly enriched but did not survive the strict FDR filtering criteria, such as DNER with 1.34-fold increase. The adjustment for multiple comparisons lowers the significance value to very stringent levels and thus decreases so called false positives. However, this happens at the expense of false negatives, which are increased by applying this procedure (Drachmann, 2008). Hence, TM1 and GPI anchored proteins among 85 enriched proteins with $p<0.05$ but $q>0.0022$ represent potential BACE1 substrates. In other words, also other proteins, which were initially excluded as hits based on the FDR corrections, might therefore be additional true hits.
The fact, that BACE1 cleavage of its substrates occurs in the TGN or in endosomes, complicates the hypothesis that BACE1 can generally control surface levels of all of its substrates. If BACE1 activity is inhibited, uncleaved substrates might be still transported to the cell surface and accumulate, such as APLP1 or CNTN-2. For other uncleaved substrates, different regulations might apply: Instead of being transported to the cell surface, they remain inside endosomes or the TGN and/or are subjected to protein degrading machineries, such as lysosomes, preventing accumulation on the surface, as it was seen for several substrate candidates, such as GLG1, LRRN1 or SEZ6L2. A third mechanism could be feasible, in which uncleaved proteins are further transported to the surface, but then again internalised and/or degraded due to lack of function. Such proteins could be candidates, for which only a mild/moderate protein increase was detected on the surface, such as L1CAM, TMEM132a or DNER. In line with this, BACE1 substrates with a short half-life might accumulate only mildly whereas substrates with a slow turnover could possibly show a stronger accumulation – as was seen for the two BACE1 substrates APLP1 and APP. APLP1 has a half-life, which is much higher than the one of APP, 308 and 43 minutes respectively (Gersbacher et al., 2013; Weidemann et al., 1989). However, APLP1 is also more subjected to BACE1 cleavage than APP (Vassar, 2014). These are two evident factors, which need to be considered, when evaluating the accumulation of a protein after protease inhibition. Nevertheless, APP with its relatively short half-life of 43 min was sufficiently labeled and successfully enriched with the SUSPECS method to demonstrate its cell surface accumulation. In summary, protein turnover mechanisms, such as internalization, recycling as well as degradation, need to be taken into account, to evaluate direct BACE1-depentent changes of surface proteins and their abundance in the outer cell membrane.
Although strong changes after BACE1 inhibition were only observed for a few proteins, these alterations in neuronal surface composition might result in functional consequences. The protein CNTN-2 is a neuronal adhesion molecule and increased surface levels of CNTN-2 have been suggested to alter cell adhesion and by this affect neurite outgrowth and axon guidance (Gautam, 2014). Thus some of the reported phenotypes of BACE1-deficient mice might be partially based on increased neuronal CNTN-2 surface levels. Further, APLP1 is an important molecule at the synapse, where it functions as transcellular adhesion molecule (Muller et al., 2017) and altered protein expression leads to dysregulated synapse formation *in vitro* and *in vivo* (Schilling et al., 2017). Therefore, the observed increased levels of APLP1 at the neuronal surface upon BACE1 inhibition and in BACE1-deficent conditions could be responsible for the reported phenotypes regarding synapse formation and maintenance (Filser et al., 2015; Savonenko et al., 2008; Zhu et al., 2016).

Worth mentioning, also BACE1 itself showed an accumulation of 1.5-fold ($p=0.054$). This might be a compensatory effect of neurons, which upregulated the expression of BACE1 in response to the loss of function. Alternatively, the inhibitor could also stabilize BACE1 and prevent its degradation as was recently shown for ADAM10 (Brummer et al., 2018). Importantly, observed changes did not only comprise putative BACE1 substrates, which would be mostly single-span and GPI-anchored proteins. A non-substrate, which showed

FDR-significant and strong accumulation after pharmacological BACE1 inhibition, was the type II membrane protein PLD3 that increased 2.3-fold. Interestingly, genetic variants in PLD3 have been linked to APP processing and an increased risk for Alzheimer's disease (Cruchaga et al., 2014). However, these findings were recently challenged and suggest a more complex role for PLD3 in AD (Fazzari et al., 2017). This study did not observe a link between BACE1 and PLD3, since BACE1 mRNA was not changed downstream of genetic PLD3 deletion (Fazzari et al., 2017). Nevertheless, PLD3 accumulated on the neuronal surface after BACE1 inhibition, which indicates a possible connection between these two proteins.
Additionally, several proteins, which are unlikely to be proteolytically affected by BACE1, showed significant alterations after FDR correction upon BACE1 inhibition. Six of these apparent non-substrates (SCL38A3, UBAC2, LMBRD1, TSPAN3, TSPAN6, TTYH3) had more than one transmembrane domain and hence were not expected to show changed protein levels. Altered abundance of these proteins therefore points towards secondary effects resulting BACE1 inhibition. Such detected indirect changes affected for example the tetraspanins TSPAN6 and TSPAN3. Tetratspanins are known to be important for membrane protein trafficking, regulation of membrane-anchored enzymes, growth factor signaling, and cell adhesion (Charrin et al., 2014). Hence, they influence a variety of cellular proteins and processes, whose dysregulation cloud lead to adverse effects after BACE1 inhibition and might be partially accountable for observed non-mechanism-based side effects in patients. On the positive side, the here detected secondary effects could be used in future studies to decipher the mechanism of unexpected side effects, for example due to enhanced or decreased activation of signaling pathways.

5.2.3 BACE1 loss of function differentially affects its substrates in secretome and surface proteome

Previously, the secretome of primary mouse neurons in response to BACE1 inhibition was analyzed using SPECS, where BACE1 inhibition reduced shedding of more than 30 substrates and substrate candidates in the secretome (Kuhn et al., 2012). The here presented study provides the cell surface proteome counterpart using SUSPECS. A meta-analysis of both studies evaluated how the effects of BACE1 inhibition in the secretome compare to the surface proteome.
A strong reduction of a protein in the secretome analysis was interpreted as main BACE1 substrate. In other words, a strong reduction of ectodomain pointed towards a protein, which was cleaved mainly or exclusively by BACE1. Conversely, this would mean that BACE1 loss of cleavage would result in strongly accumulating levels of the full-length protein if the cleavage is efficient, since no other protease could compensate. Indeed, this assumption seems to hold true for the two most reduced secretome proteins SEZ6 and SEZ6L, which decreased almost completely in the secretome upon BACE1 inhibition and showed strong accumulation of surface levels in this study. However, the protein APLP1, which in the same way as the SEZ6 proteins, was strongly reduced in the secretome and showed even stronger accumulated full-length levels in the surface proteome, was reported to be cleaved by other proteases (Eggert et al., 2004).
Sorting the substrates according to their reported reduction in the secretome after BACE inhibition and directly comparing their accumulation in the surface, demonstrated that these two tightly connected processes did not correlate well for all substrates and hence make it difficult to reliably predict a reciprocal effect. This is confirmed with following example: L1CAM was one of the proteins with a strong reduction in secretome levels, but only accumulated mildly in the surface proteome. In the same manner, GLG1, LRRN1, and NTM did not increase on the surface to the extent of their reduction in the secretome. Yet some proteins, such as APP and CNTN-2 showed only a mild reduction of ectodomain levels, but were among the strongest increases at the cell surface. However, for some proteins, such as

DNER, SEZ6L2 and TMEM132a their mild reduction of secretome levels correlated relatively well to their mild or no increase of cell surface levels. Thus, there is a reasonable correlation between changes at the cell surface and in the secretome for several substrates. Yet, a lack of correlation was observed for the BACE1 substrates CNTN2, APP, and L1CAM, where strong (or mild) effects at the surface were not accompanied by according effects in the secretome. This partially poor correlation could on the one hand be a result of the compensating processing of other proteases, as was shown for ADAM10 and BACE1 and their common substrate APP, where a loss of cleavage by one protease can lead to an up regulated processing by the other (Colombo et al., 2013). Another possible explanation would be that only a certain percentage of available full-length protein is actually shed into the secretome meaning that a minor increase in surface levels could reflect a complete block of shedding. Although, the applied mass spectrometry-based label-free protein quantification is well suited to relatively quantify changes of protein abundance, it is not suited to evaluate protein generation or turnover. To investigate those effects, a dedicated label-based mass spectrometry approach such as pulsed SILAC would be the right experimental set-up (Visscher et al., 2016).
As discussed in the prior section, other cellular processes, regulating a membrane protein's abundance at the cell surface, have to be as well considered when evaluating the effect of BACE1-inhibition, supporting the hypothesis that BACE1 alone does not control the surface levels of all its substrates.

5.2.4 BACE2 sheds VCAM1 in primary mixed glia

BACE2 is a closely related homolog of BACE1 and the two proteases are known to share substrates, such as APP, JAG1, and the SEZ6 family proteins (Yan, 2017). Still, they as well show distinct cleavage specificity, due to different tissue expression patterns with BACE1 being the main form in brain or better neurons and thus responsible for Aβ generation. Though BACE2 also cleaves APP, cleavage does not result in Aβ peptides, since it mainly occurs within the Aβ peptide domain (Bennett et al., 2000; Farzan et al., 2000). Additionally, BACE2 is expressed at only low level in all brain cell types and predominantly in peripheral tissues, such as pancreas, kidney, and colon (Bennett et al., 2000; Voytyuk et al., 2018b).
Although, current BACE inhibitors in clinical trials target BACE1, they are not specific and also inhibit BACE2 (Bennett et al., 2000; Farzan et al., 2000), which raises concerns about cross-inhibition based side effects (Bennett et al., 2000; Voytyuk et al., 2018a). Moreover, BACE2-functions and substrates in the brain are poorly described and several studies with BACE inhibitors in humans have already been terminated, because they showed non-mechanism based side effects (Egan et al., 2018; Janssen, 2018; May et al., 2011). Some of these side effects caused a change in hair color pigmentation and were mediated by BACE2 inhibition and absent processing of the melanocyte protein PMEL (Egan et al., 2018; Rochin et al., 2013). This emphasizes the need of BACE2-function and substrate identification in the brain. Specific BACE2 substrates would not only allow to predict and prevent potential side effects based on cross-inhibition, but also could help monitoring and evaluating BACE1 and BACE2 inhibition during treatment AD treatment.
In a collaborative study with I.Voytyuk (Department of Neurosciences, Katholieke Universitet Leuven, Belgium) SPECS was therefore used to determine BACE2 substrates. Recent studies reported an enriched expression of BACE2 in oligodendrocytes and astrocytes (Dominguez et al., 2005; Zeisel et al., 2015; Zhang et al., 2014). Hence, primary mixed glia cultures from BACE1 knockout animals were treated with the BACE1/2 inhibitor Compound J (CpJ) and vehicle and subjected to mass spectrometry (MS)-based secretome analysis. In other words, the effect of absent BACE2-proteolytic function was investigated in a background of BACE1 knockout. The investigation yielded 4 proteins, which were likely to be processed by BACE2, since they 1) were transmembrane type I proteins, 2) reduced by

more than 30 % upon BACE2 inhibition, and 3) MS identified only peptides derived from the proteins' ectodomains. The BACE2 substrate candidates were the Vascular cell adhesion protein 1 (VCAM1, 80 % reduction), Delta and Notch-like epidermal growth factor-related receptor (DNER, 73 % reduction), Fibroblast growth factor receptor 1 (FGFR1, 48 % reduction), and Plexin domain-containing protein 2 (PLXDC2, 35 % reduction). The strong reduction of VCAM1 and DNER suggests BACE2 as major sheddase for these two proteins in glia, whereas FGFR1 and PLXDC2 might be cleaved by additional proteases in this cell type.

In the subsequent analysis, I. Voytyuk validated VCAM1 and DNER as BACE2 substrates in primary mixed glia cultures with Western blot analysis. FGFR1 and PLXDC2 were validated in COS-1 overexpressing cells with Western blot analysis. Moreover, further investigation showed that these substrates were predominantly processed by BACE2 under inflammatory conditions, which conspicuously increased shedding of VCAM1 (Voytyuk et al., 2018b). An upregulation of VCAM1 was already observed in rat brains after injuries (Zhang et al., 2015a), in the periphery of AD patients (Lai et al., 2017), and in CSF with increasing age (Li et al., 2017a). Therefore, the results obtained in this collaborative study implicate a BACE2-function during inflammatory responses, which might be of particular importance during stages of AD, when pathology is already full-blown and acute inflammatory processes are ongoing.

5.3 MT5-MMP poses an alternative drug target in AD

Besides BACE1 and ADAM10, the matrix metalloprotease MT5-MMP has shown to have a potential impact on AD pathology. Although MT5-MMP was already linked to Alzheimer's disease (AD) in 2001, where it was localized in dystrophic neurites around Aβ-plaques in post-mortem brains of AD patients (Sekine-Aizawa et al., 2001), interest in MT5-MMP and its function only developed recently and predominantly based on two findings:
First, MT5-MMP was described as the APP η-secretase and demonstrated to cleave APP upstream of the BACE1 cleavage site and mediate the generation of alternative APP soluble and membrane-bound fragments (Willem et al., 2015). Second, MT5-MMP deficiency was shown to decrease Aβ load and thus reduce AD pathology, gliosis, and inflammation in an AD mouse model. Simultaneously, cognitive and LTP dysfunctions and LTP were improved (Baranger et al., 2016b).
Apart of a few MT5-MMP substrates and physiological functions, which were elaborated in more detail in the introduction, the protease is not well described, due to no apparent phenotype of MT5-MMP knockout in mice. The fact that loss of function of the protease does not lead to histological defects or developmental deficits in the nervous system (Komori et al., 2004) makes the protein an attractive target for therapeutic development in AD. Conversely, MT5-MMP was reported to have an impact under pathological conditions, such as sciatic nerve injury (Komori et al., 2004) and inflammatory response (Folgueras et al., 2009). Particularly this pathology-dependent behavior underlines the proteases value as potential therapeutic target for AD. However, to understand the physiological involvement of MT5-MMP is as important in order to predict and prevent putative side effects of pharmacological modulation of the protease. Therefore, this thesis aimed to elucidate the (patho-)physiological involvement of MT5-MMP.

5.3.1 MT5-MMP is not a major sheddase in physiological conditions

To identify neuronal substrates, the secretome of primary MT5-MMP knockout neurons was compared to wildtype secretome. SPECS as a proteomic discovery approach did not yield any candidates. Although the here performed study was conducted with half of the usually used

material, mass spectrometric secretome analysis identified an adequate number of glycosylated proteins compared to previous SPECS studies (Kuhn et al., 2015; Kuhn et al., 2012; Pigoni et al., 2016). MT5-MMP is highly expressed in the whole brain during late embryonic stages (embryonic day E15 to perinatal) and limited to regions of high plasticity (cortex, hippocampus, cerebellum) in the adult brain (Jaworski, 2000). The neuronal population used for the experiments were a mixture of cortical and hippocampal neurons extracted on E16.5 and obtain a high abundance of MT5-MMP. However, no significant reduction of transmembrane proteins was observed in the secretome of MT5-MMP knockout neurons, which would have indicated proteolytic transmembrane protein shedding. In general, the detected changes were very mild and overall not significant.

Only one protein was found to be significantly mildly upregulated, the sialyltransferase Beta-galactoside alpha-2,6-sialyltransferase 2 (ST6GAL2), which did not meet significant criteria after correction for false discovery rate (FDR) and is likely to be a false positive hit. Nevertheless, if ST6GAL2 was specifically upregulated in the secretome of MT5-MMP neurons, a possible scenario would be explained with the following:

ST6GAL2 is a Golgi-residing enzyme (Takashima, 2003), but activation of MT5-MMP proteolytic function happens in the trans-Golgi network (Pei, 1999). Therefore, proteolytic processing of ST6GAL2 by MT5-MMP is unlikely. However, the close homolog ST6GAL1 was reported to be cleaved by BACE1 and subsequently secreted (Kitazume et al., 2001). Whether BACE1 also cleaves ST6GAL2 was not yet investigated. However, if both homologs are BACE1 substrates, an interaction of MT5-MMP with ST6GAL2 in the Golgi could prevent cleavage by BACE1. An absence of MT5-MMP and the cleavage-protective interaction could result in increased ST6GAL2 processing by BACE1 and would result in increased levels in the secretome. This hypothesis postulates a non-proteolytic function for MT5-MMP, which was already suggested (Baranger et al., 2017; Baranger et al., 2016a) and has been shown for other membrane-bound proteases (Szabo et al., 2016). An additional explanation for the few significantly changed proteins in the MT5-MMP knockout secretome could be an involvement of the protease with the cell's glycosylation machinery. The SPECS method used for enrichment of secreted proteins is based on N-glycosylation and targets sialic acid, which is the terminal structure of such glycans (Kuhn et al., 2012; Varki et al., 2017). An interference of MT5-MMP-deficiency with sialyltransferases within the Golgi could be a reason for impaired glycosylation and in consequence result in inefficient protein enrichment with SPECS. Yet, generally impaired glycosylation would have consequences for numerous cellular mechanisms, such as cell adhesion and cell signaling, and most likely present in strong phenotypes, which are absent in MT5-MMP knockout mice (Komori et al., 2004; Varki, 2017). Another reason for absent alterations in the secretome could be functional compensation of the lost MT5-MMP activity by other membrane-bound proteases. However, this would likely affect the processing of more than one protein. Additionally, MT5-MMP could be responsible for the processing of soluble proteins, rather than membrane-bound ones. This possibility would be supported by a two studies, which described an active soluble form of MT5-MMP (Pei, 1999; Wang and Pei, 2001). This would ascribe functions to MT5-MMP that are similar to protein degradation and could explain very low and not detectable amounts of MT5-MMP-cleaved proteins in cell culture supernatant.

Importantly, in line with the neuronal secretome analysis no major proteomic changes were found in the cerebrospinal fluid (CSF) of MT5-MMP knockout animals. CSF represents the *in vivo* secretome of the whole brain, since it is topologically equivalent to the extracellular space. It contains secreted proteins and proteolytically shed ectodomains derived from of all brain cells. Rather than cell type-specific substrates, proteomic CSF analysis indicates global proteomic changes in a preserved network of different cell types *in vivo*. Only one protein was significantly changed after FDR correction in CSF upon MT5-MMP knockout: The cerebellum-derived protein cerebellin1 (CBLN1) showed a mild decrease of 52 %. CBLN1 is

a secreted protein and implicated in cerebellar synapse formation (Ito-Ishida et al., 2012). Also MT5-MMP is highly expressed in the cerebellum (Sekine-Aizawa et al., 2001) and hence a functional connection between these two proteins feasible. Further, the secreted nature of CBLN1 makes a proteolytic cleavage by the membrane-bound MT5-MMP unlikely and again points to a non-proteolytic function of the protease. Two other mildly but not significantly decreased proteins were cerebellin3 (CBLN3, 53 % reduction) and neurexin1 (NRX1, 20 % reduction), which are functionally connected to CBLN1 (Bao et al., 2006; Ito-Ishida et al., 2012; Uemura et al., 2010). Presynaptic NRXN1 interacts through CBLN1 with the postsynaptic glutamate receptor GluRδ2 and is essential for cerebellar synapse formation (Cheng et al., 2016; Uemura et al., 2010). Therefore, non-significant changes could represent downstream effects of CBLN1 reduction. However, the reduced level of CBLN1 seems to have no major consequences and not result in a cerebellar phenotype of MT5-MMP knockout animals (Komori et al., 2004; Vinueza Veloz et al., 2015).

5.3.2 MT5-MMP engages in general disease-related processes in AD pathology

The identification of direct proteolytic MT5-MMP substrates from embryonic neurons did not yield the expected outcome and prevented a categorization of the protease's function. Whereas, proteomic analysis of cerebrospinal fluid (CSF) from adult MT5-MMP knockout animals pointed towards a more pronounced function for the protease in the cerebellum under physiological conditions. In this manner, performing a more extensive proteomic analysis using CSF from MT5-MMP knockout animals in the background of the AD-mouse model 5xFAD was supposed to elucidate the protease's pathology-dependent functions. Moreover, the approach was expected to determine globally involved mechanisms in the brain that led to beneficial AD pathology upon MT5-MMP knockout (Baranger et al., 2017).

Overall, 56 proteins were found significantly changed despite application of strict significance criteria to avoid putative false positive protein hits. Two of these proteins (KIT, NPY) showed increased levels in the CSF of double transgenic 5xFAD/MT5 KO animals in comparison to 5xFAD animals without a knockout of MT5-MMP, while the remaining 54 proteins were reduced.The secreted neuropeptide Y (NPY), was increased 1.87-fold in the CSF of 5xFAD mice. This protein has been shown to have neuroprotective effects in AD neuron-like models and primary neurons, treated with toxic concentrations of β-amyloid (Aβ) peptide, where it increased production of nerve growth factor (NGF) and brain-derived neurotrophic factor BNDF (Croce et al., 2012; Croce et al., 2011). NGF and BNDF have been demonstrated to be important for the function and survival of neurons that degenerate in AD (Cuello et al., 2010; Nagahara et al., 2009). Like NGF and BNDF, NPY is protective against excitotoxicity and modulates neurogenesis (Decressac et al., 2011; Howell et al., 2005; Silva et al., 2003) and is most likely acting through these two neurotrophins. In addition, NPY was reported to be protective against CNS damage resulting from Aβ deposits and tau tangles in an AD mouse model (Rose et al., 2009). Most importantly, CSF of AD patients displayed reduced levels of NPY (Alom et al., 1990). In line with the beneficial effect of MT5-MMP-deficiency in AD-mice NPY was increased in 5xFAD-MT5 KO CSF, indicating a role for MT5-MMP in pathology-dependent regulation of NPY levels.

Proteins, which were increased in the CSF of 5xFAD animals and linked to AD-pathological mechanisms, immunological, and neurodegenerative responses, such as APP, TREM2, cathepsin proteins, FAB proteins, and NEFM, were not changed upon MT5-MMP knockout. A possible explanation for this outcome could be that MT5-MMP-deficiency interferes only with specific mechanisms during pathology progression. Disease markers like TREM2 and NEFM might be regulated independently of MT5-MMP activity and presence. Not altered CSF APP levels reflect an unaffected soluble protein amount upon MT5-MMP knockout in the 5xFAD background. Though the here used label-free mass spectrometry approach does not discriminate between different soluble APP fragments, it might be possible that MT5-

MMP-deficiency changed the ratio of soluble APP fragments. However, to confirm this hypothesis, a targeted mass spectrometry approach would be necessary. Even if the total soluble APP level was not altered in CSF of 5xFAD-MT5 KO compared to 5xFAD animals, the aggregated Aβ-plaque load was shown to be reduced in these mice (Baranger et al., 2016b).
Opposed to the above mentioned, not changed proteins, 16 significantly regulated proteins, which were increased in the CSF of 5xFAD animals, were found to be decreased upon MT5-MMP knockout. Among these proteins, vimentin (VIM) was increased 3-fold in the CSF of 5xFAD mice and decreased by over 80 % in the CSF of 5xFAD-MT5 KO animals compared to 5xFAD. Recently, VIM was detected to be enriched inside Aβ-plaques derived from postmortem human AD brain (Moya-Alvarado et al., 2016). VIM is mostly absent in healthy neurons, but was expressed in neurons within brain regions with AD pathological Aβ accumulation and neurofibrillary tangle formation, but also upon mechanical injury. Its upregulation was described as damage-response mechanism to maintain dendrites and synaptic connections (Levin et al., 2009). VIM is an intermediate filament protein and structurally similar to the astrocytic glial fibrillary acidic protein (GFAP). A conspicuous increase of GFAP and VIM expression and morphological changes are the characteristics of reactive astrogliosis and typical for neuropathological conditions (Kato et al., 1998; Pekny et al., 2014; Simpson et al., 2010). In AD brains, astrocytes and microglia were shown to be vimentin-positive, when close to Aβ-plaques (Yamada et al., 1992). Furthermore, a differential regulation of the astrocytic phosphoprotein PEA-15 (PEA15) in 5xFAD CSF and 5xFAD-MT5 KO CSF indicates a putative involvement for MT5-MMP in regulation of astrocytic gliosis: PEA15 was shown to be upregulated in cortices of AD mouse models (Takano et al., 2012) where it regulates astroglial phagocytosis of Aβ (Lv et al., 2014). An increase was also confirmed in humans by studying Aβ-plaques from post-mortem Alzheimer's disease brains (Thomason et al., 2013).
Additionally, α-enolase (ENO1) was 2-fold increased in 5xFAD CSF and decreased by 63 % when MT5-MMP was knocked out in the 5xFAD background. The protein was already shown to be enriched in AD hippocampus, where it is oxidatively modified and therefore has reduced activity (Sultana et al., 2007; Sultana et al., 2006). ENO1 is a glycolytic enzyme and involved in ATP-generation (Harris et al., 2011). Modification of ENO1 might lead to reduced glucose metabolism and therefore suggest a connection between glycolytic enzymatic impairment and reduced energy production in glucose metabolism in AD (Messier and Gagnon, 1996; Ogawa et al., 1996). As glucose metabolism is the main source of ATP production impairment of glycolytic enzymes might result in severe cellular dysfunctions eventually leading to apoptosis (Mohammad-Abdul and Butterfield, 2005). An upregulation of ENO1 during AD pathology might point to an increased protein synthesis to compensate the impaired enzymatic activity. Conversly, reduction of ENO1 upon MT5-MMP knockout in a 5xFAD background might be an indication for a healthier state of brain cells.
As for the here exemplary described proteins NPY, VIM, and ENO1, MT5-MMP could be involved in regulation of the other 14 proteins, which were increased in the CSF of 5xFAD mice and decreased upon MT5-MMP knockout in the 5xFAD background. None of the 16 proteins is a transmembrane protein and therefore unlikely to be proteolytically affected by MT5-MMP. Hence, MT5-MMP might therefore have a role in regulation of these proteins, which is based on protein-protein interaction or trafficking rather than proteolytic cleavage.
A more general approach to categorize the role of MT5-MMP in AD pathology, rather than a candidate-based search, was intended by clustering all significantly changed proteins according to their functionality and involvement in cellular mechanisms. Hence, proteins are clustered to biological processes, in which MT5-MMP might play a role in under pathological AD conditions. A clustering into biological processes, describes the pathways and larger processes, in which multiple of the identified proteins are involved and active. The majority

of proteins were classified to have oxidoreductase activity (28 %), which are proteins that catalyze the transfer of electrons from donor to an acceptor, which usually involves co-factors such as NADH or NADPH. This functional class contained e.g. several dehydrogenases, which were reduced in MT5-MMP-deficient 5xFAD CSF. Several AD studies, based on genetics, transcriptomics, proteomics and animal models suggest an involvement of aldehyde dehydrogenases in the neurodegenerative processes (Grunblatt and Riederer, 2016). Further significantly changed proteins in 5xFAD CSF upon MT5-MMP knockdown largely were involved in three biological processes: 1) cellular processes, such as cell communication, 2) metabolic processes, such as biosynthetic or catabolic processes, and 3), response to stimuli, which included cellular defense and stress responses. The fact that proteins involved in these mechanisms showed reduced CSF levels, demonstrates a pathology-dependent involvement of MT5-MMP with disease-stimulating consequences in fundamental biological processes.
Even though the here presented study did not succeed to identify physiologic proteolytic substrates of MT5-MMP, it attempted to reveal the protease's global involvement in AD pathology. In addition, it provided the basis for future candidate-based studies to determine the exact mode of action that allows the protease to regulate the above-described mechanisms under pathological conditions. Moreover, the in this work described changes and identified proteins in the CSF can be used as putative biomarkers for future MT5-MMP therapy development and studies.

5.4 Therapeutic potential of ADAM10, BACE1, and MT5-MMP modulation in AD

The membrane proteases ADAM10, BACE1, and MT5-MMP are directly involved in generation of neurotoxic and aggregating APP fragments (Kuhn et al., 2010; Vassar, 1999; Willem et al., 2015). A clinical pilot study with an approved psoriasis-drug, which stimulates ADAM10 activity, demonstrated anti-amyloidogenic potential of ADAM10 as drug target by increasing sAPPα levels in cerebrospinal fluid (CSF) of Alzheimer's disease (AD) patients (Endres et al., 2014; Tippmann et al., 2009). Unfortunately, no significant lowering of aAPPβ levels was observed and only an Aβ-reducing trend was demonstrated. In addition, only little is known about ADAM10 functions in the brain and research is just starting to reveal the full extent. Several newly described functions might therefore limit a therapeutic modulation of ADAM10 in AD (Kuhn et al., 2016; Saftig and Lichtenthaler, 2015). The here presented study contributed to assess the full involvement of ADAM10 in the brain by validating newly identified substrate candidates. One of these substrates has been shown to regulate axonal targeting in an ADAM10-dependent manner. Hence, a potential stimulation of ADAM10 activity in AD therapeutics could result in dysregulation and lead to adverse effects in patients. Notably, ADAM10 cleaves several substrates in the periphery that drive cancer progression and inflammatory disease, such as Notch, and stimulation of ADAM10 activity therefore bears a high risk potential of causing cancer (Atapattu et al., 2016; Crawford et al., 2009; Guo et al., 2012). To safely target ADAM10, a carefully dosed application of the drug would therefore be necessary in advance. Whether a reduced dosage would still lead to the observed potential anti-amyloidogenic effects remains to be seen. Maybe a combination of ADAM10 stimulation and BACE1 inhibition in low doses presents a feasible approach to get the desired Aβ-lowering effect with a minimal risk of side effects.
As rate-limiting enzyme in Aβ generation, BACE1 is the current major drug target and Aβ-lowering potential of BACE1 inhibition has been extensively demonstrated (Vassar et al., 2014). However, numerous physiological functions, besides APP-cleavage, and recent premature termination of a BACE1 inhibitors in clinical Phase II/III, raise concerns regarding the feasibility of BACE1 inhibition in AD therapeutics (Barao et al., 2016; Egan et al., 2018; Janssen, 2018; Yan, 2017). Data acquired in the scope of this work, underlines the

physiological importance and broad involvement of BACE1. Further it demonstrates that disruption of these functions might severely compromise neuronal physiology and thereby brain functions. As already implemented by several pharmaceutical companies, a mild inhibition of enzymatic BACE1 functions together with an early starting point of drug application might be a solution to avoid major interference with BACE1 physiological roles (Voytyuk et al., 2018a). Since Aβ-deposition starts already early and before any severe symptoms, a careful timing for drug administration could be compatible with low BACE1 inhibitor doses. However, if drug treatment in 'healthy' individuals is the right alternative is questionable.

An alternative drug target has appeared with MT5-MMP, whose connection to AD was known for some time, but only recently demonstrated to have beneficial potential in therapeutic development (Baranger et al., 2016b; Sekine-Aizawa et al., 2001). Yet, the full involvement of MT5-MMP in the nervous system under physiological conditions as well as its pathology-dependent function is poorly understood and may complicate its potential use as drug target in AD (Baranger et al., 2016a; Itoh, 2015). The here conducted study attempted a first step to assess the physiological function of MT5-MMP by identifying its proteolytic substrates. Obtained results indicate limited involvement of the protease in healthy conditions and are in line with prior reported studies (Komori et al., 2004). A modulation of MT5-MMP in AD therapeutics might therefore be free of adverse effects and pose a potentially safe approach. However, a specific inhibitor, which targets MT5-MMP and is highly selective over the other MMP family members, does not exist at the moment. Furthermore, the observed beneficial effects of MT5-MMP-deficiency in mice need to be confirmed in higher species, before an application in humans is feasible.

6 Summary

Alzheimer's disease (AD) is the most common form of age-related dementia and currently affects around 50 million people worldwide. As our population ages, this number is expected to increase substantially in the future. Developing disease-modulating and –preventing therapeutics poses a big clinical challenge at the time and regardless of AD research progress, the majority of clinical trials in the past have still failed. Therefore, the need to fully decipher, understand, and connect involved molecular disease mechanisms is of utmost importance for successful drug development in the future.
To this end, this thesis investigated the three proteases a disintegrin and metalloprotease 10 (ADAM 10), the beta-site APP cleaving enzyme 1 (BACE 1), and the membrane-type 5 matrix metalloprotease (MT5-MMP). They are all known to cleave the amyloid precursor protein (APP), from which the toxic Aβ peptide is generated. Hence, the proteases' direct involvement in the molecular progress of AD pathology makes them therapeutic targets in drug development. Yet, their function in the brain and their substrates are not fully known, which poses a risk of side effects during therapeutic disease modulation.
The here conducted study successfully addressed existing limitations regarding the above mentioned proteases and thus contributes to their understanding:

1. Validation of novel substrate candidates of ADAM10.
An independent biochemical experimental approach validated two newly identified substrate candidates NrCAM and NEO1 as physiological ADAM10 substrates. The two proteins demonstrate a function for ADAM10 in neurite outgrowth and regulation of axon targeting by NrCAM cleavage. This result led to the description of another central ADAM10 function in the brain.

2. Investigation of cell surface membrane composition upon pharmacological BACE1 inhibition.
a. A new method named SUSPECS (Surface-spanning protein enrichment with click sugars) was established. It allows specific biotinylation for subsequent enrichment of glycosylated transmembrane proteins at the cell surface. SUSPECS is suitable for mass spectrometry and other downstream applications such as immunoblotting or ELISA. This study validated SUSPECS as an efficient method to target the cell surface proteome and analysis of BACE1 inhibitor treated primary neurons demonstrates the strengths of this new method. More importantly, combining SUSPECS with secretome studies opens a wide range of biological applications, such as cell-secretome changes under inflammatory conditions or cross-talk between different cell types in pathology.
b. SUSPECS analysis of BACE1 inhibited neurons revealed a cell surface proteome-modulating function for BACE1. Opposed to common belief, BACE1 proteolytic cleavage is not a general mechanism to control its substrates' surface levels. Rather, the inhibition of the enzyme led to accumulation of only a subset of substrates. Other substrates showed only mild or no increase. In addition, this study shows accumulation of other biologically important proteins (for example tetraspanins), which represent secondary changes following BACE1 inhibition and could be used to decipher the mechanism of unexpected side effects (e.g. due to enhanced or decreased activation of signaling pathways). Moreover, transmembrane proteins with type 1 orientation were found to be accumulated at the cell surface, which have not been described as BACE1 substrates so far and potentially represent additional substrates.

3. Identification of MT5-MMP substrates and the protease's function in AD.
Proteomic analysis of MT5-MMP knockout neuronal secretome and cerebrospinal fluid (CSF) revealed only limited involvement of the protease under physiological conditions and did not

yield potential proteolytic substrate candidates. CSF analysis implicated a role for MT5-MMP in the regulation of CBLN1, an important protein in cerebellar synapse formation.
Investigation of global proteomic changes in CSF of an AD mouse model in the presence and absence of MT5-MMP showed a clear impact of MT5-MMP-deficiency. 56 significantly changed proteins were identified and clustered to narrow down the biological processes MT5-MMP might play a role in under pathological AD conditions. Results provide a comprehensive basis for further experimental work to study MT5-MMP's pathology-related involvement in more detail.

This study provides important information on the patho-physiological involvement of the investigated proteases ADAM10, BACE1, and MT5-MMP. The herein obtained results do not only add to the fundamental understanding of the proteases' function in the brain, but also deliver valuable insights in their potential and relevance as drug targets. Moreover, this thesis provides a profound basis and a new method for future studies in the field of disease-relevant proteases.

7 Outlook

Considering the published work and the in this thesis obtained results for the investigated proteases, ADAM10, BACE1, and MT5-MMP, BACE1 still poses the most promising drug target-candidate. In the first place, this is due to the already developed and currently tested inhibitors in advanced clinical trials (Yan, 2016) and the still unrevoked amyloid hypothesis, which implicates Aβ-generation and aggregation as a leading mechanism in the development of AD pathology (Selkoe and Hardy, 2016). The advanced stage of BACE1-inhibitor testing will demonstrate over the following years, if this direction of treatment will remain the leading one or if adjustments have to be made. A major criticism remains the occurring non-mechanism-based effects upon BACE1 inhibition and the concern of not fully understanding the full physiology behind the protease. However, over the last years, extensive progress uncovered numerous physiological BACE1 substrates and the gained knowledge is being used to monitor disease treatment and also to carefully reconsider drug dosing and treatment starting time (Vassar, 2014; Vassar et al., 2014; Voytyuk et al., 2018a). Although AD modulation with BACE1 inhibition turned out to be more demanding than expected, the failed and still ongoing clinical trials will provide a lot of valuable insights for AD treatment and further improve therapeutic development. A considerable approach could be a combination of BACE1 inhibition to counteract Aβ production and aggregation together with immunotherapeutic strategies of antibodies targeted against tau and Aβ to resolve aggregation and toxicity.

A potential therapeutic strategy targeting ADAM10 needs to prevail anti-amyloidogenic clinical relevance of increasing sAPPα levels by actually lowering Aβ levels, which was not confirmed until now (Endres et al., 2014). After all, the growing number of ADAM10 substrates in the brain reveals the physiological importance of the protease and could result in similar concerns regarding mechanistic side effects upon ADAM10 stimulation. An advantage of ADAM10 as therapeutic target is the already present and approved drug Acitretin. Yet, Acitretin is approved for treatment of psoriasis and therefore would need to still be clinically tested for applicability in AD treatment. The driving role of ADAM10 in different types of peripheral cancer and inflammation however, presents severe risk potential in ADAM10 activity-stimulating target strategies. Concluding, though ADAM10 activation showed positive results in a clinical pilot-study, it did not significantly affect Aβ levels. The latter and its emerging roles in the brain and the involvement in peripheral pathophysiology is a severe obstacle for ADAM10 activation in AD therapeutics.

A new and unexplored putative drug target is MT5-MMP. Little is known about its physiological function, but its potential in AD therapeutics is evident (Baranger et al., 2017; Baranger et al., 2016b). The results obtained in this thesis indicate that MT5-MMP function might be redundant during the embryonic period and only limited in adult stages, as seen in only mild changes of CBLN1 levels in CSF of MT5-MMP knockout animals. This may also be reflected in the observation that the analysis of MT5-MMP knockout secretome derived from embryonic neurons, revealed no major changes, thereby confirming limited or redundant physiological involvement, as already reported in literature (Komori et al., 2004) Yet, this absence of functional relevance confirms the potential of therapeutic MT5-MMP inhibition or modulation and avoids concerns about mechanism-based side effects. Nevertheless, beneficial effects of MT5-MMP absence need to be reproduced and confirmed in higher species, such as primates, before a safe application in humans is realistic. A further setback herein, is the current lack of specific and selective inhibitors for MT5-MMP, which first need to be developed to realize MT5-MMP-modulating strategies.

Abbreviations

°C	Degree Celsius
A	Ampere
AC	Accession (number)
Ac_4-ManNAz	tetra-acetylated N-azidomannosamine
AD	Alzheimer's Disease
ADAM	A disintegrin and metalloprotease
AICD	APP intracellular-domain
APP	Amyloid precursor protein
Aβ	Amyloid β-peptide
BACE	β-site APP cleaving enzyme
BP	biological process
cm	Centimeter
COS	Cercopithecus aethiops kidney fibroblast cells, SV40 transformed
Cre	Cre recombinase
CSC	cell surface capturing
CSF	Cerebrospinal fluid
CTF	C-terminal fragment
DBCO	Dibenzylcyclooctyne
DIV	Day in vitro
DTAF	Dichlorotriazinylamino fluorescein
DTT	Dithiothreitol
ER	Endoplasmic reticulum
FASP	Filter aided sample preparation
FDR	False discovery rate
g	gravitational force
GFP	Green fluorescent protein
GO	Gene ontology
GPI	Glycosylphosphatidylinositol
HEK293	Human embryonic kidney cells 293
HPLC	High performance liquid chromatography
IAA	Iodoacetamide
KO	Knockout
L	Liter
LC	Liquid chromatography
LC-MS/MS	liquid chromatography coupled to tandem mass spectrometry
LFQ	Label free quantification
m	Milli
M	Molar
min	Minute(s)
MS	Mass spectrometry
MT5-MMP	Membrane-type 5 matrix metalloprotease
NEO1	Neogenin 1
PAL	periodate oxidation and aniline-catalyzed oxime ligation
PDL	Poly-D-lysine
QARIP	Quantitative Analysis of Regulated Intramembrane Proteolysis
QARIP	Quantitative analysis of regulated intramembrane proteolysis
RIP	Regulated intramembrane proteolysis
rpm	Revolutions per minute
RT	Room temperature
sAPP	Soluble APP ectodomain
SPECS	Secretome protein enrichment with click sugars
STAGE	Stop and go extraction
SUSPECS	Surface-spanning protein enrichment with click sugars

TGN	Trans-Golgi network
TM	Transmembrane (type)
V	Volt
v/v	Volume per volume
w/v	Weight per volume
WB	Western blot
WT	Wildtype

References

Aebersold, R., and Mann, M. (2016). Mass-spectrometric exploration of proteome structure and function. Nature *537*, 347-355.

Ahmad, M., Takino, T., Miyamori, H., Yoshizaki, T., Furukawa, M., and Sato, H. (2006). Cleavage of amyloid-beta precursor protein (APP) by membrane-type matrix metalloproteinases. J Biochem *139*, 517-526.

Aisen, P.S., Gauthier, S., Ferris, S.H., Saumier, D., Haine, D., Garceau, D., Duong, A., Suhy, J., Oh, J., Lau, W.C.*, et al.* (2011). Tramiprosate in mild-to-moderate Alzheimer's disease - a randomized, double-blind, placebo-controlled, multi-centre study (the Alphase Study). Arch Med Sci *7*, 102-111.

Allan, E.R.O., Campden, R.I., Ewanchuk, B.W., Tailor, P., Balce, D.R., McKenna, N.T., Greene, C.J., Warren, A.L., Reinheckel, T., and Yates, R.M. (2017). A role for cathepsin Z in neuroinflammation provides mechanistic support for an epigenetic risk factor in multiple sclerosis. J Neuroinflammation *14*, 103.

Alom, J., Galard, R., Catalan, R., Castellanos, J.M., Schwartz, S., and Tolosa, E. (1990). Cerebrospinal fluid neuropeptide Y in Alzheimer's disease. Eur Neurol *30*, 207-210.

Alonso, A., Zaidi, T., Novak, M., Grundke-Iqbal, I., and Iqbal, K. (2001). Hyperphosphorylation induces self-assembly of tau into tangles of paired helical filaments/straight filaments. Proc Natl Acad Sci U S A *98*, 6923-6928.

Altmeppen, H.C., Prox, J., Puig, B., Kluth, M.A., Bernreuther, C., Thurm, D., Jorissen, E., Petrowitz, B., Bartsch, U., De Strooper, B.*, et al.* (2011). Lack of a-disintegrin-and-metalloproteinase ADAM10 leads to intracellular accumulation and loss of shedding of the cellular prion protein in vivo. Mol Neurodegener *6*, 36.

Alz.co.uk. World Alzheimer Report 2016 (https://www.alz.co.uk/research/world-report-2016: Alzheimer's Disease International).

Alzheimer, A. (1907). Über eine eigenartige Erkrankung der Hirnrinde. Allgemeine Zeitschrift für Psychiatrie und psychisch-gerichtliche Medizin *46*, 146-148.

Ardura-Fabregat, A., Boddeke, E., Boza-Serrano, A., Brioschi, S., Castro-Gomez, S., Ceyzeriat, K., Dansokho, C., Dierkes, T., Gelders, G., Heneka, M.T.*, et al.* (2017). Targeting Neuroinflammation to Treat Alzheimer's Disease. CNS Drugs *31*, 1057-1082.

Arumugam, T.V., Cheng, Y.L., Choi, Y., Choi, Y.H., Yang, S., Yun, Y.K., Park, J.S., Yang, D.K., Thundyil, J., Gelderblom, M.*, et al.* (2011). Evidence that gamma-secretase-mediated Notch signaling induces neuronal cell death via the nuclear factor-kappaB-Bcl-2-interacting mediator of cell death pathway in ischemic stroke. Mol Pharmacol *80*, 23-31.

Atapattu, L., Saha, N., Chheang, C., Eissman, M.F., Xu, K., Vail, M.E., Hii, L., Llerena, C., Liu, Z., Horvay, K.*, et al.* (2016). An activated form of ADAM10 is tumor selective and regulates cancer stem-like cells and tumor growth. J Exp Med *213*, 1741-1757.

Bacioglu, M., Maia, L.F., Preische, O., Schelle, J., Apel, A., Kaeser, S.A., Schweighauser, M., Eninger, T., Lambert, M., Pilotto, A.*, et al.* (2016). Neurofilament Light Chain in Blood and CSF as Marker of Disease Progression in Mouse Models and in Neurodegenerative Diseases. Neuron *91*, 56-66.

Bantscheff, M., Lemeer, S., Savitski, M.M., and Kuster, B. (2012). Quantitative mass spectrometry in proteomics: critical review update from 2007 to the present. Anal Bioanal Chem *404*, 939-965.

Bantscheff, M., Schirle, M., Sweetman, G., Rick, J., and Kuster, B. (2007). Quantitative mass spectrometry in proteomics: a critical review. Anal Bioanal Chem *389*, 1017-1031.
Bao, D., Pang, Z., Morgan, M.A., Parris, J., Rong, Y., Li, L., and Morgan, J.I. (2006). Cbln1 is essential for interaction-dependent secretion of Cbln3. Mol Cell Biol *26*, 9327-9337.
Bar-Or, A., Nuttall, R.K., Duddy, M., Alter, A., Jin Kim, H., Ifergan, I., Pennington, C.J., Bourgoin, P., Edwards, D.R., and Yong, V.W. (2003). Alyses of all matrix metalloproteinase members in leukocytes emphasize monocytes as major in¯ammatory mediators in multiple sclerosis. Brain *126*.
Baranger, K., Bonnet, A.E., Girard, S.D., Paumier, J.M., Garcia-Gonzalez, L., Elmanaa, W., Bernard, A., Charrat, E., Stephan, D., Bauer, C.*, et al.* (2017). MT5-MMP Promotes Alzheimer's Pathogenesis in the Frontal Cortex of 5xFAD Mice and APP Trafficking in vitro. Front Mol Neurosci *9*, 163.
Baranger, K., Khrestchatisky, M., and Rivera, S. (2016a). MT5-MMP, just a new APP processing proteinase in Alzheimer's disease? J Neuroinflammation *13*, 167.
Baranger, K., Marchalant, Y., Bonnet, A.E., Crouzin, N., Carrete, A., Paumier, J.M., Py, N.A., Bernard, A., Bauer, C., Charrat, E.*, et al.* (2016b). MT5-MMP is a new pro-amyloidogenic proteinase that promotes amyloid pathology and cognitive decline in a transgenic mouse model of Alzheimer's disease. Cell Mol Life Sci *73*, 217-236.
Barao, S., Moechars, D., Lichtenthaler, S.F., and De Strooper, B. (2016). BACE1 Physiological Functions May Limit Its Use as Therapeutic Target for Alzheimer's Disease. Trends Neurosci *39*, 158-169.
Bennett, B.D., Babu-Khan, S., Loeloff, R., Louis, J.C., Curran, E., Citron, M., and Vassar, R. (2000). Expression analysis of BACE2 in brain and peripheral tissues. The Journal of biological chemistry *275*, 20647-20651.
Bensimon, A., Heck, A.J., and Aebersold, R. (2012). Mass spectrometry-based proteomics and network biology. Annu Rev Biochem *81*, 379-405.
Bercher, J.D., and Blobel, C.P. (2003). Biochemical properties and functions of mem- brane-anchored metalloprotease-disintegrin proteins (ADAMs). Curr Top Dev Biol *54*, 101-123.
Beyreuther, K., and Masters, C.L. (1991). Amyloid precursor protein (APP) and beta A4 amyloid in the etiology of Alzheimer's disease: precursor-product relationships in the derangement of neuronal function. Brain Pathol *1*, 241-251.
Bi, S., and Baum, L.G. (2009). Sialic acids in T cell development and function. Biochim Biophys Acta *1790*, 1599-1610.
Bien, J., Jefferson, T., Causevic, M., Jumpertz, T., Munter, L., Multhaup, G., Weggen, S., Becker-Pauly, C., and Pietrzik, C.U. (2012). The metalloprotease meprin beta generates amino terminal-truncated amyloid beta peptide species. The Journal of biological chemistry *287*, 33304-33313.
Black, R., Rauch, C.T., Kozlosky, C., Peschon, J.J., Slack, J.L., Wolfson, M.F., Castner, B.J., Stocking, K.L., Reddy, P., Srinivasan, S.*, et al.* (1997). A metalloproteinase disintegrin that releases tumour-necrosis factor-alpha from cells. Nature *385*, 729-733.
Blobel, C.P. (2005). ADAMs: key components in EGFR signalling and development. Nat Rev Mol Cell Biol *6*, 32-43.
Braisted, J.E., Catalano, S.M., Stimac, R., Kennedy, T.E., Tessier-Lavigne, M., Shatz, C.J., and O'Leary, D.D. (2000). Netrin-1 promotes thalamic axon growth and is required for proper development of the thalamocortical projection. J Neurosci *20*, 5792-5801.
Brown, M.S., Ye, J., Rawson, R.B., and Goldstein, J.L. (2000). Regulated Intramembrane Proteolysis. Cell *100*, 391-398.
Brummer, T., Pigoni, M., Rossello, A., Wang, H., Noy, P.J., Tomlinson, M.G., Blobel, C.P., and Lichtenthaler, S.F. (2018). The metalloprotease ADAM10 (a disintegrin and metalloprotease 10) undergoes rapid, postlysis autocatalytic degradation. FASEB J *32*, 3560-3573.
Charrin, S., Jouannet, S., Boucheix, C., and Rubinstein, E. (2014). Tetraspanins at a glance. J Cell Sci *127*, 3641-3648.
Cheng, S., Seven, A.B., Wang, J., Skiniotis, G., and Ozkan, E. (2016). Conformational Plasticity in the Transsynaptic Neurexin-Cerebellin-Glutamate Receptor Adhesion Complex. Structure *24*, 2163-2173.
Chiasserini, D., Biscetti, L., Eusebi, P., Salvadori, N., Frattini, G., Simoni, S., De Roeck, N., Tambasco, N., Stoops, E., Vanderstichele, H.*, et al.* (2017). Differential role of CSF fatty acid

binding protein 3, alpha-synuclein, and Alzheimer's disease core biomarkers in Lewy body disorders and Alzheimer's dementia. Alzheimers Res Ther *9*, 52.
Chiasserini, D., Parnetti, L., Andreasson, U., Zetterberg, H., Giannandrea, D., Calabresi, P., and Blennow, K. (2010). CSF levels of heart fatty acid binding protein are altered during early phases of Alzheimer's disease. *22*, 1281-1288.
Chiba, S. (2006). Notch signaling in stem cell systems. Stem Cells *24*, 2437-2447.
Colombo, A., Wang, H., Kuhn, P.H., Page, R., Kremmer, E., Dempsey, P.J., Crawford, H.C., and Lichtenthaler, S.F. (2013). Constitutive alpha- and beta-secretase cleavages of the amyloid precursor protein are partially coupled in neurons, but not in frequently used cell lines. Neurobiol Dis *49*, 137-147.
Cox, J., Hein, M.Y., Luber, C.A., Paron, I., Nagaraj, N., and Mann, M. (2014). Accurate proteome-wide label-free quantification by delayed normalization and maximal peptide ratio extraction, termed MaxLFQ. Molecular and Cellular Proteomics *13*, 2513-2526.
Cox, J., and Mann, M. (2007). Is proteomics the new genomics? Cell *130*, 395-398.
Cox, J., and Mann, M. (2008). MaxQuant enables high peptide identification rates, individualized p.p.b.-range mass accuracies and proteome-wide protein quantification. Nat Biotechnol *26*, 1367-1372.
Cox, J., and Mann, M. (2011). Quantitative, high-resolution proteomics for data-driven systems biology. Annu Rev Biochem *80*, 273-299.
Crawford, H., Dempsey, P., Brown, G., Adam, L., and Moss, M. (2009). ADAM10 as a Therapeutic Target for Cancer and Inflammation. Current Pharmaceutical Design *15*, 2288-2299.
Croce, N., Ciotti, M.T., Gelfo, F., Cortelli, S., Federici, G., Caltagirone, C., Bernardini, S., and Angelucci, F. (2012). Neuropeptide Y protects rat cortical neurons against beta-amyloid toxicity and re-establishes synthesis and release of nerve growth factor. ACS Chem Neurosci *3*, 312-318.
Croce, N., Dinallo, V., Ricci, V., Federici, G., Caltagirone, C., Bernardini, S., and Angelucci, F. (2011). Neuroprotective effect of neuropeptide Y against beta-amyloid 25-35 toxicity in SH-SY5Y neuroblastoma cells is associated with increased neurotrophin production. Neurodegener Dis *8*, 300-309.
Cruchaga, C., Karch, C.M., Jin, S.C., Benitez, B.A., Cai, Y., Guerreiro, R., Harari, O., Norton, J., Budde, J., Bertelsen, S.*, et al.* (2014). Rare coding variants in the phospholipase D3 gene confer risk for Alzheimer's disease. Nature *505*, 550-554.
Cuello, A.C., Bruno, M.A., Allard, S., Leon, W., and Iulita, M.F. (2010). Cholinergic involvement in Alzheimer's disease. A link with NGF maturation and degradation. J Mol Neurosci *40*, 230-235.
D'Alessio, A., Esposito, B., Giampietri, C., Ziparo, E., Pober, J.S., and Filippini, A. (2012). Plasma membrane microdomains regulate TACE-dependent TNFR1 shedding in human endothelial cells. J Cell Mol Med *16*, 627-636.
De Strooper, B. (2014). Lessons from a failed gamma-secretase Alzheimer trial. Cell *159*, 721-726.
De Strooper, B., Vassar, R., and Golde, T. (2010). The secretases: enzymes with therapeutic potential in Alzheimer disease. Nat Rev Neurol *6*, 99-107.
Decressac, M., Wright, B., David, B., Tyers, P., Jaber, M., Barker, R.A., and Gaillard, A. (2011). Exogenous neuropeptide Y promotes in vivo hippocampal neurogenesis. Hippocampus *21*, 233-238.
Demyanenko, G.P., Riday, T.T., Tran, T.S., Dalal, J., Darnell, E.P., Brennaman, L.H., Sakurai, T., Grumet, M., Philpot, B.D., and Maness, P.F. (2011). NrCAM deletion causes topographic mistargeting of thalamocortical axons to the visual cortex and disrupts visual acuity. J Neurosci *31*, 1545-1558.
Deng, M., Loughran, P.A., Zhang, L., Scott, M.J., and Billiar, T.R. (2015). Shedding of the tumor necrosis factor (TNF) receptor from the surface of hepatocytes during sepsis limits inflammation through cGMP signaling. Sci Signal *8*, ra11.
Di Domenico, F., Tramutola, A., and Perluigi, M. (2016). Cathepsin D as a therapeutic target in Alzheimer's disease. Expert Opin Ther Targets *20*, 1393-1395.
Dislich, B., Wohlrab, F., Bachhuber, T., Muller, S.A., Kuhn, P.H., Hogl, S., Meyer-Luehmann, M., and Lichtenthaler, S.F. (2015). Label-free Quantitative Proteomics of Mouse Cerebrospinal Fluid Detects beta-Site APP Cleaving Enzyme (BACE1) Protease Substrates In Vivo. Mol Cell Proteomics *14*, 2550-2563.

Diz, A.C.-R., A; Skibinski, DO (2011). Multiple hypothesis testing in proteomics: a strategy for experimental work. Molecular and Cellular Protomics *10*.
Dominguez, D., Tournoy, J., Hartmann, D., Huth, T., Cryns, K., Deforce, S., Serneels, L., Camacho, I.E., Marjaux, E., Craessaerts, K.*, et al.* (2005). Phenotypic and biochemical analyses of BACE1- and BACE2-deficient mice. The Journal of biological chemistry *280*, 30797-30806.
Doody, R.S., Raman, R., Farlow, M., Iwatsubo, T., Vellas, B., Joffe, S., Kieburtz, K., He, F., Sun, X., Thomas, R.G.*, et al.* (2013). A phase 3 trial of semagacestat for treatment of Alzheimer's disease. N Engl J Med *369*, 341-350.
Doody, R.S., Thomas, R.G., Farlow, M., Iwatsubo, T., Vellas, B., Joffe, S., Kieburtz, K., Raman, R., Sun, X., Aisen, P.S.*, et al.* (2014). Phase 3 trials of solanezumab for mild-to-moderate Alzheimer's disease. N Engl J Med *370*, 311-321.
Drachmann, D. (2008). Adjusting for multiple comparisons. J Clin Res Best Pract.
Edbauer, D., Winkler, E., Haass, C., and Steiner, H. (2002). Presenilin and nicastrin regulate each other and determine amyloid beta-peptide production via complex formation. Proc Natl Acad Sci U S A *99*, 8666-8671.
Edbauer, D., Winkler, E., Regula, J.T., Pesold, B., Steiner, H., and Haass, C. (2003). Reconstitution of gamma-secretase activity. Nat Cell Biol *5*, 486-488.
Egan, M.F., Kost, J., Tariot, P.N., Aisen, P.S., Cummings, J.L., Vellas, B., Sur, C., Mukai, Y., Voss, T., Furtek, C.*, et al.* (2018). Randomized Trial of Verubecestat for Mild-to-Moderate Alzheimer's Disease. New England Journal of Medicine *378*, 1691-1703.
Eggert, S., Paliga, K., Soba, P., Evin, G., Masters, C.L., Weidemann, A., and Beyreuther, K. (2004). The proteolytic processing of the amyloid precursor protein gene family members APLP-1 and APLP-2 involves alpha-, beta-, gamma-, and epsilon-like cleavages: modulation of APLP-1 processing by n-glycosylation. The Journal of biological chemistry *279*, 18146-18156.
Eichelbaum, K., Winter, M., Berriel Diaz, M., Herzig, S., and Krijgsveld, J. (2012). Selective enrichment of newly synthesized proteins for quantitative secretome analysis. Nat Biotechnol *30*, 984-990.
Elbein, A.D. (1991). The role of N-linked oligosaccharides in glycoprotein function. Trends Biotechnol *9*, 346-352.
Elschenbroich, S., Kim, Y., Medin, J.A., and Kislinger, T. (2010). Isolation of cell surface proteins for mass spectrometry-based proteomics. Expert Rev Proteomics *7*, 141-154.
Endres, K., Fahrenholz, F., Lotz, J., Hiemke, C., Teipel, S., Lieb, K., Tuscher, O., and Fellgiebel, A. (2014). Increased CSF APPs-alpha levels in patients with Alzheimer disease treated with acitretin. Neurology *83*, 1930-1935.
Farzan, M., Schnitzler, C.E., Vasilieva, N., Leung, D., and Choe, H. (2000). BACE2, a beta -secretase homolog, cleaves at the beta site and within the amyloid-beta region of the amyloid-beta precursor protein. Proc Natl Acad Sci U S A *97*, 9712-9717.
Fazzari, P., Horre, K., Arranz, A.M., Frigerio, C.S., Saito, T., Saido, T.C., and De Strooper, B. (2017). PLD3 gene and processing of APP. Nature *541*, E1-E2.
Fenn, J.B., Mann, M., Meng, C.K., Wong, S.F., and Whitehouse, C.M. (1989). Electrospray ionisation for mass spectrometry of large biomolecules. Science *246*, 64-71.
Filser, S., Ovsepian, S.V., Masana, M., Blazquez-Llorca, L., Brandt Elvang, A., Volbracht, C., Muller, M.B., Jung, C.K., and Herms, J. (2015). Pharmacological inhibition of BACE1 impairs synaptic plasticity and cognitive functions. Biol Psychiatry *77*, 729-739.
Fleck, D., Garratt, A.N., Haass, C., and Willem, M. (2012). BACE1 Dependent Neuregulin Processing: Review. Curr Alzheimer Res *9*, 178-183.
Fleck, D., van Bebber, F., Colombo, A., Galante, C., Schwenk, B.M., Rabe, L., Hampel, H., Novak, B., Kremmer, E., Tahirovic, S.*, et al.* (2013). Dual cleavage of neuregulin 1 type III by BACE1 and ADAM17 liberates its EGF-like domain and allows paracrine signaling. J Neurosci *33*, 7856-7869.
Folch, J., Petrov, D., Ettcheto, M., Abad, S., Sanchez-Lopez, E., Garcia, M.L., Olloquequi, J., Beas-Zarate, C., Auladell, C., and Camins, A. (2016). Current Research Therapeutic Strategies for Alzheimer's Disease Treatment. Neural Plast *2016*, 8501693.
Folgueras, A.R., Valdés-Sánchez, T., Llano, E., Menéndez, L., Baamonde, A., Denlinger, B.L., Belmonte, C., Juárez, L., Lastra, A., García-Suárez, O.*, et al.* (2009). Metalloproteinase MT5-MMP

is an essential modulator of neuro-immune interactions in thermal pain stimulation. Proc Natl Acad Sci U S A *106*, 16451-16456.
Friedmann, E., Hauben, E., Maylandt, K., Schleeger, S., Vreugde, S., Lichtenthaler, S.F., Kuhn, P.H., Stauffer, D., Rovelli, G., and Martoglio, B. (2006). SPPL2a and SPPL2b promote intramembrane proteolysis of TNFalpha in activated dendritic cells to trigger IL-12 production. Nat Cell Biol *8*, 843-848.
Fukumori, A., Fluhrer, R., Steiner, H., and Haass, C. (2010). Three-amino acid spacing of presenilin endoproteolysis suggests a general stepwise cleavage of gamma-secretase-mediated intramembrane proteolysis. J Neurosci *30*, 7853-7862.
Fukumoto, H., Takahashi, H., Tarui, N., Matsui, J., Tomita, T., Hirode, M., Sagayama, M., Maeda, R., Kawamoto, M., Hirai, K*., et al.* (2010). A noncompetitive BACE1 inhibitor TAK-070 ameliorates Abeta pathology and behavioral deficits in a mouse model of Alzheimer's disease. J Neurosci *30*, 11157-11166.
Gallyas, F. (1971). Silver staining of Alzheimer's neurofibrillary changes by means of physical development. Acta Morphol Acad Sci Hung *19*, 1-8.
Gao, J., Zhang, C., Yang, B., Sun, L., Zhang, C., Westerfield, M., and Peng, G. (2012). Dcc regulates asymmetric outgrowth of forebrain neurons in zebrafish. PLoS One *7*, e36516.
Gautam, V.D.A., C.; Hebisch, M.; Kovacs, DM; Kim, DY (2014). BACE1 activity regulates cell surface contactin-2 levels_Gautam.pdf. Molecular Neurodegeneration.
Gersbacher, M.T., Goodger, Z.V., Trutzel, A., Bundschuh, D., Nitsch, R.M., and Konietzko, U. (2013). Turnover of amyloid precursor protein family members determines their nuclear signaling capability. PLoS One *8*, e69363.
Geyer, P.E., Holdt, L.M., Teupser, D., and Mann, M. (2017). Revisiting biomarker discovery by plasma proteomics. Mol Syst Biol *13*, 942.
Gibb, D.R., El Shikh, M., Kang, D.J., Rowe, W.J., El Sayed, R., Cichy, J., Yagita, H., Tew, J.G., Dempsey, P.J., Crawford, H.C*., et al.* (2010). ADAM10 is essential for Notch2-dependent marginal zone B cell development and CD23 cleavage in vivo. J Exp Med *207*, 623-635.
Glenner, G.G., and Wong, C.W. (1984). Alzheimer's disease: initial report of the purification and characterization of a novel cerebrovascular amyloid protein. 1984. Biochem Biophys Res Commun *425*, 534-539.
Goedert, M., Sisodia, S.S., and Price, D.L. (1991). Neurofibrillary tangles and β-amyloid deposits in Alzheimer's disease. Curr Opin Neurobiol *1*, 441-447.
Goldgaber, D., Lerman, M., McBride, O.W., Saffiotti, U., and Gajdusek, D.C. (1987). Characterization and chromosomal localization of a cDNA encoding brain amyloid of Alzheimer's disease. Science *235*, 877-880.
Green, R.C., Schneider, L.S., Amato, D.A., Beelen, A.P., Wilcock, G., Swabb, E.A., Zavitz, K.H., and Tarenflurbil Phase 3 Study, G. (2009). Effect of tarenflurbil on cognitive decline and activities of daily living in patients with mild Alzheimer disease: a randomized controlled trial. JAMA *302*, 2557-2564.
Grunblatt, E., and Riederer, P. (2016). Aldehyde dehydrogenase (ALDH) in Alzheimer's and Parkinson's disease. J Neural Transm (Vienna) *123*, 83-90.
Grundke-Iqbal, I., Iqbal, K., Quinlan, M., Tung, Y.C., Zaidi, M.S., and Wisniewski, H.M. (1986a). Microtubule-associated protein tau. A component of Alzheimer paired helical filaments. The Journal of biological chemistry *261*, 6084-6089.
Grundke-Iqbal, I., Iqbal, K., Tung, Y.C., Quinlan, M., Wisniewski, H.M., and Binder, L.I. (1986b). Abnormal phosphorylation of the microtubule-associated protein tau (tau) in Alzheimer cytoskeletal pathology. Proc Natl Acad Sci U S A *83*, 4913-4917.
Guo, J., He, L., Yuan, P., Wang, P., Lu, Y., Tong, F., Wang, Y., Yin, Y., Tian, J., and Sun, J. (2012). ADAM10 overexpression in human non-small cell lung cancer correlates with cell migration and invasion through the activation of the Notch1 signaling pathway. Oncol Rep *28*, 1709-1718.
Gutwein, P., Mechtersheimer, S., Riedle, S., Stoeck, A., Gast, D., Joumaa, S., Zentgraf, H., Fogel, M., and Altevogt, D.P. (2003). ADAM10-mediated cleavage of L1 adhesion molecule at the cell surface and in released membrane vesicles. FASEB J *17*.
Ha, Y. (2009). Structure and mechanism of intramembrane protease. Semin Cell Dev Biol *20*, 240-250.

Haass, C., Schlossmacher, M.G., Hung, A.Y., Vigo-Pelfrey, C., Mellon, A., Ostaszewski, B.L., Lieberburg, I., Koo, E.H., Schenk, D., Teplow, D.B., *et al.* (1992). Amyloid beta-peptide is produced by cultured cells during normal metabolism. Nature *359*, 322-325.
Haass, C., and Selkoe, D.J. (2007). Soluble protein oligomers in neurodegeneration: lessons from the Alzheimer's amyloid beta-peptide. Nat Rev Mol Cell Biol *8*, 101-112.
Hardy, J. (2009). The amyloid hypothesis for Alzheimer's disease: a critical reappraisal. J Neurochem *110*, 1129-1134.
Hardy, J., and Selkoe, D.J. (2002). The amyloid hypothesis of Alzheimer's disease: progress and problems on the road to therapeutics. Science *297*, 353-356.
Hardy, J.A., and Higgins, G.A. (1992). Alzheimer's Disease: The Amyloid Cascade Hypothesis. Science *256*, 184-185.
Harris, R.C., Essén, B., and Hultman, E. (2011). Glycogen Phosphorylase Activity in Biopsy Samples and Single Muscle Fibres of Musculus Quadriceps Femoris of Man at Rest. Scandinavian Journal of Clinical and Laboratory Investigation *36*, 521-526.
Hartmann, D., de Strooper, B., Serneels, L., Craessaerts, K., Herreman, A., Annaert, W., Umans, L., Lübke, T., Lena Illert , A., von Figura, K., *et al.* (2002). The disintegrin/metalloprotease ADAM 10 is essential for Notch signalling but not for a-secretase activity in fibroblasts. Hum Mol Genet *11*, 2615-2624.
Hayashida, K., Bartlett, A.H., Chen, Y., and Park, P.W. (2010). Molecular and cellular mechanisms of ectodomain shedding. Anat Rec (Hoboken) *293*, 925-937.
Hayashita-Kinoh, H., Kinoh, H., Okada, A., Komori, K., Itoh, Y., Chiba, T., Kajita, M., Yana, I., and Seiki, M. (2001). Membrane-type 5 matrix metalloproteinase is expressed in differentiated neurons and regulates axonal growth. Cell Growth and Differentiation *11*, 573-580.
He, W., Hu, J., Xia, Y., and Yan, R. (2014). beta-site amyloid precursor protein cleaving enzyme 1(BACE1) regulates Notch signaling by controlling the cleavage of Jagged 1 (Jag1) and Jagged 2 (Jag2) proteins. The Journal of biological chemistry *289*, 20630-20637.
Hemming, M.L., Elias, J.E., Gygi, S.P., and Selkoe, D.J. (2009). Identification of beta-secretase (BACE1) substrates using quantitative proteomics. PLoS One *4*, e8477.
Henjum, K., Almdahl, I.S., Arskog, V., Minthon, L., Hansson, O., Fladby, T., and Nilsson, L.N. (2016). Cerebrospinal fluid soluble TREM2 in aging and Alzheimer's disease. Alzheimers Res Ther *8*, 17.
Herber, J., Njavro, J., Feederle, R., Schepers, U., Müller, U.C., Bräse, S., Müller, S.A., and Lichtenthaler, S.F. (2018). Click chemistry-mediated biotinylation reveals a function for the protease BACE1 in modulating the neuronal surface glycoproteome. Mol Cell Proteomics.
Heslegrave, A., Heywood, W., Paterson, R., Magdalinou, N., Svensson, J., Johansson, P., Ohrfelt, A., Blennow, K., Hardy, J., Schott, J., *et al.* (2016). Increased cerebrospinal fluid soluble TREM2 concentration in Alzheimer's disease. Mol Neurodegener *11*, 3.
Heyden, A., Angenstein, F., Sallaz, M., Seidenbecher, C., and Montag, D. (2008). Abnormal axonal guidance and brain anatomy in mouse mutants for the cell recognition molecules close homolog of L1 and NgCAM-related cell adhesion molecule. Neuroscience *155*, 221-233.
Hogl, S., van Bebber, F., Dislich, B., Kuhn, P.H., Haass, C., Schmid, B., and Lichtenthaler, S.F. (2013). Label-free quantitative analysis of the membrane proteome of Bace1 protease knock-out zebrafish brains. Proteomics *13*, 1519-1527.
Hook, V., Toneff, T., Aaron, W., Yasothornsrikul, S., Bundey, R., and Reisine, T. (2002). Beta-amyloid peptide in regulated secretory vesicles of chromaffin cells: evidence for multiple cysteine proteolytic activities in distinct pathways for beta-secretase activity in chromaffin vesicles. Journal of Neurochemistry *81*, 237-256.
Hormann, K., Stukalov, A., Muller, A.C., Heinz, L.X., Superti-Furga, G., Colinge, J., and Bennett, K.L. (2016). A Surface Biotinylation Strategy for Reproducible Plasma Membrane Protein Purification and Tracking of Genetic and Drug-Induced Alterations. J Proteome Res *15*, 647-658.
Howard, R., McShane, R., Lindesay, J., Ritchie, C., Baldwin, A., Barber, R., Burns, A., Dening, T., Findlay, D., Holmes, C., *et al.* (2012). Donepezil and memantine for moderate-to-severe Alzheimer's disease. N Engl J Med *366*, 893-903.

Howell, O.W., Doyle, K., Goodman, J.H., Scharfman, H.E., Herzog, H., Pringle, A., Beck-Sickinger, A.G., and Gray, W.P. (2005). Neuropeptide Y stimulates neuronal precursor proliferation in the post-natal and adult dentate gyrus. J Neurochem *93*, 560-570.
Hu, Q., Noll, R.J., Li, H., Makarov, A., Hardman, M., and Graham Cooks, R. (2005). The Orbitrap: a new mass spectrometer. J Mass Spectrom *40*, 430-443.
Hu, X., Fan, Q., Hou, H., and Yan, R. (2016). Neurological dysfunctions associated with altered BACE1-dependent Neuregulin-1 signaling. J Neurochem *136*, 234-249.
Hu, X., He, W., Luo, X., Tsubota, K.E., and Yan, R. (2013). BACE1 regulates hippocampal astrogenesis via the Jagged1-Notch pathway. Cell Rep *4*, 40-49.
Huse, J.T., Pijak, D.S., Leslie, G.J., Lee, V.M., and Doms, R.W. (2000). Maturation and endosomal targeting of beta-site amyloid precursor protein-cleaving enzyme. The Alzheimer's disease beta-secretase. The Journal of biological chemistry *275*, 33729-33737.
Hussain, I., Powell, D., Howlett, D.R., Tew, D.G., Meek, T.D., Chapman, C., Gloger, I.S., Murphy, K.E., Southan, C.D., Ryan, D.M.*, et al.* (1999). Identification of a novel aspartic protease (Asp 2) as beta-secretase. Mol Cell Neurosci *14*, 419-427.
Iqbal, K., Grundke-Iqbal, I., Zaidi, T., Merz, P.A., Wen, G.Y., Shaikh, S.S., Wisniewski, H.M., Alafuzoff, I., and Winblad, B. (1986). Defective brain microtubule assembly in Alzheimer's disease. Lancet *2*, 421-426.
Ito-Ishida, A., Miyazaki, T., Miura, E., Matsuda, K., Watanabe, M., Yuzaki, M., and Okabe, S. (2012). Presynaptically released Cbln1 induces dynamic axonal structural changes by interacting with GluD2 during cerebellar synapse formation. Neuron *76*, 549-564.
Itoh, Y. (2015). Membrane-type matrix metalloproteinases: Their functions and regulations. Matrix biology : journal of the International Society for Matrix Biology *44-46*, 207-223.
Ivankov, D.N., Bogatyreva, N.S., Honigschmid, P., Dislich, B., Hogl, S., Kuhn, P.H., Frishman, D., and Lichtenthaler, S.F. (2013). QARIP: a web server for quantitative proteomic analysis of regulated intramembrane proteolysis. Nucleic Acids Res *41*, W459-464.
Janssen (2018). Update on Janssen's BACE Inhibitor Program (http://www.janssen.com/update-janssens-bace-inhibitor-program: Janssen, pharmaceutical companies of Johnson & Johnson).
Jaworski, D.M. (2000). Developmental regulation of membrane type-5 matrix metalloproteinase (MT5-MMP) expression in the rat nervous system. Brain Research *860*, 174-177.
Jefferson, T., Causevic, M., auf dem Keller, U., Schilling, O., Isbert, S., Geyer, R., Maier, W., Tschickardt, S., Jumpertz, T., Weggen, S.*, et al.* (2011). Metalloprotease meprin beta generates nontoxic N-terminal amyloid precursor protein fragments in vivo. The Journal of biological chemistry *286*, 27741-27750.
Jin, M., Shepardson, N., Yang, T., Chen, G., Walsh, D., and Selkoe, D.J. (2011). Soluble amyloid beta-protein dimers isolated from Alzheimer cortex directly induce Tau hyperphosphorylation and neuritic degeneration. Proc Natl Acad Sci U S A *108*, 5819-5824.
Jorissen, E., Prox, J., Bernreuther, C., Weber, S., Schwanbeck, R., Serneels, L., Snellinx, A., Craessaerts, K., Thathiah, A., Tesseur, I.*, et al.* (2010). The disintegrin/metalloproteinase ADAM10 is essential for the establishment of the brain cortex. J Neurosci *30*, 4833-4844.
Josic, D., and Clifton, J.G. (2007). Mammalian plasma membrane proteomics. Proteomics *7*, 3010-3029.
Kang, J., Lemaire, H.G., Unterbeck, A., Salbaum, J.M., Masters, C.L., Grzeschik, K.H., Multhaup, G., Beyreuther, K., and Müller-Hill, B. (1987). The precursor of Alzheimer's disease amyloid A4 protein resembles a cell-surface receptor. Nature *325*, 733-736.
Kato, S., Gondo, T., Hoshii, Y., Takahashi, M., Yamada, M., and Ishihara, T. (1998). Confocal observation of senile plaques in Alzheimer's disease: senile plaque morphology and relationship between senile plaques and astrocytes. Pathol Int *48*, 332-340.
Kennedy, M.E., Stamford, A.W., Chen, X., Cox, K., Cumming, J.N., Dockendorf, M.F., Egan, M., Ereshefsky, L., Hodgson, R.A., Hyde, L.A.*, et al.* (2016). The BACE1 inhibitor verubecestat (MK-8931) reduces CNS β-amyloid in animal models and in Alzheimer's disease patients. Sci Transl Med *8*, 363ra150.
Keren-Shaul, H., Spinrad, A., Weiner, A., Matcovitch-Natan, O., Dvir-Szternfeld, R., Ulland, T.K., David, E., Baruch, K., Lara-Astaiso, D., Toth, B.*, et al.* (2017). A Unique Microglia Type Associated with Restricting Development of Alzheimer's Disease. Cell *169*, 1276-1290 e1217.

Kim, M., Suh, J., Romano, D., Truong, M.H., Mullin, K., Hooli, B., Norton, D., Tesco, G., Elliott, K., Wagner, S.L., *et al.* (2009). Potential late-onset Alzheimer's disease-associated mutations in the ADAM10 gene attenuate {alpha}-secretase activity. Hum Mol Genet *18*, 3987-3996.
Kimura, R., and Ohno, M. (2009). Impairments in remote memory stabilization precede hippocampal synaptic and cognitive failures in 5XFAD Alzheimer mouse model. Neurobiol Dis *33*, 229-235.
Kisler, K., Nelson, A.R., Montagne, A., and Zlokovic, B.V. (2017). Cerebral blood flow regulation and neurovascular dysfunction in Alzheimer disease. Nat Rev Neurosci *18*, 419-434.
Kitazume, S., Tachida, Y., Oka, R., Shirotani, K., Saido, T.C., and Hashimoto, Y. (2001). Alzheimer's beta-secretase, beta-site amyloid precursor protein-cleaving enzyme, is responsible for cleavage secretion of a Golgi-resident sialyltransferase. Proc Natl Acad Sci U S A *98*, 13554-13559.
Komori, K., Nonaka, T., Okada, A., Kinoh, H., Hayashita-Kinoh, H., Yoshida, N., Yana, I., and Seiki, M. (2004). Absence of mechanical allodynia and Aβ-fiber sprouting after sciatic nerve injury in mice lacking membrane-type 5 matrix metalloproteinase. FEBS letters *557*, 125-128.
Kuhn, P., Voss, M., Haug-Kröper, M., Schröder, B., Schepers, U., Bräse, S., Haass, C., Lichtenthaler, S., and Fluhrer, R. (2015). Secretome analysis identifies novel signal Peptide peptidase-like 3 (Sppl3) substrates and reveals a role of Sppl3 in multiple Golgi glycosylation pathways. Molecular and Cellular Protomics *14*, 1584-1598.
Kuhn, P.H., Colombo, A.V., Schusser, B., Dreymueller, D., Wetzel, S., Schepers, U., Herber, J., Ludwig, A., Kremmer, E., Montag, D., *et al.* (2016). Systematic substrate identification indicates a central role for the metalloprotease ADAM10 in axon targeting and synapse function. Elife *5*.
Kuhn, P.H., Koroniak, K., Hogl, S., Colombo, A., Zeitschel, U., Willem, M., Volbracht, C., Schepers, U., Imhof, A., Hoffmeister, A., *et al.* (2012). Secretome protein enrichment identifies physiological BACE1 protease substrates in neurons. EMBO J *31*, 3157-3168.
Kuhn, P.H., Wang, H., Dislich, B., Colombo, A., Zeitschel, U., Ellwart, J.W., Kremmer, E., Rossner, S., and Lichtenthaler, S.F. (2010). ADAM10 is the physiologically relevant, constitutive alpha-secretase of the amyloid precursor protein in primary neurons. EMBO J *29*, 3020-3032.
Lai, K.S.P., Liu, C.S., Rau, A., Lanctôt, K.L., Köhler, C.A., Pakosh, M., Carvalho, A.F., and Herrmann, N. (2017). Peripheral inflammatory markers in Alzheimer's disease: a systematic review and meta-analysis of 175 studies. J Neurol Neurosurg Psychiatry *88*, 876-882.
Lal, M., and Caplan, M. (2011). Regulated intramembrane proteolysis: signaling pathways and biological functions. Physiology (Bethesda) *26*, 34-44.
Lammich, S., Kojro, E., Postina, R., Gilbert, S., Pfeiffer, R., Jasionowski, M., Haass, C., and Fahrenholz, F. (1999). Constitutive and regulated alpha-secretase cleavage of Alzheimer's amyloid precursor protein by a disintegrin metalloprotease. Proc Natl Acad Sci U S A *96*, 3922-3927.
Lang, A.E. (2010). Clinical trials of disease-modifying therapies for neurodegenerative diseases: the challenges and the future. Nat Med *16*, 1223-1226.
Laughlin, S.T., and Bertozzi, C.R. (2007). Metabolic labeling of glycans with azido sugars and subsequent glycan-profiling and visualization via Staudinger ligation. Nat Protoc *2*, 2930-2944.
Lépinoux-Chambaud, C., and Eyer, J. (2013). Review on intermediate fila- ments of the nervous system and their pathological alterations. Histochem Cell Biol *140*, 13-22.
Levin, E.C., Acharya, N.K., Sedeyn, J.C., Venkataraman, V., D'Andrea, M.R., Wang, H.Y., and Nagele, R.G. (2009). Neuronal expression of vimentin in the Alzheimer's disease brain may be part of a generalized dendritic damage-response mechanism. Brain Res *1298*, 194-207.
Li, G., Shofer, J.B., Petrie, E.C., Yu, C.E., Wilkinson, C.W., Figlewicz, D.P., Shutes-David, A., Zhang, J., Montine, T.J., Raskind, M.A., *et al.* (2017a). Cerebrospinal fluid biomarkers for Alzheimer's and vascular disease vary by age, gender, and APOE genotype in cognitively normal adults. Alzheimers Res Ther *9*, 48.
Li, H., Han, J., Pan, J., Liu, T., Parker, C.E., and Borchers, C.H. (2017b). Current trends in quantitative proteomics - an update. J Mass Spectrom *52*, 319-341.
Li, H.L., Wang, H.H., Liu, S.J., Deng, Y.Q., Zhang, Y.J., Tian, Q., Wang, X.C., Chen, X.Q., Yang, Y., Zhang, J.Y., *et al.* (2007). Phosphorylation of tau antagonizes apoptosis by stabilizing beta-catenin, a mechanism involved in Alzheimer's neurodegeneration. Proc Natl Acad Sci U S A *104*, 3591-3596.
Li, Q., and Sudhof, T.C. (2004). Cleavage of amyloid-beta precursor protein and amyloid-beta precursor-like protein by BACE 1. The Journal of biological chemistry *279*, 10542-10550.

Li, Q.X., Fuller, S.J., Beyreuther, K., and Masters, C.L. (1999). The amyloid precursor protein of Alzheimer disease in human brain and blood. Journal of Leukocyte Biology *66*, 567-574.
Liang, Z., and Li, Q.X. (2018). Discovery of Selective, Substrate-Competitive, and Passive Membrane Permeable Glycogen Synthase Kinase-3beta Inhibitors: Synthesis, Biological Evaluation, and Molecular Modeling of New C-Glycosylflavones. ACS Chem Neurosci.
Lichtenthaler, S.F., Haass, C., and Steiner, H. (2011). Regulated intramembrane proteolysis--lessons from amyloid precursor protein processing. J Neurochem *117*, 779-796.
Lin, X., Koelsch, G., Wu, S., Downs, D., Dashti, A., and Tang, J. (2000). Human aspartic protease memapsin 2 cleaves the β-secretase site of β-amyloid precursor protein. Proc Natl Acad Sci U S A *97*, 1456–1460.
Lis, H., and Sharon, N. (1993). Protein glycosylation. Structural and functional aspects. Eur J Biochem *218*, 1-27.
Liu, L., and Duff, K. (2008). A technique for serial collection of cerebrospinal fluid from the cisterna magna in mouse. J Vis Exp.
Llano (1999). Identification and charakterisation of human MT5-MMP, a new membrane-bound activator of progelatinase A overexpressed in brain tumors_Llano et al.1999.pdf.
Lonergan, E., and Luxenberg, J. (2009). Valproate preparations for agitation in dementia. Cochrane Database Syst Rev, CD003945.
Luxan, G., D'Amato, G., MacGrogan, D., and de la Pompa, J.L. (2016). Endocardial Notch Signaling in Cardiac Development and Disease. Circ Res *118*, e1-e18.
Lv, J., Ma, S., Zhang, X., Zheng, L., Ma, Y., Zhao, X., Lai, W., Shen, H., Wang, Q., and Ji, J. (2014). Quantitative proteomics reveals that PEA15 regulates astroglial Abeta phagocytosis in an Alzheimer's disease mouse model. J Proteomics *110*, 45-58.
Makarov, A. (2000). Electrostatic Axially Harmonic Orbital Trapping: A High-Performance Technique of Mass Analysis. Analytical chemistry *72*, 1156-1162.
Mao, X., Ou, M.T., Karuppagounder, S.S., Kam, T.I., Yin, X., Xiong, Y., Ge, P., Umanah, G.E., Brahmachari, S., Shin, J.H.*, et al.* (2016). Pathological alpha-synuclein transmission initiated by binding lymphocyte-activation gene 3. Science *353*.
Maretzky, T., Schulte, M., Ludwig, A., Rose-John, S., Blobel, C., Hartmann, D., Altevogt, P., Saftig, P., and Reiss, K. (2005). L1 is sequentially processed by two differently activated metalloproteases and presenilin/gamma-secretase and regulates neural cell adhesion, cell migration, and neurite outgrowth. Mol Cell Biol *25*, 9040-9053.
Masters, C.L., Simms, G., Weinman, N.A., Multhaup, G., McDonald, B.L., and Beyreuther, K. (1985). Amyloid plaque core protein in Alzheimer disease and Down syndrome. PNAS *82*, 4245–4249.
Mathias, R., Chen, Y.-S., Goode, R.J.A., Kapp, E.A., Mathivanan, S., Moritz, R.L., Zhu, H.-J., and Simpson, R.J. (2011). Tandem application of cationic colloidal silica and Triton X-114 for plasma membrane protein isolation and purification: Towards developing an MDCK protein database. Proteomics *11*, 1238-1253.
May, P.C., Dean, R.A., Lowe, S.L., Martenyi, F., Sheehan, S.M., Boggs, L.N., Monk, S.A., Mathes, B.M., Mergott, D.J., Watson, B.M.*, et al.* (2011). Robust central reduction of amyloid-beta in humans with an orally available, non-peptidic beta-secretase inhibitor. J Neurosci *31*, 16507-16516.
Meissner, F., and Mann, M. (2014). Quantitative shotgun proteomics: considerations for a high-quality workflow in immunology. Nat Immunol *15*, 112-117.
Mende, M., Bednarek, C., Wawryszyn, M., Sauter, P., Biskup, M.B., Schepers, U., and Brase, S. (2016). Chemical Synthesis of Glycosaminoglycans. Chem Rev *116*, 8193-8255.
Messier, C., and Gagnon, M. (1996). Glucose regulation and cognitive functions: relation to Alzheimer's disease and diabetes. Behavioural Brain Research *75*, 1-11.
Mi, H., Muruganujan, A., Casagrande, J.T., and Thomas, P.D. (2013). Large-scale gene function analysis with the PANTHER classification system. Nat Protoc *8*, 1551-1566.
Mirzaei, H., and Carrasco, M. (2016). Advances in Experimental Medicine and Biology, Vol 919 (Springer Nature: Springer International Publishing AG).
Mohammad-Abdul, H., and Butterfield, D.A. (2005). Protection against amyloid beta-peptide (1-42)-induced loss of phospholipid asymmetry in synaptosomal membranes by tricyclodecan-9-

xanthogenate (D609) and ferulic acid ethyl ester: implications for Alzheimer's disease. Biochim Biophys Acta *1741*, 140-148.
Mouton, P.R., Martin, L.J., Calhoun, M.E., G., D.F., and Price, D.L. (1998). Cognitive decline strongly correlates with cortical atrophy in Alzheimer's dementia. Neurobiol Aging *19*, 371-377.
Moya-Alvarado, G., Gershoni-Emek, N., Perlson, E., and Bronfman, F.C. (2016). Neurodegeneration and Alzheimer's disease (AD). What Can Proteomics Tell Us About the Alzheimer's Brain? Mol Cell Proteomics *15*, 409-425.
Mullan, M., Crawford, F., Axelman, K., Houlden, H., Lilius, L., Winblad, B., and Lannfelt, L. (1992). A pathogenic mutation for probable Alzheimer's disease in the APP gene at the N-terminus of beta-amyloid. Nat Genet *1*, 345-347.
Muller, S.A., Scilabra, S.D., and Lichtenthaler, S.F. (2016). Proteomic Substrate Identification for Membrane Proteases in the Brain. Front Mol Neurosci *9*, 96.
Muller, U.C., Deller, T., and Korte, M. (2017). Not just amyloid: physiological functions of the amyloid precursor protein family. Nat Rev Neurosci *18*, 281-298.
Nagahara, A.H., Merrill, D.A., Coppola, G., Tsukada, S., Schroeder, B.E., Shaked, G.M., Wang, L., Blesch, A., Kim, A., Conner, J.M.*, et al.* (2009). Neuroprotective effects of brain-derived neurotrophic factor in rodent and primate models of Alzheimer's disease. Nat Med *15*, 331-337.
Nesvizhskii, A.I., Vitek, O., and Aebersold, R. (2007). Analysis and validation of proteomic data generated by tandem mass spectrometry. Nat Methods *4*, 787-797.
Oakley, H., Cole, S.L., Logan, S., Maus, E., Shao, P., Craft, J., Guillozet-Bongaarts, A., Ohno, M., Disterhoft, J., Van Eldik, L.*, et al.* (2006). Intraneuronal beta-amyloid aggregates, neurodegeneration, and neuron loss in transgenic mice with five familial Alzheimer's disease mutations: potential factors in amyloid plaque formation. J Neurosci *26*, 10129-10140.
Ogawa, M., Fukuyama, H., Ouchi, Y., Yamauchi, H., and Kimura, J. (1996). Altered energy metabolism in Alzheimer's disease. Journal of the Neurological Sciences *139*, 78-82.
Olsen, J.V., Macek, B., Lange, O., Makarov, A., Horning, S., and Mann, M. (2007). Higher-energy C-trap dissociation for peptide modification analysis. Nat Methods *4*, 709-712.
Ong, S.E., Blagoev, B., Kratchmarova, I., Kristensen, D.B., Steen, H., Pandey, A., and Mann, M. (2010). Stable isotope labeling by amino acids in cell culture, SILAC, as a simple and accurate approach to expression proteomics. Mol Cell Proteomics *1*, 376-386.
Ong, S.E., and Mann, M. (2005). Mass spectrometry-based proteomics turns quantitative. Nat Chem Biol *1*, 252-262.
Pan, D., and Rubin, G.M. (1997). Kuzbanian controls proteolytic processing of Notch and mediates lateral inhibition during Drosophila and vertebrate neurogenesis. Cell *90*, 271-280.
Pan, Y., Short, J.L., Choy, K.H., Zeng, A.X., Marriott, P.J., Owada, Y., Scanlon, M.J., Porter, C.J., and Nicolazzo, J.A. (2016). Fatty Acid-Binding Protein 5 at the Blood-Brain Barrier Regulates Endogenous Brain Docosahexaenoic Acid Levels and Cognitive Function. J Neurosci *36*, 11755-11767.
Pei, D. (1999). Identification and characterization of the fifth membrane-type matrix metalloproteinase MT5-MMP. The Journal of biological chemistry *274*, 8925-8932.
Pekny, M., Wilhelmsson, U., and Pekna, M. (2014). The dual role of astrocyte activation and reactive gliosis. Neurosci Lett *565*, 30-38.
Perry, R.H., Cooks, R.G., and Noll, R.J. (2008). Orbitrap mass spectrometry: instrumentation, ion motion and applications. Mass Spectrom Rev *27*, 661-699.
Petzold, A. (2005). Neurofilament phosphoforms: surrogate markers for axonal injury, degeneration and loss. J Neurol Sci *233*, 183-198.
Pierfelice, T., Alberi, L., and Gaiano, N. (2011). Notch in the vertebrate nervous system: an old dog with new tricks. Neuron *69*, 840-855.
Pigoni, M., Wanngren, J., Kuhn, P.H., Munro, K.M., Gunnersen, J.M., Takeshima, H., Feederle, R., Voytyuk, I., De Strooper, B., Levasseur, M.D.*, et al.* (2016). Seizure protein 6 and its homolog seizure 6-like protein are physiological substrates of BACE1 in neurons. Mol Neurodegener *11*, 67.
Porlan, E., Marti-Prado, B., Morante-Redolat, J.M., Consiglio, A., Delgado, A.C., Kypta, R., Lopez-Otin, C., Kirstein, M., and Farinas, I. (2014). MT5-MMP regulates adult neural stem cell functional quiescence through the cleavage of N-cadherin. Nat Cell Biol *16*, 629-638.

Portelius, E., Mattsson, N., Andreasson, U., Blennow, K., and Zetterberg, H. (2011). Novel aβ isoforms in Alzheimer's disease - their role in diagnosis and treatment. Curr Pharm Des *17*, 2594-2602.
Postina, R., Schroeder, A., Dewachter, I., Bohl, J., Schmitt, U., Kojro, E., Prinzen, C., Endres, K., Hiemke, C., Blessing, M.*, et al.* (2004). A disintegrin-metalloproteinase prevents amyloid plaque formation and hippocampal defects in an Alzheimer disease mouse model. J Clin Invest *113*, 1456-1464.
Prinzen, C., Trumbach, D., Wurst, W., Endres, K., Postina, R., and Fahrenholz, F. (2009). Differential gene expression in ADAM10 and mutant ADAM10 transgenic mice. BMC Genomics *10*, 66.
Prox, J., Bernreuther, C., Altmeppen, H., Grendel, J., Glatzel, M., D'Hooge, R., Stroobants, S., Ahmed, T., Balschun, D., Willem, M.*, et al.* (2013). Postnatal disruption of the disintegrin/metalloproteinase ADAM10 in brain causes epileptic seizures, learning deficits, altered spine morphology, and defective synaptic functions. J Neurosci *33*, 12915-12928, 12928a.
Querfurth, H.W., and LaFerla, F.M. (2010). Alzheimer's Disease. The New England Journal of Medicine *362*, 329-344.
Rappsilber, J., Mann, M., and Ishihama, Y. (2007). Protocol for micro-purification, enrichment, pre-fractionation and storage of peptides for proteomics using StageTips. Nat Protoc *2*, 1896-1906.
Reiss, K., and Saftig, P. (2009). The "A Disintegrin And Metalloprotease" (ADAM) family of sheddases: Physiological and cellular functions. Seminars in Cell & Developmental Biology *20*, 126-137.
Rochin, L., Hurbain, I., Serneels, L., Fort, C., Watt, B., Leblanc, P., Marks, M.S., De Strooper, B., Raposo, G., and van Niel, G. (2013). BACE2 processes PMEL to form the melanosome amyloid matrix in pigment cells. Proc Natl Acad Sci U S A *110*, 10658-10663.
Rose, J.B., Crews, L., Rockenstein, E., Adame, A., Mante, M., Hersh, L.B., Gage, F.H., Spencer, B., Potkar, R., Marr, R.A.*, et al.* (2009). Neuropeptide Y fragments derived from neprilysin processing are neuroprotective in a transgenic model of Alzheimer's disease. J Neurosci *29*, 1115-1125.
Rudd, P.M., Elliott, T., Cresswell, P., Wilson, I.A., and Dwek, R.A. (2001). Glycosylation and the immune system. Science *291*, 2370-2376.
Ryan, S.D., Whitehead, S.N., Swayne, L.A., Moffat, T.C., Hou, W., Ethier, M., Bourgeois, A.J., Rashidian, J., Blanchard, A.P., Fraser, P.E.*, et al.* (2009). Amyloid-beta42 signals tau hyperphosphorylation and compromises neuronal viability by disrupting alkylacylglycerophosphocholine metabolism. Proc Natl Acad Sci U S A *106*, 20936-20941.
Sabido, E., Selevsek, N., and Aebersold, R. (2012). Mass spectrometry-based proteomics for systems biology. Curr Opin Biotechnol *23*, 591-597.
Saftig, P., and Lichtenthaler, S.F. (2015). The alpha secretase ADAM10: A metalloprotease with multiple functions in the brain. Prog Neurobiol *135*, 1-20.
Saftig, P., and Reiss, K. (2011). The "A Disintegrin And Metalloproteases" ADAM10 and ADAM17: novel drug targets with therapeutic potential? Eur J Cell Biol *90*, 527-535.
Salloway, S., Sperling, R., Fox, N.C., Blennow, K., Klunk, W., Raskind, M., Sabbagh, M., Honig, L.S., Porsteinsson, A.P., Ferris, S.*, et al.* (2014). Two phase 3 trials of bapineuzumab in mild-to-moderate Alzheimer's disease. N Engl J Med *370*, 322-333.
Sandbrink, R., Masters, C.L., and Beyreuther, K. (1994). APP gene family: unique age-associated changes in splicing of Alzheimer's betaA4-amyloid protein precursor. neurobiol Dis *1*, 13-24.
Sankaranarayanan, S., Holahan, M.A., Colussi, D., Crouthamel, M.C., Devanarayan, V., Ellis, J., Espeseth, A., Gates, A.T., Graham, S.L., Gregro, A.R.*, et al.* (2009). First demonstration of cerebrospinal fluid and plasma A beta lowering with oral administration of a beta-site amyloid precursor protein-cleaving enzyme 1 inhibitor in nonhuman primates. J Pharmacol Exp Ther *328*, 131-140.
Satoh, J.K., Y.; Yamamoto, Y.; Kawana, N.; Ishida, T.; Saito, Y.; Arima, K. (2014). PLD3 is acumulated on neuritic plaques in Alzheimer's disease brains. Alzheimer's Research & Therapy.
Savonenko, A.V., Melnikova, T., Laird, F.M., Stewart, K.A., Price, D.L., and Wong, P.C. (2008). Alteration of BACE1-dependent NRG1/ErbB4 signaling and schizophrenia-like phenotypes in BACE1-null mice. Proc Natl Acad Sci U S A *105*, 5585-5590.
Schilling, S., Mehr, A., Ludewig, S., Stephan, J., Zimmermann, M., August, A., Strecker, P., Korte, M., Koo, E.H., Muller, U.C.*, et al.* (2017). APLP1 Is a Synaptic Cell Adhesion Molecule,

Supporting Maintenance of Dendritic Spines and Basal Synaptic Transmission. J Neurosci *37*, 5345-5365.
Schlondorff, J., and Blobel, C.P. (1999). Metalloprotease-disintegrins: modular proteins capable of promoting cell-cell interactions and triggering signals by protein-ectodomain shedding. J Cell Sci *112*, 3603-3617.
Schmitt, U., Hiemke, C., Fahrenholz, F., and Schroeder, A. (2006). Over-expression of two different forms of the α-secretase ADAM10 affects learning and memory in mice. Behavioural Brain Research *175*, 278-284.
Schuur, M., Ikram, M.A., van Swieten, J.C., Isaacs, A., Vergeer-Drop, J.M., Hofman, A., Oostra, B.A., Breteler, M.M.B., and van Duijn, C.M. (2011). Cathepsin D gene and the risk of Alzheimer's disease: A population-based study and meta-analysis. Neurobiology of Aging *32*, 1607-1614.
Sekine-Aizawa, Y., Hama, E., Watanabe, K., Tsubuki, S., Kanai-Azuma, M., Kanai, Y., Arai, H., Aizawa, H., Iwata, N., and Saido, T.C. (2001). Matrix metalloproteinase (MMP) system in brain: identification and characterization of brain-specific MMP highly expressed in cerebellum. Euro J Neurosci *13*, 935-948.
Selkoe, D.J. (1991). The Molecular Pathology of Alzheimer's Disease. Neuron *6*, 487-498.
Selkoe, D.J. (2004). Cell biology of protein misfolding: the examples of Alzheimer's and Parkinson's diseases. Nat Cell Biol *6*, 1054-1061.
Selkoe, D.J. (2011). Alzheimer's disease. Cold Spring Harb Perspect Biol *3*.
Selkoe, D.J., and Hardy, J. (2016). The amyloid hypothesis of Alzheimer's disease at 25 years. EMBO Mol Med *8*, 595-608.
Serdaroglu, A., Muller, S.A., Schepers, U., Brase, S., Weichert, W., Lichtenthaler, S.F., and Kuhn, P.H. (2017). An optimised version of the secretome protein enrichment with click sugars (SPECS) method leads to enhanced coverage of the secretome. Proteomics *17*.
Seubert, P., Oltersdorf, T., Lee, M.G., Barbour, R., Blomquist, C., Davis, D.L., Bryant, K., Fritz, L.C., Galasko, D., Thal, L.J.*, et al.* (1993). Secretion of beta-amyloid precursor protein cleaved at the amino terminus of the beta-amyloid peptide. Nature *361*, 260-263.
Seubert, P., Vigo-Pelfrey, C., Esch, F., Lee, M., Dovey, H., Davis, D., Sinha, S., Schlossmacher, M., Whaley, J., Swindlehurst, C.*, et al.* (1992). Isolation and quantification of soluble Alzheimer's beta-peptide from biological fluids. Nature *359*, 325-327.
Shariati, S.A., and De Strooper, B. (2013). Redundancy and divergence in the amyloid precursor protein family. FEBS letters *587*, 2036-2045.
Sharma, K., Schmitt, S., Bergner, C.G., Tyanova, S., Kannaiyan, N., Manrique-Hoyos, N., Kongi, K., Cantuti, L., Hanisch, U.K., Philips, M.A.*, et al.* (2015). Cell type- and brain region-resolved mouse brain proteome. Nat Neurosci *18*, 1819-1831.
Shevchenko, A., Tomas, H., Havlis, J., Olsen, J.V., and Mann, M. (2006). In-gel digestion for mass spectrometric characterization of proteins and proteomes. Nat Protoc *1*, 2856-2860.
Shimshek, D.R., Kim, J., Hubner, M.R., Spergel, D.J., Buchholz, F., Casanova, E., Stewart, A.F., Seeburg, P.H., and Sprengel, R. (2002). Codon-improved Cre recombinase (iCre) expression in the mouse. Genesis *32*, 19-26.
Shoji, M., Golde, T.E., Ghiso, J., Cheung, T.T., Estus, S., Shaffer, L.M., Cai, X.D., McKay, D.M., Tintner, R., Frangione, B.*, et al.* (1992). Production of the Alzheimer amyloid beta protein by normal proteolytic processing. Science *258*, 126-129.
Silva, A., Pinheiro, P.S., Carvalho, A.P., Carvalho, C.M., Jakobsen, B., Zimmer, J., and Malva, J.O. (2003). Activation of neuropeptide Y receptors is neuroprotective against excitotoxicity in organotypic hippocampal slice cultures. FASEB J *17*, 1118-1120.
Simpson, J.E., Ince, P.G., Lace, G., Forster, G., Shaw, P.J., Matthews, F., Savva, G., Brayne, C., Wharton, S.B., Function, M.R.C.C.*, et al.* (2010). Astrocyte phenotype in relation to Alzheimer-type pathology in the ageing brain. Neurobiol Aging *31*, 578-590.
Sinha, S., Anderson, J.P., Barbour, R., Basi, G.S., Caccavello, R., Davis, D., Doan, M., Dovey, H.F., Frigon, N., Hong, J.*, et al.* (1999). Purification and cloning of amyloid precursor protein beta-secretase from human brain. Nature *402*, 537-540.
Sisodia, S.S., Koo, E.H., Beyreuther, K., Unterbeck, A., and Price, D.L. (1990). Evidence that beta-amyloid protein in Alzheimer's disease is not derived by normal processing. Science *248*, 492-495.

Solanas, G., Cortina, C., Sevillano, M., and Batlle, E. (2011). Cleavage of E-cadherin by ADAM10 mediates epithelial cell sorting downstream of EphB signalling. Nat Cell Biol *13*, 1100-1107.
Stachel, S.J., Coburn, C.A., Steele, T.G., Jones, K.G., Loutzenhiser, E.F., Gregro, A.R., Rajapakse, H.A., Lai, M.T., Crouthamel, M.C., Xu, M.*, et al.* (2004). Structure-based design of potent and selective cell-permeable inhibitors of human beta-secretase (BACE-1). J Med Chem *47*, 6447-6450.
Stasyk, T., and Huber, L.A. (2004). Zooming in: fractionation strategies in proteomics. Proteomics *4*, 3704-3716.
Steen, H., and Mann, M. (2004). The ABC's (and XYZ's) of peptide sequencing. Nat Rev Mol Cell Biol *5*, 699-711.
Steiner, H., Fluhrer, R., and Haass, C. (2008). Intramembrane proteolysis by gamma-secretase. The Journal of biological chemistry *283*, 29627-29631.
Strassnig, M., and Ganguli, M. (2005). About a Peculiar Disease of the Cerebral Cortex; Alzheimer's Original Case Revisited. Psychiatry *2*, 30-33.
Stutzer, I., Selevsek, N., Esterhazy, D., Schmidt, A., Aebersold, R., and Stoffel, M. (2013). Systematic proteomic analysis identifies beta-site amyloid precursor protein cleaving enzyme 2 and 1 (BACE2 and BACE1) substrates in pancreatic beta-cells. The Journal of biological chemistry *288*, 10536-10547.
Suh, J., Choi, S.H., Romano, D.M., Gannon, M.A., Lesinski, A.N., Kim, D.Y., and Tanzi, R.E. (2013). ADAM10 missense mutations potentiate beta-amyloid accumulation by impairing prodomain chaperone function. Neuron *80*, 385-401.
Sultana, R., Boyd-Kimball, D., Cai, J., Pierce, W.M., Klein, J.B., Merchant, M.J., and Butterfield, D.A. (2007). Proteomics analysis of the Alzheimer's disease hippocampal proteome. J Alzheimers Dis *11*, 153-164.
Sultana, R., Boyd-Kimball, D., Poon, H.F., Cai, J., Pierce, W.M., Klein, J.B., Merchant, M., Markesbery, W.R., and Butterfield, D.A. (2006). Redox proteomics identification of oxidized proteins in Alzheimer's disease hippocampus and cerebellum: an approach to understand pathological and biochemical alterations in AD. Neurobiol Aging *27*, 1564-1576.
Swaney, D.L., Wenger, C.D., and Coon, J.J. (2010). Value of using multiple proteases for large-scale mass spectrometry-based proteomics. J Proteome Res *9*, 1323-1329.
Szabo, R., Lantsman, T., Peters, D.E., and Bugge, T.H. (2016). Delineation of proteolytic and non-proteolytic functions of the membrane-anchored serine protease prostasin. Development *143*, 2818-2828.
Tabatabaei-Jafari, H., Shaw, M.E., and Cherbuin, N. (2015). Cerebral atrophy in mild cognitive impairment: A systematic review with meta-analysis. Alzheimers Dement (Amst) *1*, 487-504.
Takano, M., Maekura, K., Otani, M., Sano, K., Nakamura-Hirota, T., Tokuyama, S., Min, K.S., Tomiyama, T., Mori, H., and Matsuyama, S. (2012). Proteomic analysis of the brain tissues from a transgenic mouse model of amyloid beta oligomers. Neurochem Int *61*, 347-355.
Takashima, S. (2003). Comparison of the Enzymatic Properties of Mouse -Galactoside 2,6-Sialyltransferases, ST6Gal I and II. Journal of Biochemistry *134*, 287-296.
Takino, T., Koshikawa, N., Miyamori, H., Tanaka, M., Sasaki, T., Okada, Y., Seiki, M., and Sato, H. (2003). Cleavage of metastasis suppressor gene product KiSS-1 protein/metastin by matrix metalloproteinases. Oncogene *22*, 4617-4626.
Tanzi, R.E., Bird, E.D., Latt, S.A., and Neve, R.L. (1987). The amyloid beta protein gene is not duplicated in brains from patients with Alzheimer's disease. Science *238*, 666-669.
Thomason, L.A., Smithson, L.J., Hazrati, L.N., McLaurin, J., and Kawaja, M.D. (2013). Reactive astrocytes associated with plaques in TgCRND8 mouse brain and in human Alzheimer brain express phosphoprotein enriched in astrocytes (PEA-15). FEBS letters *587*, 2448-2454.
Tippmann, F., Hundt, J., Schneider, A., Endres, K., and Fahrenholz, F. (2009). Up-regulation of the alpha-secretase ADAM10 by retinoic acid receptors and acitretin. FASEB J *23*, 1643-1654.
Tusher, V.G., Tibshirani, R., and Chu, G. (2001). Significance analysis of microarrays applied to the ionizing radiation response. Proc Natl Acad Sci U S A *98*, 5116-5121.
Uemura, T., Lee, S.J., Yasumura, M., Takeuchi, T., Yoshida, T., Ra, M., Taguchi, R., Sakimura, K., and Mishina, M. (2010). Trans-synaptic interaction of GluRdelta2 and Neurexin through Cbln1 mediates synapse formation in the cerebellum. Cell *141*, 1068-1079.

Ulrich, J.D., and Holtzman, D.M. (2016). TREM2 Function in Alzheimer's Disease and Neurodegeneration. ACS Chem Neurosci *7*, 420-427.
Vandenberghe, R., Rinne, J.O., Boada, M., Katayama, S., Scheltens, P., Vellas, B., Tuchman, M., Gass, A., Fiebach, J.B., Hill, D.*, et al.* (2016). Bapineuzumab for mild to moderate Alzheimer's disease in two global, randomized, phase 3 trials. Alzheimers Res Ther *8*, 18.
Varki, A. (2017). Biological roles of glycans. Glycobiology *27*, 3-49.
Varki, A., Cummings, R.D., Esko, J.D., Stanley, P., W Hart, G.W., Aebi, M., Darvill, A.G., Kinoshita, T., Packer, N.H., Prestegard, J.H.*, et al.* (2017). Essentials Of Glycobiology, 3 edn (Cold Spring Harbor NY: Cold Spring Harbor Laboratory Press).
Vassar, R. (1999). Beta-Secretase Cleavage of Alzheimer's Amyloid Precursor Protein by the Transmembrane Aspartic Protease BACE. Science *286*, 735-741.
Vassar, R. (2014). BACE1 inhibitor drugs in clinical trials for Alzheimer's disease. Alzheimer's Research & Therapy.
Vassar, R., Kuhn, P.H., Haass, C., Kennedy, M.E., Rajendran, L., Wong, P.C., and Lichtenthaler, S.F. (2014). Function, therapeutic potential and cell biology of BACE proteases: current status and future prospects. J Neurochem *130*, 4-28.
Vinueza Veloz, M.F., Zhou, K., Bosman, L.W., Potters, J.W., Negrello, M., Seepers, R.M., Strydis, C., Koekkoek, S.K., and De Zeeuw, C.I. (2015). Cerebellar control of gait and interlimb coordination. Brain Struct Funct *220*, 3513-3536.
Visscher, M., De Henau, S., Wildschut, M.H.E., van Es, R.M., Dhondt, I., Michels, H., Kemmeren, P., Nollen, E.A., Braeckman, B.P., Burgering, B.M.T.*, et al.* (2016). Proteome-wide Changes in Protein Turnover Rates in C. elegans Models of Longevity and Age-Related Disease. Cell Rep *16*, 3041-3051.
Voss, M., Schroder, B., and Fluhrer, R. (2013). Mechanism, specificity, and physiology of signal peptide peptidase (SPP) and SPP-like proteases. Biochim Biophys Acta *1828*, 2828-2839.
Voytyuk, I., De Strooper, B., and Chavez-Gutierrez, L. (2018a). Modulation of gamma- and beta-Secretases as Early Prevention Against Alzheimer's Disease. Biol Psychiatry *83*, 320-327.
Voytyuk, I., Mueller, S.A., Herber, J., Snellinx, A., Moechars, D., van Loo, G., Lichtenthaler, S.F., and De Strooper, B. (2018b). BACE2 distribution in major brain cell types and identification of novel substrates. Life Science Alliance *1*, e201800026.
Wang, J.Z., and Liu, F. (2008). Microtubule-associated protein tau in development, degeneration and protection of neurons. Prog Neurobiol *85*, 148-175.
Wang, X., and Pei, D. (2001). Shedding of membrane type matrix metalloproteinase 5 by a furin-type convertase: a potential mechanism for down-regulation. The Journal of biological chemistry *276*, 35953-35960.
Wang, X., Yi, J., Lei, J., and Pei, D. (1999). Expression, purification and charaterization of recombinant mouse MT5-MMP protein products. FEBS J *462*, 261-266.
Wang, Z.Y., Han, Z.M., Liu, Q.F., Tang, W., Ye, K., and Yao, Y.Y. (2015). Use of CSF alpha-synuclein in the differential diagnosis between Alzheimer's disease and other neurodegenerative disorders. Int Psychogeriatr *27*, 1429-1438.
Warren, K.M., Reeves, T.M., and Phillips, L.L. (2012). MT5-MMP, ADAM-10, and N-cadherin act in concert to facilitate synapse reorganization after traumatic brain injury. J Neurotrauma *29*, 1922-1940.
Washburn, M.P., Wolters, D., and Yates, J.R. (2001). Large-scale analysis of the yeast proteome by multidimensional protein identification technology. Nature Biotechnology *19*, 242-247.
Weber, S., and Saftig, P. (2012). Ectodomain shedding and ADAMs in development. Development *139*, 3693-3709.
Weekens, M.P. (2010). Comparative Analysis of thechniques to purifiy Plasma Membrane Proteins_Weekens et al.2010. Journal of Biomolecular Techniques.
Weidemann, A., G., K., Bunke, D., Fischer, P., Salbaum, J.M., Masters, C.L., and Beyreuther, K. (1989). Identification, biogenesis, and localization of precursors of Alzheimer's disease A4 amyloid protein. Cell *57*, 115-126.
Weidemann, A., Paliga, K., Dürrwang, U., Reinhard, F.B., Schuckert, O., Evin, G., and Masters, C.L. (1999). Proteolytic processing of the Alzheimer's disease amyloid precursor protein within its

cytoplasmic domain by caspase-like proteases. The Journal of biological chemistry *274*, 5823-5829.
Willem, M., Tahirovic, S., Busche, M.A., Ovsepian, S.V., Chafai, M., Kootar, S., Hornburg, D., Evans, L.D., Moore, S., Daria, A.*, et al.* (2015). eta-Secretase processing of APP inhibits neuronal activity in the hippocampus. Nature *526*, 443-447.
Wisniewski, J.R. (2011). Tools for phospho- and glycoproteomics of plasma membranes. Amino Acids *41*, 223-233.
Wollscheid, B., Bausch-Fluck, D., Henderson, C., O'Brien, R., Bibel, M., Schiess, R., Aebersold, R., and Watts, J.D. (2009). Mass-spectrometric identification and relative quantification of N-linked cell surface glycoproteins. Nat Biotechnol *27*, 378-386.
Wu, Z., Ni, J., Liu, Y., Teeling, J.L., Takayama, F., Collcutt, A., Ibbett, P., and Nakanishi, H. (2017). Cathepsin B plays a critical role in inducing Alzheimer's disease-like phenotypes following chronic systemic exposure to lipopolysaccharide from Porphyromonas gingivalis in mice. Brain Behav Immun *65*, 350-361.
Yamada, T., Kawamata, T., Walker, D.G., and McGeer, P.L. (1992). Vimentin immunoreactivity in normal and pathological human brain tissue. Acta Neuropathol *84*, 157-162.
Yan, R. (2016). Stepping closer to treating Alzheimer's disease patients with BACE1 inhibitor drugs. Transl Neurodegener *5*, 13.
Yan, R. (2017). Physiological Functions of the beta-Site Amyloid Precursor Protein Cleaving Enzyme 1 and 2. Front Mol Neurosci *10*, 97.
Yan, R., Bienkowski, M.J., Shuck, M.E., Miao, H., Tory, M.C., Pauley, A.M., Brashier, J.R., Stratman, N.C., Mathews, W.R., Buhl, A.E.*, et al.* (1999). Membrane-anchored aspartyl protease with Alzheimer's disease beta-secretase activity. Nature *402*, 533-537.
Yang, Y., and Wang, J.Z. (2018). Nature of Tau-Associated Neurodegeneration and the Molecular Mechanisms. J Alzheimers Dis *62*, 1305-1317.
Yu, L.R., Stewart, N.A., and T.D., V. (2010). Proteomics: The deciphering of the functional genome. In Essentials of Genomic and Personalized Medicine, G.S. Ginsburg, and H.F. Willard, eds. (Academic Press: Elsevier).
Zeisel, A., Muñoz-Manchado, A.B., Codeluppi, S., Lönnerberg, P., La Manno, G., Juréus, A., Marques, S., Munguba, H., He, L., Betsholtz, C.*, et al.* (2015). Brain structure. Cell types in the mouse cortex and hippocampus revealed by single-cell RNA-seq. Science *347*, 1138-1142.
Zeng, Y., Ramya, T.N., Dirksen, A., Dawson, P.E., and Paulson, J.C. (2009). High-efficiency labeling of sialylated glycoproteins on living cells. Nat Methods *6*, 207-209.
Zhang, D., Yuan, D., Shen, J., Yan, Y., Gong, C., Gu, J., Xue, H., Qian, Y., Zhang, W., He, X.*, et al.* (2015a). Up-regulation of VCAM1 Relates to Neuronal Apoptosis After Intracerebral Hemorrhage in Adult Rats. Neurochem Res *40*, 1042-1052.
Zhang, Y., Chen, K., Sloan, S.A., Bennett, M.L., Scholze, A.R., O'Keeffe, S., Phatnani, H.P., Guarnieri, P., Caneda, C., Ruderisch, N.*, et al.* (2014). An RNA-sequencing transcriptome and splicing database of glia, neurons, and vascular cells of the cerebral cortex. J Neurosci *34*, 11929-11947.
Zhang, Z., Song, M., Liu, X., Su Kang, S., Duong, D.M., Seyfried, N.T., Cao, X., Cheng, L., Sun, Y.E., Ping Yu, S.*, et al.* (2015b). Delta-secretase cleaves amyloid precursor protein and regulates the pathogenesis in Alzheimer's disease. Nat Commun *6*, 8762.
Zhou, L., Barao, S., Laga, M., Bockstael, K., Borgers, M., Gijsen, H., Annaert, W., Moechars, D., Mercken, M., Gevaert, K.*, et al.* (2012). The neural cell adhesion molecules L1 and CHL1 are cleaved by BACE1 protease in vivo. The Journal of biological chemistry *287*, 25927-25940.
Zhu, K., Xiang, X., Filser, S., Marinkovic, P., Dorostkar, M.M., Crux, S., Neumann, U., Shimshek, D.R., Rammes, G., Haass, C.*, et al.* (2016). Beta-Site Amyloid Precursor Protein Cleaving Enzyme 1 Inhibition Impairs Synaptic Plasticity via Seizure Protein 6. Biol Psychiatry.
Zubarev, R.A., and Makarov, A. (2013). Orbitrap mass spectrometry. Anal Chem *85*, 5288-5296.

Supplementary data

Supplementary data 1: Significantly changed proteins in the CSF of 5xFAD-MT5 KO mice compared to 5xFAD animals. Proteins, which significantly changed (56 proteins) in the CSF of 5xFAD mice upon knockdown of MT5-MMP are listed sorted by their p-value. In addition to the change in protein level (LFQ intensity ratio 5xFAD-MT5 KO/5xFAD) and p-value, the table indicates the subcellular location of each protein according to reviewed Uniprot annotations (+ = annotation exists for the listed compartment location: Cytoplasm, nucleus, membrane, mitochondrion or secreted (extracellular space)).

Uniprot accession	Protein names	Gene names	Cytoplasm	Nucleus	Membrane	Mitochon-drion	Secreted	5xFAD-MT5 KO/ 5xFAD	p-value ↓	FDR significant
P05532	Mast/stem cell growth factor receptor Kit	Kit	+		+			1.64	1.35E-04	+
P20152	Vimentin	Vim	+					0.14	1.45E-04	+
P50247	Adenosylhomocysteinase	Ahcy	+					0.24	1.55E-04	+
Q9R171	Cerebellin-1	Cbln1			+		+	0.66	1.64E-04	+
P68372	Tubulin beta-4B chain	Tubb4b	+					0.06	3.06E-04	+
P57774	Neuropeptide Y	Npy					+	1.87	5.15E-04	+
Q91VI7	Ribonuclease inhibitor	Rnh1	+					0.22	5.71E-04	+
P15626	Glutathione S-transferase Mu 2	Gstm2	+					0.20	5.72E-04	+
P07901	Heat shock protein HSP 90-alpha	Hsp90aa1	+		+			0.15	5.97E-04	+
Q00915	Retinol-binding protein 1	Rbp1	+					0.14	6.05E-04	+
Q9WTX5	S-phase kinase-associated protein 1	Skp1	+	+				0.47	6.58E-04	+
P63242; Q8BGY2	Eukaryotic translation initiation factor 5A-1/2	Eif5a; Eif5a2	+	+	+			0.32	6.86E-04	+
Q8R1G2	Carboxymethylenebutenolidase homolog	Cmbl	+					0.21	8.07E-04	+
Q9DCD0	6-phosphogluconate dehydrogenase, decarboxylating	Pgd	+					0.32	8.36E-04	+
Q62148	Retinal dehydrogenase 2	Aldh1a2	+					0.11	9.27E-04	+
P11499	Heat shock protein HSP 90-beta	Hsp90ab1	+					0.22	1.05E-03	+
P16045	Galectin-1	Lgals1					+	0.27	1.26E-03	+
Q9R0P3	S-formylglutathione hydrolase	Esd	+					0.20	1.35E-03	+
Q62426	Cystatin-B	Cstb	+					0.50	1.69E-03	+
Q61598	Rab GDP dissociation inhibitor beta	Gdi2	+		+			0.31	1.73E-03	+
Q99PT1	Rho GDP-dissociation inhibitor 1	Arhgdia	+					0.44	1.89E-03	+
P24549	Retinal dehydrogenase 1	Aldh1a1	+					0.19	2.00E-03	+
P14069	Protein S100-A6	S100a6	+	+	+			0.35	2.01E-03	+
O55023	Inositol monophosphatase 1	Impa1	+					0.53	2.02E-03	+
P45376	Aldose reductase	Akr1b1	+					0.16	2.37E-03	+
P35700	Peroxiredoxin-1	Prdx1	+					0.31	2.55E-03	+
Q62048	Astrocytic phosphoprotein PEA-15	Pea15	+					0.39	2.59E-03	+
P17182	Alpha-enolase	Eno1	+		+			0.37	2.65E-03	+
P16858	Glyceraldehyde-3-phosphate dehydrogenase	Gapdh	+	+				0.17	2.72E-03	+
P26350	Prothymosin alpha	Ptma		+				0.20	2.99E-03	+
P63017	Heat shock cognate 71 kDa protein	Hspa8	+	+	+			0.38	3.08E-03	+
P68254	14-3-3 protein theta	Ywhaq	+					0.36	3.56E-03	+

Q01853	Transitional endoplasmic reticulum ATPase	Vcp	+	+				0.08	3.56E-03	+
P19157; P46425	Glutathione S-transferase P 1/2	Gstp1; Gstp2	+	+		+		0.34	3.72E-03	+
P17751	Triosephosphate isomerase	Tpi1	+					0.29	3.76E-03	+
P01942	Hemoglobin subunit alpha	Hba	+				+	0.12	3.94E-03	+
P15105	Glutamine synthetase	Glul	+			+		0.12	4.07E-03	+
P99029	Peroxiredoxin-5, mitochondrial	Prdx5	+			+		0.38	4.29E-03	+
P68510	14-3-3 protein eta	Ywhah	+					0.26	4.32E-03	+
Q61316	Heat shock 70 kDa protein 4	Hspa4	+					0.32	4.80E-03	+
Q9CQV8	14-3-3 protein beta/alpha	Ywhab	+					0.34	4.82E-03	+
O88844	Isocitrate dehydrogenase [NADP] cytoplasmic	Idh1	+					0.35	4.83E-03	+
P48758	Carbonyl reductase [NADPH] 1	Cbr1	+					0.22	5.68E-03	+
Q99LX0	Protein deglycase DJ-1	Park7	+	+	+	+		0.38	5.97E-03	+
P68037	Ubiquitin-conjugating enzyme E2 L3	Ube2l3	+	+				0.39	6.03E-03	+
P18760	Cofilin-1	Cfl1	+	+	+			0.41	6.26E-03	+
P23492	Purine nucleoside phosphorylase	Pnp	+					0.20	6.35E-03	+
P10649	Glutathione S-transferase Mu 1	Gstm1	+					0.29	6.39E-03	+
Q9DBF1	Alpha-aminoadipic semialdehyde dehydrogenase	Aldh7a1	+	+		+		0.16	6.45E-03	+
P06151	L-lactate dehydrogenase A chain	Ldha	+					0.28	7.12E-03	+
P48036	Annexin A5	Anxa5			+		+	0.31	7.47E-03	+
P28474	Alcohol dehydrogenase class-3	Adh5	+					0.19	8.52E-03	+
P02088	Hemoglobin subunit beta-1	Hbb-b1	+					0.16	9.42E-03	+
Q99LD8	N(G),N(G)-dimethylarginine dimethylaminohydrolase 2	Ddah2	+			+		0.28	1.06E-02	+
P56480	ATP synthase subunit beta, mitochondrial	Atp5b			+	+		0.14	1.14E-02	+
Q02053	Ubiquitin-like modifier-activating enzyme 1	Uba1	+	+		+		0.16	1.18E-02	+

Supplementary data 2: Protein class clustering of significantly changed proteins in the CSF of 5xFAD-MT5 KO mice compared to 5xFAD animals. Significantly changed proteins (56 proteins) in the CSF of 5xFAD mice upon knockdown of MT5-MMP are classified and clustered by PANTHER based on their Gene Ontology annotations into functional protein classes. Proteins are given with their Uniprot accession number and change in protein level (LFQ intensity ratio 5xFAD-MT5 KO/5xFAD).

Protein class	Uniprot Accession	Gene Names	Protein Names	5xFAD-MT5 KO/ 5xFAD
Oxidoreductase	P16858	Gapdh	Glyceraldehyde-3-phosphate dehydrogenase	0.17
	Q9DCD0	Pgd	6-phosphogluconate dehydrogenase, decarboxylating	0.32
	P35700	Prdx1	Peroxiredoxin-1	0.30
	Q9DBF1	Aldh7a1	Alpha-aminoadipic semialdehyde dehydrogenase	0.15
	P99029	Prdx5	Peroxiredoxin-5, mitochondrial	0.37
	Q62148	Aldh1a2	Retinal dehydrogenase 2	0.11
	P06151	Ldha	L-lactate dehydrogenase A chain	0.28
	P28474	Adh5	Alcohol dehydrogenase class-3	0.18
	P24549	Aldh1a1	Retinal dehydrogenase 1	0.18
	P45376	Akr1b1	Aldose reductase	0.16

Hydrolase	Q99LX0	Park7	Protein deglycase DJ-1	0.37
	P50247	Ahcy	Adenosylhomocysteinase	0.24
	Q99LD8	Ddah2	N(G),N(G)-dimethylarginine dimethylaminohydrolase 2	0.27
	Q9R0P3	Esd	S-formylglutathione hydrolase	0.19
	O55023	Impa1	Inositol monophosphatase 1	0.52
	P56480	Atp5b	ATP synthase subunit beta, mitochondrial	0.13
Nucleic acid binding	Q91VI7	Rnh1	Ribonuclease inhibitor	0.21
	Q99LX0	Park7	Protein deglycase DJ-1	0.37
	P56480	Atp5b	ATP synthase subunit beta, mitochondrial	0.13
Chaperone	P11499	Hsp90ab1	Heat shock protein HSP 90-beta	0.21
	Q9CQV8	Ywhab	14-3-3 protein beta/alpha	0.34
	P68254	Ywhaq	14-3-3 protein theta	0.35
	P68510	Ywhah	14-3-3 protein eta	0.26
	P07901	Hsp90aa1	Heat shock protein HSP 90-alpha	0.14
Signaling molecule	P14069	S100a6	Protein S100-A6	0.34
	P16045	Lgals1	Galectin-1	0.27
	Q99PT1	Arhgdia	Rho GDP-dissociation inhibitor 1	0.43
	P57774	Npy	(Pro-)Neuropeptide Y	1.86
Enzyme modulator	Q00915	Rbp1	Retinol-binding protein 1	0.13
	Q61598	Gdi2	Rab GDP dissociation inhibitor beta	0.31
	Q99PT1	Arhgdia	Rho GDP-dissociation inhibitor 1	0.43
	Q62426	Cstb	Cystatin-B	0.50
Ligase	P68037	Ube2l3	Ubiquitin-conjugating enzyme E2 L3	0.39
	Q02053	Uba1	Ubiquitin-like modifier-activating enzyme 1	0.16
	P15105	Glul	Glutamine synthetase	0.12
Transfer/carrier protein	Q02053	Uba1	Ubiquitin-like modifier-activating enzyme 1	0.16
	P68037	Ube2l3	Ubiquitin-conjugating enzyme E2 L3	0.39
Transferase	P23492	Pnp	Purine nucleoside phosphorylase	0.20
	Q61598	Gdi2	Rab GDP dissociation inhibitor beta	0.31
Transproter	P56480	Atp5b	ATP synthase subunit beta, mitochondrial	0.13
Cell adhesion molecule	P16045	Lgals1	Galectin-1	0.27
Calcium-binding protein	P14069	S100a6	Protein S100-A6	0.34
Isomerase	P17751	Tpi1	Triosephosphate isomerase	0.29
Lyase	P17182	Eno1	Alpha-enolase	0.36

Supplementary data 3: Biological process clustering of significantly changed proteins in the CSF of 5xFAD-MT5 KO mice compared to 5xFAD animals. Significantly changed proteins (56 proteins) in the CSF of 5xFAD mice upon knockdown of MT5-MMP are classified and clustered by PANTHER based on their Gene Ontology annotations according to their involvement in biological processes. Proteins are given with their Uniprot accession number and change in protein level (LFQ intensity ratio 5xFAD-MT5 KO/5xFAD). Main processes are separated by a solid line. Sub-categories (sub) within a main process are separated by a dashed line.

Biological process	Uniprot AC	Gene Name	Protein Name	5xFAD-MT5 KO/ 5xFAD
Biological regulation	P05532	Kit	Mast/stem cell growth factor receptor Kit	1.64
	P35700	Prdx1	Peroxiredoxin-1	0.31
	P99029	Prdx5	Peroxiredoxin-5, mitochondrial	0.38
	Q99LD8	Ddah2	N(G),N(G)-dimethylarginine dimethylaminohydrolase 2	0.28
	O55023	Impa1	Inositol monophosphatase 1	0.53
	P57774	Npy	(Pro-)Neuropeptide Y	1.87
Cellular component organisation/biogenesis				0.06
	P68372	Tubb4b	Tubulin beta-4B chain	
	Q61316	Hspa4	Heat shock 70 kDa protein 4	0.32
	Q01853	Vcp	Transitional endoplasmic reticulum ATPase	0.08

	P18760	Cfl1	Cofilin-1	0.41
Cellular process	P63017	Hspa8	Heat shock cognate 71 kDa protein	0.38
	Q99LX0	Park7	Protein deglycase DJ-1	0.38
	P16045	Lgals1	Galectin-1	0.27
	P68037	Ube2l3	Ubiquitin-conjugating enzyme E2 L3	0.39
	Q91VI7	Rnh1	Ribonuclease inhibitor	0.22
	Q02053	Uba1	Ubiquitin-like modifier-activating enzyme 1	0.16
	P68372	Tubb4b	Tubulin beta-4B chain	0.06
	P35700	Prdx1	Peroxiredoxin-1	0.31
	P99029	Prdx5	Peroxiredoxin-5, mitochondrial	0.38
	P17751	Tpi1	Triosephosphate isomerase	0.29
	P50247	Ahcy	Adenosylhomocysteinase	0.24
	Q99LD8	Ddah2	N(G),N(G)-dimethylarginine dimethylaminohydrolase 2	0.28
	P18760	Cfl1	Cofilin-1	0.41
sub: cell comminucation	P05532	Kit	Mast/stem cell growth factor receptor Kit	1.64
	Q9CQV8	Ywhab	14-3-3 protein beta/alpha	0.34
	P68510	Ywhah	14-3-3 protein eta	0.26
	Q61598	Gdi2	Rab GDP dissociation inhibitor beta	0.31
	Q01853	Vcp	Transitional endoplasmic reticulum ATPase	0.08
	Q00915	Rbp1	Retinol-binding protein 1	0.14
	O55023	Impa1	Inositol monophosphatase 1	0.53
	Q99PT1	Arhgdia	Rho GDP-dissociation inhibitor 1	0.44
	P57774	Npy	(Pro-)Neuropeptide Y	1.87
sub: cell cycle	P14069	S100a6	Protein S100-A6	0.35
	Q9CQV8	Ywhab	14-3-3 protein beta/alpha	0.34
	P68254	Ywhaq	14-3-3 protein theta	0.36
	P68510	Ywhah	14-3-3 protein eta	0.26
	P68372	Tubb4b	Tubulin beta-4B chain	0.06
	Q01853	Vcp	Transitional endoplasmic reticulum ATPase	0.08
Developmental process	P05532	Kit	Mast/stem cell growth factor receptor Kit	1.64
	Q00915	Rbp1	Retinol-binding protein 1	0.14
Immune system process	Q91VI7	Rnh1	Ribonuclease inhibitor	0.22
	Q61316	Hspa4	Heat shock 70 kDa protein 4	0.32
Localization	P63017	Hspa8	Heat shock cognate 71 kDa protein	0.38
	Q61598	Gdi2	Rab GDP dissociation inhibitor beta	0.31
	Q01853	Vcp	Transitional endoplasmic reticulum ATPase	0.08
Metabolic process				
sub: bisynthetic process	Q99LX0	Park7	Protein deglycase DJ-1	0.38
	Q91VI7	Rnh1	Ribonuclease inhibitor	0.22
	P17751	Tpi1	Triosephosphate isomerase	0.29
	Q99LD8	Ddah2	N(G),N(G)-dimethylarginine dimethylaminohydrolase 2	0.28
sub: catabolic process	P63017	Hspa8	Heat shock cognate 71 kDa protein	0.38
	P68037	Ube2l3	Ubiquitin-conjugating enzyme E2 L3	0.39
	Q91VI7	Rnh1	Ribonuclease inhibitor	0.22
	Q02053	Uba1	Ubiquitin-like modifier-activating enzyme 1	0.16
	P35700	Prdx1	Peroxiredoxin-1	0.31
	P99029	Prdx5	Peroxiredoxin-5, mitochondrial	0.38
	P17751	Tpi1	Triosephosphate isomerase	0.29
	Q01853	Vcp	Transitional endoplasmic reticulum ATPase	0.08
	O55023	Impa1	Inositol monophosphatase 1	0.53
sub: coenzyme metabolic process	P50247	Ahcy	Adenosylhomocysteinase	0.24
sub: generation of precursor metabolites and energy	P16858	Gapdh	Glyceraldehyde-3-phosphate dehydrogenase	0.17
	P17182	Eno1	Alpha-enolase	0.37
	P17751	Tpi1	Triosephosphate isomerase	0.29
	P06151	Ldha	L-lactate dehydrogenase A chain	0.28
	P56480	Atp5b	ATP synthase subunit beta, mitochondrial	0.14
sub: nitrogen compound metabolic process	P63017	Hspa8	Heat shock cognate 71 kDa protein	0.38
	Q99LX0	Park7	Protein deglycase DJ-1	0.38

	Q91VI7	Rnh1	Ribonuclease inhibitor	0.22
	Q01853	Vcp	Transitional endoplasmic reticulum ATPase	0.08
	P50247	Ahcy	Adenosylhomocysteinase	0.24
	Q99LD8	Ddah2	N(G),N(G)-dimethylarginine dimethylaminohydrolase 2	0.28
	P15105	Glul	Glutamine synthetase	0.12
sub: phosphate-containing compound metabolic process	P63017	Hspa8	Heat shock cognate 71 kDa protein	0.38
	P05532	Kit	Mast/stem cell growth factor receptor Kit	1.64
	Q01853	Vcp	Transitional endoplasmic reticulum ATPase	0.08
	O55023	Impa1	Inositol monophosphatase 1	0.53
sub: primary metabolic process	P63017	Hspa8	Heat shock cognate 71 kDa protein	0.38
	Q91VI7	Rnh1	Ribonuclease inhibitor	0.22
	P14069	S100a6	Protein S100-A6	0.35
	P11499	Hsp90ab1	Heat shock protein HSP 90-beta	0.22
	Q99LX0	Park7	Protein deglycase DJ-1	0.38
	P68037	Ube2l3	Ubiquitin-conjugating enzyme E2 L3	0.39
	P48036	Anxa5	Annexin A5	0.31
	Q91VI7	Rnh1	Ribonuclease inhibitor	0.22
	Q9DCD0	Pgd	6-phosphogluconate dehydrogenase,	0.32
	Q02053	Uba1	Ubiquitin-like modifier-activating enzyme 1	0.16
	P17751	Tpi1	Triosephosphate isomerase	0.29
	Q01853	Vcp	Transitional endoplasmic reticulum ATPase	0.08
	P50247	Ahcy	Adenosylhomocysteinase	0.24
	Q99LD8	Ddah2	N(G),N(G)-dimethylarginine dimethylaminohydrolase 2	0.28
	P06151	Ldha	L-lactate dehydrogenase A chain	0.28
	O55023	Impa1	Inositol monophosphatase 1	0.53
	P28474	Adh5	Alcohol dehydrogenase class-3	0.19
	P15105	Glul	Glutamine synthetase	0.12
	P07901	Hsp90aa1	Heat shock protein HSP 90-alpha	0.15
	P56480	Atp5b	ATP synthase subunit beta, mitochondrial	0.14
sub: sulfur compound metabolic process	P50247	Ahcy	Adenosylhomocysteinase	0.24
Multicellular process	P05532	Kit	Mast/stem cell growth factor receptor Kit	1.64
	Q9R171	Cbln1	Cerebellin-1	0.66
	Q61598	Gdi2	Rab GDP dissociation inhibitor beta	0.31
	Q00915	Rbp1	Retinol-binding protein 1	0.14
Response to stimulus				
sub: behavior	P57774	Npy	(Pro-)Neuropeptide Y	1.87
sub: cellular defense response	Q91VI7	Rnh1	Ribonuclease inhibitor	0.22
sub: response to abiotic stimulus	P63017	Hspa8	Heat shock cognate 71 kDa protein	0.38
sub: response to external stimulus	Q01853	Vcp	Transitional endoplasmic reticulum ATPase	0.08
sub: response to stress	P63017	Hspa8	Heat shock cognate 71 kDa protein	0.38
	P11499	Hsp90ab1	Heat shock protein HSP 90-beta	0.22
	Q99LX0	Park7	Protein deglycase DJ-1	0.38
	Q02053	Uba1	Ubiquitin-like modifier-activating enzyme 1	0.16
	P35700	Prdx1	Peroxiredoxin-1	0.31
	P99029	Prdx5	Peroxiredoxin-5, mitochondrial	0.38
	Q01853	Vcp	Transitional endoplasmic reticulum ATPase	0.08
	P07901	Hsp90aa1	Heat shock protein HSP 90-alpha	0.15

Acknowledgement

I would like to express my gratitude to my supervisor Prof. Stefan Lichtenthaler who gave me the opportunity to work and grow in his lab and for his support and guidance during my PhD.

I am grateful to my colleagues within and beyond the lab for the constant collaboration and fruitful scientific and personal discussions.

My special gratitude goes to my friends and family for their unconditional support during these years.

List of Publications

A part of the presented data has been published in the following manuscripts:

Click chemistry-mediated biotinylation reveals a function for the protease BACE1 in modulating the neuronal surface glycoproteome
Herber J., Njavro J., Feederle R., Schepers U., Müller U.C., Bräse S., Müller S.A., Lichtenthaler S.F.
Molecular and Cellular Proteomics 2018 May 1; doi: 10.1074/mcp.RA118.000608. PMID: 29716

BACE2 distribution in major brain cell types and identification of novel substrates
Voytyuk I., Mueller S.A., **Herber J**., Snellinx A., Moechars D., van Loo G., Lichtenthaler S.F., De Strooper B.
Life Science Alliance 2018; 1; e201800026

Systematic substrate identification indicates a central role for the metalloprotease ADAM10 in axon targeting and synapse function.
Kuhn P.H., Colombo A.V., Schusser B., Dreymueller D., Wetzel S., Schepers U., **Herber J.**, Ludwig A., Kremmer E., Montag D., Müller U., Schweizer M., Saftig P., Bräse S., Lichtenthaler S. F.
Elife 2016 Jan 23;5. pii: e12748. doi: 10.7554/eLife.12748. PMID: 26802628